Hippocampus-cortex communication during sleep

Dissertation

zur Erlangung des Grades eines
Doktors der Naturwissenschaften

der Mathematisch-Naturwissenschaftlichen Fakultät
und
der Medizinischen Fakultät
der Eberhard-Karls-Universität Tübingen

vorgelegt
von

Ernesto Edgardo Durán Rodríguez
aus Santiago, Chile

Juni - 2020

Tag der mündlichen Prüfung: 30.06.2020

Dekan der Math. - Nat. Fakultät: Prof. Dr. W. Rosenstiel
Dekan der Medizinischen Fakultät: Prof. Dr. I.B.Autenrieth

1. Berichterstatter: Prof. Dr. Jan Born

2. Berichterstatter: Dr. Pablo Fuentealba

Prüfungskommission:

Prof. Dr. Jan Born

Dr. Pablo Fuentealba

Dr. Andreas Burgalossi

Prof. Dr. Andreas Nieder

Erklärung / Declaration:

Ich erkläre, dass ich die zur Promotion eingereichte Arbeit mit dem Titel:

"*Hippocampus-cortex communication during sleep"* selbständig verfasst, nur die angegebenen Quellen und Hilfsmittel benutzt und wörtlich oder inhaltlich übernommene Stellen als solche gekennzeichnet habe. Ich versichere an Eides statt, dass diese Angaben wahr sind und dass ich nichts verschwiegen habe. Mir ist be-kannt, dass die falsche Abgabe einer Versicherung an Eides statt mit Freiheitsstrafe bis zu drei Jahren oder mit Geldstrafe bestraft wird.

I hereby declare that I have produced the work entitled:

"*Hippocampus-cortex communication during sleep"*, submitted for the award of a doctorate, on my own (without external help), have used only the sources and aids indicated and have marked passages included from other works, whether verbatim or in content, as such. I swear upon oath that these statements are true and that I have not concealed anything. I am aware that making a false declaration under oath is punishable by a term of imprisonment of up to three years or by a fine.

Tübingen, den ....

Datum / Date Unterschrift / Signature

Contents

Abstract 1
1 Introduction 2
1.1 Sleep and sleep stages 2
1.2. Slow-wave sleep specific electrical oscillations 4
1.2.1 Slow oscillations 4
1.2.2 Spindles 5
1.2.3 Ripples 5
1.2.4 Temporal interaction among slow oscillations, spindles and ripples 6
1.3 Role of thalamus in hippocampus-cortex interaction 7
1.4 Aim 8
2 Study I: Simultaneous appearance of different sleep stages in hippocampus and cortex 9
3 Study II: Temporal association among slow oscillations, spindles and ripples 10
4 Study III: Selective modulation of thalamic neurons by hippocampal ripples 11
5 Discussion and conclusions 13
5.1 Hippocampus and cortex communication during sleep stages 13
5.2 Role of slow oscillations, spindles and ripples in the hippocampal-cortex communication 14
5.3 Hippocampal ripples modulation of thalamic neurons 16
5.4 Future directions 17
6 List of publications and statement of contribution 18
7 Acknowledgements 19
8 References 20
9 Appended publications 26
A.1 Sleep stage dynamic between hippocampus and cortex 26
A.2 Temporal associations between sleep slow oscillations, spindles and ripples 26
A.3 Midline thalamic neurons are differentially engaged during hippocampus network oscillations 26

Abstract

Sleep is critically involved in the formation of long-term memory and is thought to rely on a dialogue between hippocampus and neocortex. The communication between these structures has been proposed to be from the hippocampus to the neocortex. In rodents in the course of sleep, the brain alternates between stages of slow-wave sleep (SWS) and rapid eye movement (REM) sleep. Although sleep stages have been widely investigated, the precise temporal dynamic in hippocampus and cortex has remained largely unresolved. The sleep stages dynamic in hippocampus and cortex might determine the direction of the communication in both areas. Moreover, the hippocampus-cortex communication can be investigated not only in the dynamic of sleep stages, but also restricted to SWS. The interaction between hippocampus and cortex during SWS has been proposed to be top-down regulated by the neocortical slow oscillation (SO) that drives spindles in thalamo-cortical networks and ripples in hippocampal networks. Hippocampal ripples nested in spindles might support the hippocampal-to-neocortical communication. Despite that, these oscillations have been functionally coupled, the temporal association in hippocampus and cortex is not well understood. Furthermore, the thalamus is a central hub that is intimately connected to hippocampus. The thalamus is thought to play an important role in the communication between hippocampus and cortex. However, how thalamic neurons interact with hippocampus is still not clear. Here, we characterized in rats the sleep stages dynamic between neocortex and hippocampus. In addition, we examined the temporal relationships between the specific oscillations during SWS. Lastly, we examined the temporal relationship between thalamic neurons and hippocampal ripples. We simultaneously recorded the electroencephalogram (EEG) from skull electrodes over frontal and parietal cortex and the local field potential (LFP) from the medial prefrontal cortex and dorsal hippocampus (dHC) in order to determine the sleep stage dynamic and the temporal relationship between SOs, spindles and ripples. In addition, we performed simultaneous recordings of thalamic neurons and hippocampal ripples. Our results showed that SWS appeared simultaneously in the hippocampus and the cortex, however REM sleep appeared earlier in the hippocampus. Analysis of the specific oscillations during SWS showed that spindles in the hippocampus are orchestrated by SOs and these spindles

modulated hippocampal ripples. Moreover, hippocampal ripples inhibited specifically one class of thalamic neurons. These findings indicated a specific hippocampal-cortex communication, which has clear implications not only for our understanding of the organization of sleep and sleep rhythms, but possibly also for its functions, e.g., in memory formation.

1 Introduction

The communication in the brain describes a process in which an area, conveys certain aspects of its current functional state to another area (Schnitzler & Gross, 2005). In this scenario, sleep is an ideal temporal frame that might allow the neuronal activity transfer between brain regions. Sleep is characterized by the absence of body movement and the absence of reaction to the external stimulus (Tobler, 1995). Although sleep results from a reduction of external behavior, there is an increase of the internal activity in the brain (Sejnowski & Destexhe, 2000). As a consequence of the neuronal activity, large brain territories become synchronized in specific oscillatory rhythms (Schnitzler & Gross, 2005). The brain oscillations determine the sleep and sleep stages (Lesku et al., 2006). During the sleep stages the hippocampus and the cortex establish a very precise temporal coordination (Siapas & Wilson, 1998; Mölle et al., 2006; 2009; Wierzynski et al., 2009). This coordination is thought to support the communication between both brain areas, in order to transfer the hippocampal neuronal activity to different cortical networks.

1.1 Sleep and sleep stages

Sleep is an essential state that involves the whole organism. Sleep deprivation and sleep disruptions cause severe cognitive and emotional problems (Killgore, 2010; Vandekerckhove et al., 2010). Animals deprived of sleep for several weeks show temperature and weight dysregulation and ultimately die of infections and tissue lesions (Rechtschaffen et al., 1995). Sleep is defined by several criteria, as a typical body posture, physical quiescence, an increase threshold for arousal, rapid state reversibility, and regulatory capacity (Tobler, 1995). The definition of sleep in vertebrates is assessed by

using behavioural and electrophysiological criteria (Rechtschaffen et al., 1968; Neckelmann, 1994) based on electroencephalogram (EEG) and electromyogram (EMG). These electrophysiological criteria allow differentiating in mammals between the two principal sleep stages; slow-wave sleep (SWS) and rapid eye movement (REM) sleep (Tobler, 1995; Lesku et al., 2006). SWS is characterized by a predominant high-amplitude delta activity (<4.0 Hz) and a reduced EMG activity, and REM sleep is characterized by a predominant theta activity (5.0–10.0 Hz), phasic muscle twitches, and a minimum EMG activity. Sleep also is characterized by a cyclic alternation of these two stages, i.e. SWS and REM sleep. In humans, the first part of the night (early sleep) is characterized by high amounts of SWS, whereas REM sleep prevails during the second half (late sleep) (Ackermann & Borbely, 1993). Additionally, in rodents and cats, a transition state between SWS and REM sleep can be discriminated, which is called intermediate stage (IS) (Gottesmann et al., 1984; Glin et al., 1991; Benington et al., 1994). IS is characterized by a decrease in delta activity, a progressive increase of theta activity and the presence of sleep spindles (10.0–16.0 Hz).

Although sleep involves the whole brain, recent findings have suggested that sleep and sleep stages can also locally occur restricted to specific networks and regions (Mahowald et al., 2005; Krueger et al., 2008). For example, in human neocortex, local activations were recorded while SWS was simultaneously present in other regions (Nobili et al., 2011). In mice, intrusions of sleep-like activity patterns were observed in local neocortical networks during prolonged wake periods and immediately after spontaneous awakening (Vyazovskiy et al., 2011, 2014). In simultaneous scalp and intracranial recordings in human patients, most slow waves and spindles were found to occur only in local neocortical networks (Nir et al., 2011). The different sleep stages are often thought to fulfill specific functions (Ackermann & Rasch, 2014). The functions allocated to the different sleep stages are typically not established within only a single structure such as the neocortex, but rely on interactions between cortical and subcortical networks (Tsunematsu et al., 2011; Pignatelli et al., 2012). For example, memory formation is assumed to involve the co-coordinate dialogue between neocortex and hippocampus (Buzsáki, 1989). However, it is not clear that the different sleep stages can also locally appear in these brain regions. Here, we determined the dynamic of sleep stages in hippocampus and neocortex.

Understanding the dynamic of sleep stages has strong implications on understanding the hippocampus and cortex communication and its functions, e.g., memory process.

1.2 Slow-wave sleep specific electrical oscillations

The sleep and the sleep stages are characterized by a specific brain activity (Tobler, 1995; Lesku et al., 2006). SWS is characterized by the presence of cortical SOs, thalamo-cortical spindles and hippocampal ripples. These oscillations establish a very precise temporal coordination that is thought to support the hippocampal and cortical dialog (Born et al., 2006).

1.2.1 Slow oscillations

The SO is a prominent signal record in EEG during SWS, which is defined by the < 1 Hz frequency band (Steriade et al., 1993a). SOs comprise alterations between periods of neuronal membrane depolarization accompanied by sustained firing (upstates) and periods of membrane hyperpolarization associated with neuronal silence (downstate) (Steriade et al., 1993a; 1993b). Thus, the SO represents a spontaneous event during which cortical neurons are alternately silent and active for a specific time window. The generations and propagation of SO depend principally on the cortex, substantially involving subcortical structures like the thalamus (Steriade et al., 1993b; Crunelli & Hughes, 2010; Neske, 2016, Gent et al., 2018). Although SO is primordially a neocortical phenomenon, it can also be recorded in hippocampus (Wolansky et al., 2006; Staresina & Bergmann et al., 2015). Moreover, high density EEG recordings in humans have demonstrated that SOs originate most frequently in prefrontal cortex and propagate to posterior cortical regions, despite the occurrence of other origins and directions of propagation (Massimini et al, 2004). The importance of the SO resides in the fact that it modulates other rhythms that are generated in subcortical regions. For example, the cortical SO drives the generation of spindle oscillations in thalamocortical feedback loops (Steriade et al., 1993b; 1993c).

1.2.2 Spindles

Spindles are brief oscillations event between 10.0-16.0 Hz that typically appear during sleep (De Gennaro & Ferrara, 2003). A single spindle is recognized based on ~5 to 20 successive deflections of the human EEG signal (Lüthi, 2014). These deflections reach a maximum at the middle of the spindle event, gradually increasing before ("waxing") and decreasing after ("waning"). In humans, spindles are divided into two types that have different frequencies, topographic distributions, and functional roles (De Gennaro & Ferrara, 2003; Rasch & Born, 2013). The neuronal mechanisms of spindle generation are the results of synaptic interactions in the thalamocortical network (Steriade et al., 1993c). Spindle activity originates in the thalamus as a result of mutual interactions between GABAergic neurons of the nucleus reticularis which function as pacemaker, and the glutamatergic thalamo-cortical projections which widespread the propagation of spindles to cortical regions (Contreras et al., 1997). The thalamus is divided into different nuclei and they establish a precise neuroanatomical projection to cortex (Herrero et al., 2002; Van der Werf et al., 2002; Xiao et al., 2009). Eventually, each cortex territory reflects spindles differently depending on thalamus-cortical networks. High density EEG recordings in rats showed that spindles can reach the whole cortex simultaneously, but they can also be restricted to anterior or posterior areas (Kim et al., 2015) and hippocampus (Sullivan et al., 2014). Interestingly, the importance of the spindles in hippocampus resides on modulating hippocampal ripples (Clemens et al., 2007; 2011; Staresina & Bergmann et al., 2015).

1.2.3 Ripples

Ripples are characteristic hippocampal oscillations that appear during different behaviours (immobility, drinking, eating and grooming) and during SWS (Buzsáki et al., 1983; 2015). Ripples correspond to high frequency oscillations observed at around 100–200 Hz, particularly in the hippocampal CA1 sub-region (Buzsaki et al., 1992). These oscillations are emergent population event as a result of synchronous output of cooperating CA1 pyramidal cells (Buzsáki et al., 1992). Ripples may serve to induce synaptic enhancement in target structures of the hippocampus. Indeed, they are associated with a robustly enhanced transient excitability in the hippocampus and its partner structures

(Chrobak and Buzsáki, 1994; Csicsvari et al., 1999, Logothetis et al., 2012). For example, ripples drive the spike timing relationship between hippocampal and cortical neurons (Wierzynski et al., 2009). Although these hippocampal oscillations enhance transient excitability in some brain areas, at the same time they can generate transient inhibition in subcortical areas (Logothetis et al., 2012; Yang et al., 2019).

1.2.4 Temporal interaction between slow oscillations, spindles and ripples.

It has been proposed that hippocampus and cortex establish a dialog during SWS (Buzsáki, 1989). In the hippocampus-cortex dialog, the SOs coordinate the reactivation of hippocampal ripples in synchrony with thalamo-cortical spindle activity (Born et al., 2006). This reactivation is thought to be the mechanism by which temporarily stored memories are integrated into long-term storage. In line with this idea, several studies have demonstrated the role of cortical SOs in the coordination of thalamic spindles and hippocampal ripples, together with their role in memory process (Sirota et al., 2013; Mölle et al., 2006; 2009; Staresina & Bergmann et al., 2015; Maingret et al., 2016; Latchoumane & Ngo et al., 2017). Although upstate of the SO modulates the spindles, this modulation increased after learning and during SWS (Mölle et al, 2011). Moreover, it has been shown that strengthening of the temporal coordination among hippocampal ripples, cortical SO and spindles can enhance the consolidation of hippocampus-dependent spatial memory (Maingret et al., 2016). In addition, it has been demonstrated that optogenetic stimulation of thalamic spindles in phase with cortical SO upstate, improves the consolidation of hippocampus dependent memory during sleep (Latchoumane & Ngo et al., 2017). Despite numerous studies showing the influence of cortical SO in the coordination of thalamic spindles and hippocampal ripples, there is little evidence that SOs in cortex can also drive spindles in hippocampus, and that these spindles modulate hippocampal ripples. In light of the strong implications for understanding the hippocampus-cortex dialog, here we determined the cortical and hippocampal SO modulation, in the functional coupling between spindles and ripples in hippocampus during SWS.

1.3 The role of thalamus in hippocampus-cortex interaction

Numerous studies have investigated the hippocampus-cortex interaction during sleep (Rasch & Born., 2013). During the last decade growing evidence showed that subcortical structures can facilitate the hippocampus-cortex communication where thalamus play an important role (Van der Werf et al., 2002; Saalman, 2014; Vertes et al., 2015). The thalamus is a heterogeneous structure that projects mainly to cortex and also to subcortical areas (Jones, 2012). The different nuclei of thalamus have been named according to the functions in which they participate or according to anatomical position. The midline nuclei of thalamus is a narrow band, which extends from the dorsal (third ventricle) to the ventral formed by several nuclei (Van der Werf et al., 2002). The neurons in midline thalamus are characterized by the differential expression of calcium-binding proteins (Winsky et al., 1992; Arai et al., 1994). The differential expression of these proteins suggests that midline thalamus is composed by type of neurons with a distinctive neurochemical profile.

Midline thalamus is intimately connected with hippocampus and cortex (Van der Werf et al., 2002). The neurons in the ventral part of the midline thalamus project specifically into hippocampus (Vertes et al., 2006). Meanwhile, hippocampus projects into midline thalamus via the subiculum (Canteras et al., 1992; O'Mara et al., 2009). The neurons of the dorsal part of the midline thalamus project specifically into prefrontal cortex (Berendse & Groenewegen, 1991; Bubser & Deutch, 1998; Moga et al., 1995; Otake & Nakamura, 1998). Concurrently, prefrontal cortex projects back to midline thalamus (Huang et al., 2006; Vertes et al., 2006). Thus, midline thalamus corresponds to a specific hub that not just projects, but also allows the communication to hippocampus and cortex. Although the specific role of the midline thalamus is still unknown, different studies associate these nuclei with different cognitive functions (Van der Werf et al., 2002). The midline of thalamus has specifically been associated with different aspects of memory process (Loureiro et al., 2012 Cholvin el at., 2013). Historically, these functions have also been associated with hippocampus and prefrontal areas (Rasch & Born 2013). Giving the relevance of the midline thalamus in the communication of hippocampus with cortex it has

become pertinent to investigate the relation between these nuclei and hippocampus. In particular, we determined the temporal relationship between midline thalamic neurons and hippocampal ripples.

1.4 Aim

The aim of this research during the course of my PhD was to investigate the temporal interaction between hippocampus and cortex during sleep, and the role of thalamus in this process. In order to investigate the hippocampus-cortex interactions I performed three different but interconnected studies. In the first study, I performed experiments to characterize the hippocampus-cortex dynamic in different sleep stages. Therefore, I recorded in hippocampus and cortex simultaneously during sleep. In the second study, I performed additional analysis to characterize the temporal association between slow oscillations, spindles and ripples during slow-wave sleep. Finally, to investigate the role of thalamus in the hippocampus-cortex interaction, I performed additional experiments to record thalamic neurons and hippocampal ripples simultaneously.

2 Study I: Simultaneous appearance of different sleep stages in hippocampus and cortex

In this study, we aimed to determine the temporal coordination of the sleep stages in hippocampus and cortex. Here, we wanted to investigate whether the sleep and sleep stages come up simultaneously or at different time in hippocampus and cortex. The sleep stages dynamic might determine the direction of the communication in hippocampus and cortex. For this purpose, we used simultaneous recordings (12 h during the light phase) of two EEG (frontal and parietal) and two local field potential (LFP) electrodes, in medial prefrontal cortex (mPFC) and dorsal hippocampus (dHC) and one electromyogram (EMG) electrode in the neck muscle (the electrode locations are shown in publication A.1, Figure 1). The simultaneous recordings allowed us to characterize the sleep stages at the same time in different brain areas (for representative example see publication A.1 Figure 2A). The different vigilance states (wakefulness, SWS, IS, and REM sleep) were determined off-line using 10-s epochs through visual inspection. Each single EEG and LFP recording was independently classified together with the associated EMG recording.

We determined the congruence (i.e. co-occurrence) of sleep stages between the frontal EEG and each of the three other recording sites (i.e. parietal EEG and LFP signals from mPFC and dHC). The congruence in wake and sleep stage occurrence was high in wake (>92.0%) and SWS (>96.5%), somewhat lower for REM sleep (>87.0%), and distinctly lower for IS (<36.5%, see publication A.1 Figure 2B). Interestingly, IS and REM sleep showed different dynamics in hippocampus and cortex. IS episodes were overall rather short (0.31 ± 0.04 min) and most often identified in EEG recordings (see publication A.1, Figure 2C). During the time that IS was present in frontal EEG, REM sleep was most often present in hippocampus (see publication A.1, Figure 4B). We found that REM sleep in 36.6% of all epochs started earlier in hippocampal LFP recordings than in cortex. The greatest difference between REM sleep occurrence in dHC and parietal EEG recordings where REM sleep occurred with an average delay of 17.2 ± 1.1 s (publication A.1, Figure 3B). During the intervals of early local REM sleep in hippocampus, there was high theta activity in the cortical EEG activity that was synchronized with the hippocampal theta. However, the detection of REM sleep in the EEG signal is hampered by strong concurring

SWS-related oscillatory activity (see publication A.1, Figure 5A). The earlier REM onset in hippocampus was also accompanied by earlier muscle atonia, another hallmark of REM sleep (see publication A.1, Figure 5E). In sum, our results indicated that SWS appeared simultaneously in the whole brain, meanwhile REM sleep appeared early in hippocampus and then in cortex.

3 Study II: Temporal dynamic between slow oscillations, spindles and ripples

In this study, we aimed to characterize the temporal coordination between SOs, spindles and ripples, which might support the hippocampus-cortex communication. For this propose, we used the same simultaneous recordings of EEGs and LFP previously published (see publication A.1). We identified the SOs associated with spindles. We found that the co-occurrence of the SOs with spindles was more prominent in EEG than in LFP recordings (see publication A.2, Figure 3). In accordance with previous studies, we found a clear temporal relationship between SOs and spindles in both EEG recordings (Mölle et al., 2006; 2009; Latchoumane & Ngo et al., 2017). Spindles occurrence was diminished for a more or less extended interval around the SO downstate peak, and distinctly increased during the subsequent SO upstate, reaching a maximum ~500 ms after the SO downstate peak.

We also identified the SOs that appeared simultaneously with hippocampal ripples. We found the percentage of SOs co-occurring with hippocampal ripples was comparable in cortex and hippocampus ~38% (publication A.2, Table 2). Event correlation histograms of ripple events, referenced to the SO downstate peak, indicated a suppression of hippocampal ripples around the downstate peak of SOs in the frontal and parietal EEG, followed by an increased ripple occurrence during the SO upstate (publication A.2, Figure 4A). However, this significant decrease and subsequent increase of ripples were not clear for mPFC SOs. Event correlation histograms between hippocampal SO and ripple showed the upstate-related increase in ripple events, and in addition, hippocampal SOs were accompanied by a second increase in ripples which preceded the SO downstate peak (publication A.2, Figure 4A). The temporal association between hippocampal SOs and

ripples indicated the presence of two types of ripples (publication A.2, Supplementary Figure 4).

Finally, we assessed to the co-occurrence of SOs with spindles and hippocampal ripples which has been proposed as a mechanism for consolidation of memories (Staresina & Bergmann et al., 2015; Latchoumane & Ngo et al., 2016). We first assessed to the role of SO, we compared the average power spectra of the dHC LFP around the spindle, between spindles that did and did not co-occur with an SO event. The spectra indicated an increase in ripple power around the spindle which did not differ between spindles occurring in isolation and spindles co-occurring with an SO (publication A.2, Figure 6), suggesting that the presence of an SO does not substantially add to the spindle-related modulation of ripple power. We second assessed to the role of spindles, we compared average power spectra of the dHC LFP around the SO downstate peak, between SOs that did and did not co-occur with a spindle. The spectra showed a suppression of ripple power around the SO downstate peak that was most distinct for isolated SOs (publication A.2, Figure 7). Interestingly, ripple power was distinctly higher during SOs that co-occurred with spindles than during SOs occurring in isolation. Overall, these results suggest that the spindles are the primary factor driving hippocampal ripple activity, whereas the SO appears to be restricted to the suppression of ripple activity during the hyperpolarizing downstate.

4 Study III: Selective modulation of thalamic neurons by hippocampal ripples.

In this study, we aimed to determine the temporal coordination between thalamus and hippocampus. This coordination might play an important role in the hippocampus-cortex interaction. For this purpose, we performed simultaneous recordings of thalamic neurons and hippocampal ripples in anesthetized mice. The neuronal oscillations characterized during natural SWS can also be reproduced under anesthesia: slow, large-amplitude waves in field potential, which are generated by the alternation of hyperpolarized and depolarized states of cortical neurons (Chauvette et al., 2011). After the recordings, the thalamic neurons were labeled with neurobiotin using the juxtacellular labeling method (Pinault, 1996). Juxtacellular labeling method allowed us to characterize the position,

morphology and neurochemical profile of the neurons. Neurons were recorded from the most midline thalamic nuclei (publication A.3, Figure. 1a). Midline thalamic neurons did not show obvious distinct morphological types. In order to characterize the neurochemical profiles of thalamic neurons, we tested the neurobiotin-labelled cells for expressing the immunoreactivity for two calcium-binding proteins (publication A.3, Figure. 1b): calretinin (CR) and calbindin (CB). Nearly half of the labelled thalamic neurons expressed calbindin (CB+, 45.6%) or calretinin (CR+, 49.4%). Interestingly, CR+ neurons showed a lower firing rate than CR- neurons (publication A.3, Figure 3).

In order to assess the spike timing of individual thalamic neurons with respect to ripples, we computed the event correlation histogram between the simultaneously recorded hippocampal ripples and the action potentials of individual neurons in the midline thalamus, considering the onset of ripple episodes as reference. Our analysis showed that all midline thalamic neurons seemed to slightly increase their discharge probability just before the onset of sharp wave-ripples (publication A.3, Figure. 6a–c). Interestingly, CR− neurons did not exhibit major changes in their discharge probability during ripples (publication A.3, Figure. 6d, f). In contrast, the spike timing of CR+ neurons were significantly modulated by ripples (publication A.3, Figure. 6c, f). Indeed, the firing rate of CR+ cells was significantly inhibited during ripple episodes, and slightly activated immediately before and after the high frequency episodes (publication A.3, Figure. 6f). In sum, different midline thalamic neuronal type might be selectively recruited during hippocampal ripples, which supports the view that the thalamus is important in the dialogue between hippocampus and cortex.

5 Discussion and conclusions

Numerous studies showed that the hippocampus establishes a precise temporal coordination with cortex during sleep (Siapas & Wilson, 1998; Siapas et al., 2005; Mölle et al., 2006; Wierzynski et al., 2009). Our findings extend these observations by showing the temporal coordination between hippocampus and cortex during the different sleep stages, and between the SWS-specific electrical oscillations.

5.1 Hippocampus and cortex communication during sleep stages

We compared the appearance of sleep stages in EEG recordings (frontal and parietal cortex) and in LFP recordings (mPFC and dHC) in rats. We found that SWS simultaneously appeared in hippocampus and cortex. The simultaneous appearance of SWS suggests that this sleep stage reflects a rather unitary phenomenon that catches widespread areas of the brain. SWS is also known to synchronize activities in several other brain regions, thereby allowing precise communication between neuronal networks (Siapas & Wilson 1998; Mölle et al., 2006; Crunelli & Hughes, 2010). Interestingly, hippocampal-cortical networks showed that cells in prefrontal cortex fired consistently after hippocampal cells and that they were driven by hippocampal ripples (Wierzynsk et al., 2009). This provides an evidence at the single cell-pair level for highly consistent directional interactions between hippocampus and cortex during SWS. Moreover, there is evidence reported an increased firing in rats' barrel cortex (Vyazovskiy et al., 2009) and hippocampus (Grosmark et al., 2012) across the transition from SWS to REM sleep. Thus, the high congruence in the occurrence of SWS in the hippocampus and cortex might play a fundamental role not only in coordinating their fire temporal coincidence, but also in coordinating the increase of the neuronal firing rate in hippocampus and cortex.

Moreover, we found differences in IS and REM sleep occurrences that appeared to reflect a disparate regulation of those sleep stages in hippocampus and cortex. We found that IS epochs mainly occurred in EEG recordings covering frontal cortical signal, and while the frontal cortex was in IS, the hippocampal showed already the presence of REM sleep. The synchronization of oscillations reflects the temporal precise interaction of brain areas (Fries, 2005). In line with this idea, the disparate regulation of IS and REM sleep

might provide a time window to break the communication between hippocampus and cortex. In this view, hippocampus is disconnected and the temporal coordination with cortex might vanish. Also, our data showed that when REM sleep occurs earlier in the hippocampus than neocortex, SWS-related activity still capturing neocortical networks, in the presence of REM-related theta activity in the EEG, at that time, probably represents volume-conducted hippocampal theta activity. These results suggest that hippocampus might also drive the entrance into REM sleep in cortex, in order to re-establish the dialog between both brain areas. The mechanisms that then, with some delay, make neocortical networks to ultimately synchronize to the hippocampal theta rhythm remain to be clarified. In sum, our data suggest that sleep and SWS is a global phenomenon with a simultaneous impact on different brain regions. However, this data also provides that the occurrence of REM sleep in many cases begins substantially earlier in hippocampal than neocortical networks. Moreover, the early occurrence of REM sleep suggest that hippocampus determine this sleep stage in the cortical networks and the direction of the communication between both brain areas.

5.2 Role of slow oscillations, spindles and ripples in the hippocampal-cortex communication

According to the two-stage model of memory consolidation, during SWS the memory traces in hippocampus migrate to neocortical sites for a long-lasting storage (Buzsáki, 1989). It has been proposed that the repeated reactivation of hippocampal memory representations is under top-down control of the cortical SO (Born et al., 2006; Marshall et al., 2006). The SO upstates are thought to facilitate the emergence of spindles (Steriade et al., 1993c), which modulate the ripples in the hippocampus (Diekelmann & Born, 2010; Staresina & Bergmann et al., 2015; Latchoumane & Ngo et al., 2016). In agreement with recent results (Swift et al., 2018) we found that spindle onsets were followed by an increase in hippocampal ripple activity (see publication A.2, Figure 5). This increase did not depend on whether or not the spindle co-occurred with a SO suggesting that, once a spindle is released, it dominates the regulation of hippocampal ripple activity. In addition, our results showed that the presence of SO associated with spindles modulated

the hippocampal ripples activity. Overall, the temporal pattern is consistent with the scenario where top-down SO sets the frame for a global time-window for hippocampal-cortical communication.

Interestingly, our data confirmed previous findings of a robust increase in spindle activity accompanying the early upstate of SOs in EEG recordings (Mölle et al., 2009, 2011; Nir et al., 2011), which supports the view that membrane depolarization of cortico-thalamic projections during the SO upstate are driving the generation of spindle activity in thalamic networks (Steriade et al.,1993a; 1993b). A coupling of spindles to SO upstates was not observed in hippocampal LFP recordings, which is likewise compatible with the notion that such coupling originates in cortico-thalamic feedback loops. SOs and spindles in hippocampal LFP recordings likely represent travelling waves that reach these networks via thalamic and cortical projections (Vertes et al., 2007; Wolansky et al., 2006; Varela et al., 2014). Indeed, the hippocampus itself is not capable of generating SOs (Isomura et al., 2006).

Our data also shows that hippocampal ripples are associated with the cortical SO upstates. In the EEG recordings this upstate-related increase was preceded by a decrease in ripple activity during the prior SO downstate. Ripple occurrence significantly increased also following the onset of spindles in the parietal EEG, and hippocampal ripples were preceded by increased spindle activity in all channels (publication A.2, Figure 5B). Moreover, hippocampal ripple power was increased during spindles regardless of whether the spindles co-occurred with an SO or not. On the other side, ripple activity was significantly higher when a spindle co-occurred with a SO than during an isolated SO. Altogether these observations suggest that the spindle is the primary regulator of hippocampal ripple activity even in the presence of an SO. The influence of the SO, appears to be mainly restricted to a downstate-related suppression of ripples, indicating that the downstates of these global SOs also effectively inactivate hippocampal circuitry (Behrens et al., 2005). The pathways of spindle effects on hippocampal ripple activity are unclear, but likely involve the nucleus reuniens of the thalamus (Vertes et al., 2006; Cassel et al., 2013).

In sum, we found an intricate relationship between SOs, spindles and ripples. This functional coupling may provide a mechanism for temporally fine-tuned communication between the hippocampus and neocortex during SWS.

5.3 Hippocampal ripples modulation of thalamic neurons

Simultaneous recording of thalamus and hippocampus showed that hippocampal ripples modulate thalamic neurons differentially. The hippocampal ripples exerted a transient inhibition in the fire rate of CB+ thalamic neurons. Previous studies indicated that ripples exerted extensive modulation over ample brain areas (Chrobak and Buzsáki, 1994; Csicsvari et al., 1999; Logothetis et al., 2012). Indeed, most of the cerebral cortex is selectively activated during the ripples, whereas thalamus and others subcortical territories were strongly and consistently inhibited (Logothetis et al., 2012; Yang et al., 2019). In addition, an evidence showed that ripples drove the spike timing relationship between hippocampal and cortical neurons (Wierzynski et al., 2009). These findings suggested that during SWS, synergistic thalamo-cortical activity may be orchestrating a privileged interaction state between hippocampus and cortex by differentially silencing the output of midline thalamic nuclei.

Spindle activity originates in the thalamus and propagates to cortical regions by thalamo-cortical projections (Steriade et al 1993a). Midline thalamus is intimately connected with hippocampus (Van der Werf et al., 2002). The neurons of the ventral part of the midline thalamus project specifically to hippocampus meanwhile hippocampus projects back to the whole midline thalamus (Canteras et al., 1992; Vertes et al., 2006; O'Mara et al., 2009). Thus, the neuronal activity in midline thalamus might modulates spindles activity appearance in the hippocampus. Moreover, according to our data (study II) spindle onsets precede systematically the appearance of ripples in hippocampus. Furthermore, ripples exert a feedback inhibition over a specific type of thalamic neurons. All together these data suggest a close loop between thalamus and hippocampus that might modulate the hippocampus and cortex dialog.

5.4 Future directions

This thesis contributes to the current understanding of the hippocampus and cortex communication during sleep. Moreover, we are able now to describe this communication in the dynamic of sleep stages, as well as, in the dynamic of the oscillations during SWS. Most importantly, after these studies, we will be able to open new questions and hopefully new directions for future research. Due to numerous studies which demonstrated that sleep improves memories (Smith, 2001; Marshall & Born, 2007), it would be important to demonstrate if hippocampal-cortex dissociation during REM sleep is necessary for the consolidation of memories. In addition, it would be important to determine the neuronal mechanism that allows the dissociation between hippocampus and cortex during the transition from SWS to REM sleep. Moreover, our data suggest that spindles modulate the appearance of ripples in hippocampus. Further experiments would explore with more details the thalamic contribution to the ripple generation in hippocampus, together with determining the neuronal mechanism that allows the coordination between spindles and ripples. Finally, according to system consolidation model, the spindles and ripples co-exist during the SWS and they are orchestrated by SOs (Rasch & Born, 2013). In a compelling agreement with this conjecture, our results showed that ripples were modulated by spindles in hippocampus, and these spindles were orchestrated by SO. It would be important that further experiments determine if the association between these oscillations during sleep can be influenced by previous learning. Moreover, and most important determine the causal role of a hippocampo-cortical dialog during SWS in memory consolidation.

6 List of publications and statement of contribution

1 “Sleep stage dynamics in neocortex and hippocampus”. Ernesto Durán, Carlos N Oyanedel, Niels Niethard, Marion Inostroza & Jan Born. Sleep, 2018.

E. Durán, CN Oyanedel, M. Inostroza and J. Born designed experiments. J. Born supervised the study. E. Durán, CN Oyanedel and N. Niethard analyzed the electrophysiological data and performed the statistical analysis. E. Durán performed the reconstruction of electrode positions. E. Durán and CN. Oyanedel prepared figures. E. Durán, CN Oyanedel and J. Born wrote the manuscript and revision inclusions of crucial comments given by N. Niethard and M. Inostroza.

2 “Temporal associations between sleep slow oscillations, spindles and ripples”. Carlos N Oyanedel, Ernesto Durán, Niels Niethard, Marion Inostroza & Jan Born. Submitted, 2020.

E. Durán, CN Oyanedel, M. Inostroza and J. Born designed experiments. J. Born supervised the study. E. Durán, CN Oyanedel and N. Niethard analyzed the electrophysiological data and performed the statistical analysis. E. Durán and CN. Oyanedel prepared the figures. E. Durán, CN Oyanedel and J. Born wrote the manuscript.

3 “Midline thalamic neurons are differentially engaged during hippocampus network oscillations”. Ariel Lara-Vásquez, Nelson Espinosa, Ernesto Durán, Marcelo Stockle & Pablo Fuentealba. Scientific Reports, 2016

P. Fuentealba designed experiments and supervised the study. A. Lara-Vásquez and E. Durán performed experiments and anatomical reconstructions. N. Espinosa and M. Stockle analyzed the electrophysiological data and performed the statistical analysis. A. Lara-Vásquez and P. Fuentealba prepared the figures. P. Fuentealba wrote the manuscript and revisions inclusions of crucial comments given by A. Lara-Vásquez, N. Espinosa and E. Durán

7 Acknowledgements

I sincerely thank Jan Born for giving me the opportunity to pursue my PhD studies in his lab. His support and scientific guidance have been immense to improve this work. I really appreciate his permanent optimism and constructive comments, even for negative results. I thank Pablo Fuentealba for giving me the option to complete part of my PhD in his lab. I sincerely appreciate his persistence in teaching me to be rigorous and precise in describing the scientific phenomenon. I thank Marion Inostroza for her collaboration with Pablo Fuentealba and for giving me the opportunity to be part of the animal group in the Institute for Medical Psychology and Behavioural Neurobiology, University Tübingen. I sincerely appreciate the effort and the contribution of Carlos Oyanedel in my research project. His help and friendship were invaluable from the beginning of my stay in Germany. I thank Niels Niethard for his contribution and comments on my work.

I sincerely appreciate the friends who were available in any time to share my happiness as well as my sad moments. I would like to express my gratitude towards all of them even those I have not mentioned. I must thank Ravit Kotikalapudi, Marius Nann and Joao Santiago for their sincere friendship. I will be indebted to them forever.

I deeply thank Maria Paz for being my partner. I appreciate her company and the happiness that she always shared with me. I sincerely thank her extraordinary patience and her immense love during these years. She gave me the strength to overcome some bad moments.

I sincerely thank my family for their unconditional love. Finally, and most important I deeply thank Dalia Rodríguez, my mother, the most important person in my life.

8 References

Ackermann, D., & Borbely, A. A. (1993). All-night dynamics of the human sleep EEG. *Journal of sleep research*, *2*(2), 70-81.

Ackermann, S., & Rasch, B. (2014). Differential effects of non-REM and REM sleep on memory consolidation?. *Current neurology and neuroscience reports*, 14(2), 430.

Andrillon, T., Nir, Y., Staba, R. J., Ferrarelli, F., Cirelli, C., Tononi, G., & Fried, I. (2011). Sleep spindles in humans: insights from intracranial EEG and unit recordings. *Journal of Neuroscience*, 31(49), 17821-17834.

Arai, R.Y., Jacobowitz, D. M., & Deura, S. (1994). Distribution of calretinin, calbindin-D28k, and parvalbumin in the rat thalamus. *Brain research bulletin*, 33(5), 595-614.

Behrens, C. J., van den Boom, L. P., de Hoz, L., Friedman, A., & Heinemann, U. (2005). Induction of sharp wave–ripple complexes in vitro and reorganization of hippocampal networks. *Nature neuroscience*, *8*(11), 1560.

Benington, J. H., & Heller, H. C. (1994). REM-sleep timing is controlled homeostatically by accumulation of REM-sleep propensity in non-REM sleep. *American Journal of Physiology-Regulatory, Integrative and Comparative Physiology*, *266*(6), R1992-R2000.

Berendse, H. W., and Groenewegen, H. J. (1991). Restricted cortical termination fields of the midline and intralaminar thalamic nuclei in the rat. Neuroscience 42, 73–102.

Born, J., Rasch, B., & Gais, S. (2006). Sleep to remember. *The Neuroscientist*, *12*(5), 410-424.

Bubser, M., & Deutch, A. Y. (1998). Thalamic paraventricular nucleus neurons collateralize to innervate the prefrontal cortex and nucleus accumbens. *Brain research*, *787*(2), 304-310.

Buzsaki, G., Horvath, Z., Urioste, R., Hetke, J., & Wise, K. (1992). High-frequency network oscillation in the hippocampus. *Science*, *256*(5059), 1025-1027.

Buzsáki, G. (1989). Two-stage model of memory trace formation: a role for "noisy" brain states. *Neuroscience*, 31(3), 551-570.

Buzsáki, G., & Vanderwolf, C. H. (1983). Cellular bases of hippocampal EEG in the behaving rat. *Brain Research Reviews*, *6*(2), 139-171.

Buzsáki, G. (2015). Hippocampal sharp wave-ripple: A cognitive biomarker for episodic memory and planning. *Hippocampus*, 25(10), 1073-1188.

Canteras, N. S., & Swanson, L. W. (1992). Projections of the ventral subiculum to the amygdala, septum, and hypothalamus: a PHAL anterograde tract-tracing study in the rat. *Journal of Comparative Neurology*, *324*(2), 180-194.

Cassel, J. C., De Vasconcelos, A. P., Loureiro, M., Cholvin, T., Dalrymple-Alford, J. C., & Vertes, R. P. (2013). The reuniens and rhomboid nuclei: neuroanatomy, electrophysiological characteristics and behavioral implications. *Progress in neurobiology*, *111*, 34-52.

Chauvette, S., Crochet, S., Volgushev, M., & Timofeev, I. (2011). Properties of slow oscillation during slow-wave sleep and anesthesia in cats. *Journal of Neuroscience*, *31*(42), 14998-15008.

Cholvin, T., Loureiro, M., Cassel, R., Cosquer, B., Geiger, K., Nogueira, D.D.S., Raingard, H., Robelin, L., Kelche, C., de Vasconcelos, A.P. and Cassel, J.C. (2013). The ventral midline thalamus contributes to strategy shifting in a memory task requiring both prefrontal cortical and hippocampal functions. *Journal of Neuroscience*, *33*(20), 8772-8783.

Chrobak, J. J., & Buzsáki, G. (1994). Selective activation of deep layer (V-VI) retrohippocampal cortical neurons during hippocampal sharp waves in the behaving rat. *Journal of Neuroscience*, *14*(10), 6160-6170.

Clemens, Z., Mölle, M., Erőss, L., Barsi, P., Halász, P., & Born, J. (2007). Temporal coupling of parahippocampal ripples, sleep spindles and slow oscillations in humans. *Brain*, *130*(11), 2868-2878.

Clemens, Z., Mölle, M., Erőss, L., Jakus, R., Rásonyi, G., Halász, P., & Born, J. (2011). Fine-tuned coupling between human parahippocampal ripples and sleep spindles. *European Journal of Neuroscience*, 33(3), 511-520.

Contreras, D., Destexhe, A., Sejnowski, T. J., & Steriade, M. (1997). Spatiotemporal patterns of spindle oscillations in cortex and thalamus. *Journal of Neuroscience*, *17*(3), 1179-1196.

Crunelli, V., & Hughes, S. W. (2010). The slow (< 1 Hz) rhythm of non-REM sleep: a dialogue between three cardinal oscillators. *Nature neuroscience*, *13*(1), 9.

Csicsvari, J., Hirase, H., Czurkó, A., Mamiya, A., & Buzsáki, G. (1999). Oscillatory coupling of hippocampal pyramidal cells and interneurons in the behaving rat. *Journal of Neuroscience*, *19*(1), 274-287.

De Gennaro, L., & Ferrara, M. (2003). Sleep spindles: an overview. *Sleep medicine reviews*, *7*(5), 423-440.

Diekelmann, S., & Born, J. (2010). The memory function of sleep. *Nature Reviews Neuroscience*, *11*(2), 114.

Fries, P. (2005). A mechanism for cognitive dynamics: neuronal communication through neuronal coherence. *Trends in cognitive sciences*, *9*(10), 474-480.

Gent, T. C., Bandarabadi, M., Herrera, C. G., & Adamantidis, A. R. (2018). Thalamic dual control of sleep and wakefulness. *Nature neuroscience*, *21*(7), 974.

Glin, L., Arnaud, C., Berracochea, D., Galey, D., Jaffard, R., & Gottesmann, C. (1991). The intermediate stage of sleep in mice. *Physiology & behavior*, *50*(5), 951-953.

Gottesmann, C., Gandolfo, G., & Zernicki, B. (1984). Intermediate stage of sleep in the cat. *Journal de physiologie*, *79*(5), 365-372.

Grosmark, A. D., Mizuseki, K., Pastalkova, E., Diba, K., & Buzsáki, G. (2012). REM sleep reorganizes hippocampal excitability. *Neuron*, *75*(6), 1001-1007.

Herrero, M. T., Barcia, C., & Navarro, J. (2002). Functional anatomy of thalamus and basal ganglia. *Child's Nervous System*, *18*(8), 386-404.

Huang, H., Ghosh, P., & van den Pol, A. N. (2006). Prefrontal cortex–projecting glutamatergic thalamic paraventricular nucleus-excited by hypocretin: a feedforward circuit that may enhance cognitive arousal. *Journal of Neurophysiology*, *95*(3), 1656-1668.

Isomura, Y., Sirota, A., Özen, S., Montgomery, S., Mizuseki, K., Henze, D. A., & Buzsáki, G. (2006). Integration and segregation of activity in entorhinal-hippocampal subregions by neocortical slow oscillations. *Neuron*, *52*(5), 871-882.

Jones, E. G. (2012). *The thalamus*. Springer Science & Business Media.

Killgore, W. D. (2010). Effects of sleep deprivation on cognition. In *Progress in brain research* (Vol. 185, pp. 105-129). Elsevier.

Kim, D., Hwang, E., Lee, M., Sung, H., & Choi, J. H. (2015). Characterization of topographically specific sleep spindles in mice. *Sleep*, 38(1), 85-96.

Krueger, J. M., Rector, D. M., Roy, S., Van Dongen, H. P., Belenky, G., & Panksepp, J. (2008). Sleep as a fundamental property of neuronal assemblies. *Nature Reviews Neuroscience*, *9*(12), 910.

Latchoumane, C. F. V., Ngo, H. V. V., Born, J., & Shin, H. S. (2017). Thalamic spindles promote memory formation during sleep through triple phase-locking of cortical, thalamic, and hippocampal rhythms. *Neuron*, *95*(2), 424-435.

Lesku, J. A., Roth II, T. C., Amlaner, C. J., & Lima, S. L. (2006). A phylogenetic analysis of sleep architecture in mammals: the integration of anatomy, physiology, and ecology. *The American Naturalist*, *168*(4), 441-453.

Logothetis, N.K., Eschenko, O., Murayama, Y., Augath, M., Steudel, T., Evrard, H.C., Besserve, M. and Oeltermann, A. (2012). Hippocampal–cortical interaction during periods of subcortical silence. *Nature*, *491*(7425), 547.

Loureiro, M., Cholvin, T., Lopez, J., Merienne, N., Latreche, A., Cosquer, B., Geiger, K., Kelche, C., Cassel, J.C. and de Vasconcelos, A.P., (2012). The ventral midline thalamus (reuniens and rhomboid nuclei) contributes to the persistence of spatial memory in rats. *Journal of Neuroscience*, *32*(29), 9947-9959.

Lüthi, A. (2014). Sleep spindles: where they come from, what they do. *The Neuroscientist*, *20*(3), 243-256.

Mahowald, M. W., & Schenck, C. H. (2005). Insights from studying human sleep disorders. *Nature*, 437(7063), 1279.

Maingret, N., Girardeau, G., Todorova, R., Goutierre, M., & Zugaro, M. (2016). Hippocampo-cortical coupling mediates memory consolidation during sleep. *Nature neuroscience*, 19(7), 959.

Marshall, L., Helgadóttir, H., Mölle, M., & Born, J. (2006). Boosting slow oscillations during sleep potentiates memory. *Nature*, 444(7119), 610.

Marshall, L., & Born, J. (2007). The contribution of sleep to hippocampus-dependent memory consolidation. *Trends in cognitive sciences*, 11(10), 442-450.

Massimini, M., Huber, R., Ferrarelli, F., Hill, S., & Tononi, G. (2004). The sleep slow oscillation as a traveling wave. *Journal of Neuroscience*, *24*(31), 6862-6870.

Moga, M. M., Weis, R. P., & Moore, R. Y. (1995). Efferent projections of the paraventricular thalamic nucleus in the rat. *Journal of Comparative Neurology*, *359*(2), 221-238.

Mölle, M., Bergmann, T. O., Marshall, L., & Born, J. (2011). Fast and slow spindles during the sleep slow oscillation: disparate coalescence and engagement in memory processing. *Sleep*, *34*(10), 1411-1421.

Mölle, M., Yeshenko, O., Marshall, L., Sara, S. J., & Born, J. (2006). Hippocampal Sharp Wave- Ripples Linked to Slow. *J Neurophysiol*, *96*, 62-70.

Mölle, M., Eschenko, O., Gais, S., Sara, S. J., & Born, J. (2009). The influence of learning on sleep slow oscillations and associated spindles and ripples in humans and rats. *European Journal of Neuroscience*, *29*(5), 1071-1081.

Nádasdy, Z., Hirase, H., Czurkó, A., Csicsvari, J., & Buzsáki, G. (1999). Replay and time compression of recurring spike sequences in the hippocampus. *Journal of Neuroscience*, *19*(21), 9497-9507.

Neckelmann, D., Olsen, Ø. E., Fagerland, S., & Ursin, R. (1994). The reliability and functional validity of visual and semiautomatic sleep/wake scoring in the Møll-Wistar rat. *Sleep*, *17*(2), 120-131.

Neske, G. T. (2016). The slow oscillation in cortical and thalamic networks: mechanisms and functions. *Frontiers in neural circuits*, *9*, 88.

Nir, Y., Staba, R. J., Andrillon, T., Vyazovskiy, V. V., Cirelli, C., Fried, I., & Tononi, G. (2011). Regional slow waves and spindles in human sleep. *Neuron*, *70*(1), 153-169.

Nobili, L., Ferrara, M., Moroni, F., De Gennaro, L., Russo, G.L., Campus, C., Cardinale, F. and De Carli, F. (2011). Dissociated wake-like and sleep-like electro-cortical activity during sleep. *Neuroimage*, *58*(2), 612-619.

O'mara, S. M., Sanchez-Vives, M. V., Brotons-Mas, J. R., & O'hare, E. (2009). Roles for the subiculum in spatial information processing, memory, motivation and the temporal control of behaviour. *Progress in Neuro-Psychopharmacology and Biological Psychiatry*, *33*(5), 782-790.

Otake, K., & Nakamura, Y. (1998). Single midline thalamic neurons projecting to both the ventral striatum and the prefrontal cortex in the rat. *Neuroscience*, *86*(2), 635-649.

Pignatelli, M., Beyeler, A., & Leinekugel, X. (2012). Neural circuits underlying the generation of theta oscillations. *Journal of Physiology-Paris*, *106*(3-4), 81-92.

Pinault, D. (1996). A novel single-cell staining procedure performed in vivo under electrophysiological control: morpho-functional features of juxtacellularly labeled thalamic cells and other central neurons with biocytin or Neurobiotin. *Journal of neuroscience methods*, *65*(2), 113-136.

Rasch, B., & Born, J. (2013). About sleep's role in memory. *Physiological reviews*, *93*(2), 681-766.

Rechtschaffen, A., & Bergmann, B. M. (1995). Sleep deprivation in the rat by the disk-over-water method. *Behavioural brain research*, *69*(1-2), 55-63.

Rechtschaffen, A. Kales, A. (1968). A manual for standardized terminology, techniques and scoring system for sleep stages in human subjects. *Brain information service/Brain Research Institute, University of California*.

Saalmann, Y. B. (2014). Intralaminar and medial thalamic influence on cortical synchrony, information transmission and cognition. *Frontiers in systems neuroscience*, *8*, 83.

Schnitzler, A., & Gross, J. (2005). Normal and pathological oscillatory communication in the brain. *Nature reviews neuroscience*, *6*(4), 285.

Sejnowski, T. J., & Destexhe, A. (2000). Why do we sleep? 1. *Brain research*, *886*(1-2), 208-223.

Siapas, A. G., & Wilson, M. A. (1998). Coordinated interactions between hippocampal ripples and cortical spindles during slow-wave sleep. *Neuron*, *21*(5), 1123-1128.

Siapas, A. G., Lubenov, E. V., & Wilson, M. A. (2005). Prefrontal phase locking to hippocampal theta oscillations. *Neuron*, *46*(1), 141-151.

Sirota, A., Csicsvari, J., Buhl, D., & Buzsáki, G. (2003). Communication between neocortex and hippocampus during sleep in rodents. *Proceedings of the National Academy of Sciences*, *100*(4), 2065-2069.

Smith, C. (2001). Sleep states and memory processes in humans: procedural versus declarative memory systems. *Sleep medicine reviews*, 5(6), 491-506.

Staresina, B.P., Bergmann, T.O., Bonnefond, M., Van Der Meij, R., Jensen, O., Deuker, L., Elger, C.E., Axmacher, N. and Fell, J. (2015). Hierarchical nesting of slow oscillations, spindles and ripples in the human hippocampus during sleep. *Nature neuroscience*, 18(11), 1679.

Steriade, M., Nunez, A., & Amzica, F. (1993a). A novel slow (< 1 Hz) oscillation of neocortical neurons in vivo: depolarizing and hyperpolarizing components. *Journal of neuroscience*, *13*(8), 3252-3265.

Steriade, M., Nuñez, A., & Amzica, F. (1993b). Intracellular analysis of relations between the slow (< 1 Hz) neocortical oscillation and other sleep rhythms of the electroencephalogram. *Journal of Neuroscience*, *13*(8), 3266-3283.

Steriade, M., McCormick, D. A., & Sejnowski, T. J. (1993c). Thalamocortical oscillations in the sleeping and aroused brain. *Science*, 262(5134), 679-685.

Sullivan, D., Mizuseki, K., Sorgi, A., & Buzsáki, G. (2014). Comparison of sleep spindles and theta oscillations in the hippocampus. *Journal of Neuroscience*, *34*(2), 662-674.

Swift, K. M., Gross, B. A., Frazer, M. A., Bauer, D. S., Clark, K. J., Vazey, E. M., & Poe, G. R. (2018). Abnormal Locus Coeruleus sleep activity alters sleep signatures of memory consolidation and impairs place cell stability and spatial memory. *Current Biology*, *28*(22), 3599-3609.

Tobler, I. (1995). Is sleep fundamentally different between mammalian species?. *Behavioural brain research*, *69*(1-2), 35-41.

Tsunematsu, T., Kilduff, T. S., Boyden, E. S., Takahashi, S., Tominaga, M., & Yamanaka, A. (2011). Acute optogenetic silencing of orexin/hypocretin neurons induces slow-wave sleep in mice. *Journal of Neuroscience*, *31*(29), 10529-10539.

Vandekerckhove, M., & Cluydts, R. (2010). The emotional brain and sleep: an intimate relationship. *Sleep medicine reviews*, *14*(4), 219-226.

Vertes, R. P. (2006). Interactions among the medial prefrontal cortex, hippocampus and midline thalamus in emotional and cognitive processing in the rat. *Neuroscience*, *142*(1), 1-20.

Vertes, R. P., Linley, S. B., & Hoover, W. B. (2015). Limbic circuitry of the midline thalamus. *Neuroscience & Biobehavioral Reviews*, *54*, 89-107.

Vyazovskiy, V. V., Olcese, U., Hanlon, E. C., Nir, Y., Cirelli, C., & Tononi, G. (2011). Local sleep in awake rats. *Nature*, *472*(7344), 443.

Vyazovskiy, V. V., Cui, N., Rodriguez, A. V., Funk, C., Cirelli, C., & Tononi, G. (2014). The dynamics of cortical neuronal activity in the first minutes after spontaneous awakening in rats and mice. *Sleep*, *37*(8), 1337-1347.

Van der Werf, Y. D., Witter, M. P., & Groenewegen, H. J. (2002). The intralaminar and midline nuclei of the thalamus. Anatomical and functional evidence for participation in processes of arousal and awareness. *Brain research reviews*, *39*(2-3), 107-140.

Wierzynski, C. M., Lubenov, E. V., Gu, M., & Siapas, A. G. (2009). State-dependent spike-timing relationships between hippocampal and prefrontal circuits during sleep. *Neuron*, *61*(4), 587-596.

Winsky, L., Montpied, P., Arai, R., Martin, B. M., & Jacobowitz, D. M. (1992). Calretinin distribution in the thalamus of the rat: immunohistochemical and in situ hybridization histochemical analyses. *Neuroscience*, *50*(1), 181-196.

Wilson, M. A., & McNaughton, B. L. (1994). Reactivation of hippocampal ensemble memories during sleep. *Science*, *265*(5172), 676-679.

Wolansky, T., Clement, E. A., Peters, S. R., Palczak, M. A., & Dickson, C. T. (2006). Hippocampal slow oscillation: a novel EEG state and its coordination with ongoing neocortical activity. *Journal of Neuroscience*, *26*(23), 6213-6229.

Xiao, D., Zikopoulos, B., & Barbas, H. (2009). Laminar and modular organization of prefrontal projections to multiple thalamic nuclei. *Neuroscience*, *161*(4), 1067-1081.

Yang, M., Logothetis, N. K., & Eschenko, O. (2019). Occurrence of hippocampal ripples is associated with activity suppression in the mediodorsal thalamic nucleus. *Journal of Neuroscience*, *39*(3), 434-444.

9 Appended publications

A.1 Sleep stage dynamic in neocortex and hippocampus

A.2 Temporal associations between sleep slow oscillations, spindles and ripples

A.3 Midline thalamic neurons are differentially engaged during hippocampus network oscillations

SLEEPJ, 2018, 1–11

doi: 10.1093/sleep/zsy060
Advance Access Publication Date: 16 April 2018
Original Article

ORIGINAL ARTICLE

Sleep stage dynamics in neocortex and hippocampus

Ernesto Durán[1,2,3,†], Carlos N. Oyanedel[1,2,†], Niels Niethard[1], Marion Inostroza[1,‡] and Jan Born[1,4,*,‡]

[1]Institute of Medical Psychology and Behavioral Neurobiology, University of Tübingen, Tübingen, Germany, [2]Graduate School of Neural and Behavioural Science, International Max Planck Research School, Tübingen, Germany, [3]Laboratorio de Circuitos Neuronales, Departamento de Psiquiatría, Centro Interdisciplinario de Neurociencias, Pontificia Universidad Católica de Chile, Santiago, Chile and [4]Center for Integrative Neuroscience, University of Tübingen, Tübingen, Germany

*Corresponding author. Jan Born, Institute of Medical Psychology and Behavioral Neurobiology, University of Tübingen, FIN-Building, Otfried-Müller-Strasse 25, 72076 Tübingen, Germany. Email: jan.born@uni-tuebingen.de.
†These authors contributed equally to this work.
‡Shared senior authorship

Abstract

Mammalian sleep comprises the stages of slow-wave sleep (SWS) and rapid eye movement (REM) sleep. Additionally, a transition state is often discriminated which in rodents is termed intermediate stage (IS). Although these sleep stages are thought of as unitary phenomena affecting the whole brain in a congruent fashion, recent findings have suggested that sleep stages can also appear locally restricted to specific networks and regions. Here, we compared in rats sleep stages and their transitions between neocortex and hippocampus. We simultaneously recorded the electroencephalogram (EEG) from skull electrodes over frontal and parietal cortex and the local field potential (LFP) from the medial prefrontal cortex and dorsal hippocampus. Results indicate a high congruence in the occurrence of sleep and SWS (>96.5%) at the different recording sites. Congruence was lower for REM sleep (>87%) and lowest for IS (<36.5%). Incongruences occurring at sleep stage transitions were most pronounced for REM sleep which in 36.6 per cent of all epochs started earlier in hippocampal LFP recordings than in the other recordings, with an average interval of 17.2 ± 1.1 s between REM onset in the hippocampal LFP and the parietal EEG ($p < 0.001$). Earlier REM onset in the hippocampus was paralleled by a decrease in muscle tone, another hallmark of REM sleep. These findings indicate a region-specific regulation of REM sleep which has clear implications not only for our understanding of the organization of sleep, but possibly also for the functions, e.g. in memory formation, that have been associated with REM sleep.

Statement of Significance

Sleep in mammals comprises the core sleep stages of slow-wave sleep (SWS) and rapid eye movement (REM) sleep which are thought of as unitary phenomena expressing themselves in a coherent way throughout the brain. We compared the occurrence of sleep and sleep stages in electroencephalogram recordings of cortical activity and local field potential recordings from prefrontal cortex and hippocampus. Although SWS congruently occurred in signals covering neocortical and hippocampal activity, REM sleep often started substantially earlier in the hippocampus than in neocortical networks. The findings indicate a region-specific regulation of REM sleep with implications for the functions commonly attributed to this stage.

Key words: slow-wave sleep; intermediate stage; REM sleep; prefrontal cortex; hippocampus; theta activity; muscle atonia

Submitted: 14 November, 2017; **Revised:** 15 February, 2018

Introduction

Classically, sleep and its composing sleep stages have been thought of as homogenous states that capture the whole organism, or at least the whole brain. Based on such concept, sleep was defined using behavioral criteria, such as physical quiescence and increased arousal thresholds. The most widely accepted approach to characterize sleep is polysomnography which includes the simultaneous recording of electroencephalographic (EEG) and electromyographic (EMG) recordings and, additionally in humans, electrooculographic recordings [1, 2]. These signals allow us to differentiate in mammals the two principal sleep stages of slow-wave sleep (SWS) and rapid eye movement (REM) sleep [3, 4]. Additionally, in rodents and cats, a transition state between SWS and REM sleep can be discriminated which is called intermediate stage (IS) [5–7]. Although all these sleep stages are considered as global phenomena, in recent years evidence has accumulated suggesting that sleep and sleep stages might not congruently take place in the whole brain, but can also locally occur restricted to specific networks and regions [8]. For example, in human neocortex, local activations were recorded while SWS was simultaneously present in other regions [9]. In mice, intrusions of sleep-like activity patterns were observed in local neocortical networks during prolonged wake periods and immediately after spontaneous awakening [10, 11]. In simultaneous scalp and intracranial recordings in human patients, most slow waves and spindles hallmarking the EEG during SWS were found to occur only in local neocortical networks [12].

The findings of these studies mostly examine activity within neocortical networks, underlining the local nature of phenomena defining sleep stages like spindles and slow waves. However, much less is known about the congruence in the occurrence of entire sleep stages between different brain structures. This is important, on the one hand, because the different sleep stages are often thought to fulfill specific functions. For example, "dual process theories" of memory formation during sleep assume that SWS supports consolidation of declarative memory, whereas REM sleep supports consolidation of procedural memory [13, 14]. On the other hand, the functions allocated to the different sleep stages are typically not established within only a single structure such as the neocortex, but rely on interactions between cortical and subcortical interactions. Thus, memory formation during SWS is assumed to involve the co-ordinate dialogue between neocortex and hippocampus [15, 16]. Indeed, consistent with a region-specific organization of sleep stages, intracranial recordings in human patients revealed that spindles occur in the hippocampus several minutes before sleep onset [17]. In a recent first systematic examination of sleep stages in the rat neocortex and hippocampus, both regions were found to concurrently be in different sleep stages nearly as often as they were in the same [18]. In light of the strong implications of these findings for the understanding of sleep and its functions, we here sought to confirm and extend those previous experiments. In rats, we recorded the EEG via skull electrodes over the frontal and parietal cortex and, additionally, local field potentials (LFPs) from medial prefrontal cortex (mPFC) and dorsal hippocampus (dHC). Our results reveal a high congruence in the occurrence of SWS at the different recording sites, which was decreased with regard to REM sleep. In many cases, the hippocampus appeared to enter REM sleep, together with a decrease in muscle tone, substantially earlier compared with the other recording sites.

Materials and Methods

Animals

The recordings were performed in five male Long Evans rats (Janvier, Le Genest-Saint-Isle, France, 280–340 g, 14–18 weeks old). Animals were kept on a 12 hr/12 hr light/dark cycle with lights off at 19:00 hr. Water and food were available ad libitum. All experimental procedures were approved by the University of Tübingen and the local institutions in charge of animal welfare (Regierungspräsidium Tübingen).

Surgery

Standard surgical procedures were followed as described previously [19]. Animals were anesthetized with an intraperitoneal injection of fentanyl (0.005 mg/kg of body weight), midazolam (2.0 mg/kg), and medetomidin (0.15 mg/kg). They were placed into a stereotaxic frame and were supplemented with isoflurane (0.5%) if necessary. The scalp was exposed and five holes were drilled into the skull. Three EEG screw electrodes were implanted: one frontal electrode (AP: +2.6 mm, ML: −1.5 mm, with reference to Bregma), one parietal electrode (AP: −2.0 mm, ML: −2.5 mm), and one occipital reference electrode (AP: −10.0 mm, ML: 0.0 mm). Additionally, two platinum electrodes were implanted to record LFP signals: one into the right mPFC (AP: +3.0 mm, ML: +0.5 mm, DV: −3.6 mm) and one into the right dHC (AP: −3.1 mm, ML: +3.0 mm, DV: −3.6 mm). Electrode positions were confirmed by histological analysis. One stainless steel wire electrode was implanted in the neck muscle for EMG recordings. Electrodes were connected to a six-channel electrode pedestal (PlasticsOne, USA) and fixed with cold polymerizing dental resin and the wound was sutured. Rats had at least 5 days for recovery.

Electrophysiological recordings

Rats were habituated to the recording box (dark grey PVC, 30 × 30 cm, 40 cm high) for 2 days, 12 hr per day, before actual recordings started. Experimental recordings were performed for 12 hr during the light phase, starting at 7:00 hr. The rat's behavior was simultaneously tracked using a video camera mounted on the recording box. EEG, LFP, and EMG signals were continuously recorded and digitalized using a CED Power 1401 converter and Spike2 software (Cambridge Electronic Design, UK). During the recordings, the electrodes were connected through a swiveling commutator to an amplifier (Model 15A54, Grass Technologies, USA). The screw electrode in the occipital skull served as reference for all EEG, LFP, and EMG recordings. Filtering was for the EEG between 0.1 and 300 Hz, for LFP signals a high-pass filter of 0.1 Hz was applied, and for the EMG between 30 and 300 Hz. Signals were sampled at 1 kHz.

Histology

After the last recording session, electrolytic lesions were made at the tip of the electrodes to verify their precise location (dHC and mPFC). Rats were deeply anesthetized with a lethal dose of fentanyl, midazolam, and medetomidin and intracardially perfused with saline (0.9%, wt/vol) followed by a 4 per cent

paraformaldehyde fixative solution. After extraction from the skull, brains were post-fixed in 4 per cent paraformaldehyde fixative solution for 1 day. Brains were then sliced into coronal sections (70 μm) and stained with 0.5 per cent toluidine blue (Figure 1).

Sleep stage characterization

The sleep stages (SWS, IS, and REM sleep) and wakefulness were determined offline for subsequent 10 s epochs through visual inspection. For classification of sleep stages, standard criteria were followed as described by Neckelmann et al. [2] and Bjorvatn et al. [20]. Accordingly, the wake stage was characterized by predominant low-amplitude fast activity associated with increased EMG tonus. SWS was characterized by predominant high-amplitude delta activity (<4.0 Hz) and reduced EMG activity, and REM sleep by predominant theta activity (5.0–10.0 Hz), phasic muscle twitches, and minimum EMG activity. IS was identified by a decrease in delta activity, a progressive increase of theta activity and the presence of sleep spindles (10–16 Hz). Sleep stage classification was independently performed for the frontal and parietal EEG signals and the mPFC and dHC LFP signals. Each single EEG and LFP record was independently classified (together with the associated EMG record) by two experienced experimenters (interscorer agreement > 89.9%). Consensus was achieved afterwards for epochs with discrepant classification. In addition to the classical scoring based on subsequent 10 s intervals, we rescored recordings using 2 s intervals, to examine dissociations of sleep stages at a finer temporal resolution. Analyses based on the scoring of 2 s intervals confirmed essential all results of the classical 10 s scoring and will not be reported here in detail.

Data analyses

Time spent asleep and in the different sleep stages, number of episodes, and average duration of an episode in each sleep stage was calculated for the whole 12 hr recording period. Also, for each sleep stage, the co-occurrence between any two recording sites was calculated by determining the percentage of 10 s epochs with co-occurrence of the specific sleep stage with the number of epochs with occurrence of this sleep stage in at least one of the recordings set to 100 per cent. This report is limited to the congruence between the frontal EEG signal which we used as reference (as it is most commonly used in rodent sleep research) and the three other recording sites.

To examine whether the timing of transitions into or out of specific sleep stages systematically differed between recording sites, we calculated average “delay times” for each recording site. For this purpose, the signal at the four recording sites was scanned, and whenever a transition into the sleep stage of interest occurred at one site, this time point was set to zero. Then, the transition delays for all the remaining channels were calculated based on the difference relative to this reference time point. For each recording site, the delay times to enter a specific sleep stage were averaged across all transitions into this sleep stage.

To characterize sleep stage transitions, power spectra were calculated based on MATLAB (Mathworks, USA) algorithms and the FieldTrip toolbox [21]. To this end, fast Fourier transformation (FFT) was applied to Hanning tapered blocks of 10,000 data points (corresponding to 10 s epochs), to calculate the single-sided amplitude spectrum within 0.1–25 Hz, before and after the onset of a sleep stage of interest. Power values were also used to generate time-frequency plots. Phase coherence between the dHC signal and the signal in each of the three other channels was calculated based on the frequency domain of each signal’s Fourier representation computed with FieldTrip (ft_freqanalysis).

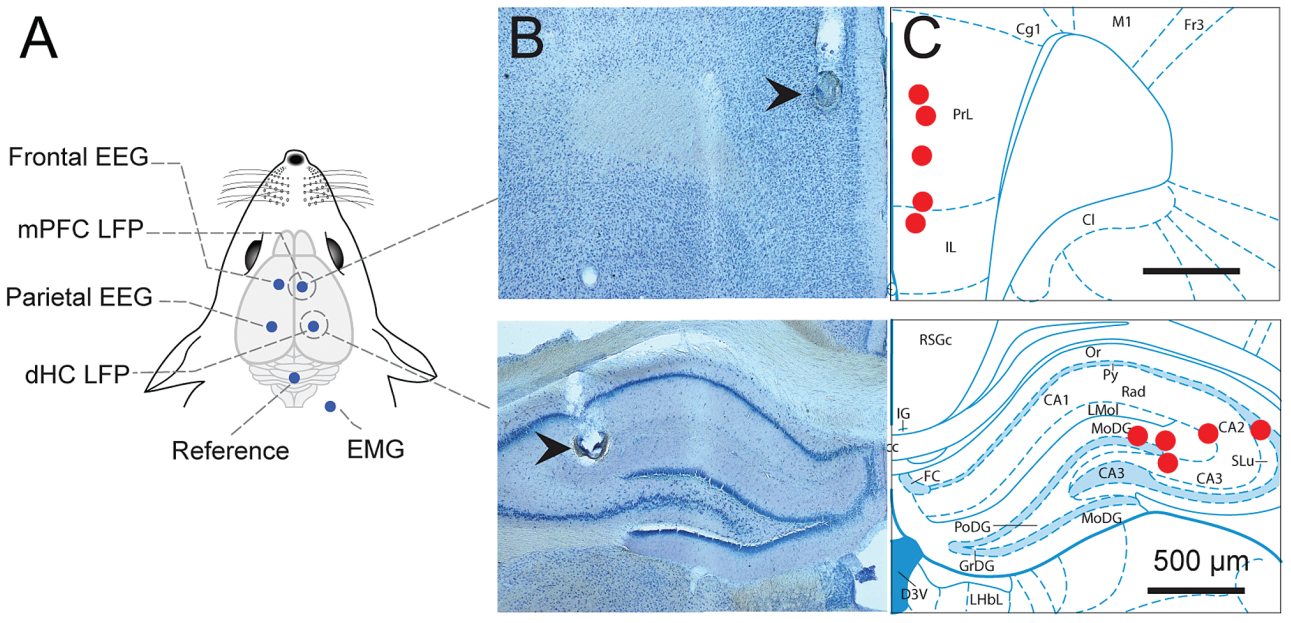

Figure 1. Electrode positions. (A) Schema of recordings. For EEG recordings, two skull electrodes were placed above the frontal and parietal lobe, respectively, of the left hemisphere; for LFP recordings, electrodes were inserted in the mPFC and dHC, respectively, in the right hemisphere. An EMG electrode was implanted into the neck muscle. The reference for EEG, LFP, and EMG recordings was a screw electrode placed above the occipital lobe. (B) Coronal histological sections showing electrode implantation sites (arrows) in the mPFC (left top) and dHC (left bottom). (C) Maps of electrode positions for mPFC (top) and dHC (bottom) LFP recordings (3.0 and −3.22 mm anteroposterior referenced to Bregma, respectively) across five animals. EEG = Electroencephalogram; LFP = Local field potential; EMG = Electromyogram; mPFC = Medial prefrontal cortex; dHC = Dorsal hippocampus.

To calculate EMG amplitude, the signal was root mean squared (rms), then filtered using a third-order low pass Butterworth filter of 0.2 Hz, and down-sampled to a rate of 100 Hz.

Statistical analyses

Kolmogorov–Smirnov test was used to assure normality of the distribution for each parameter. Differences in sleep stage classifications between recording sites were assessed using repeated measures analyses of variance (ANOVA) with a recording Site factor (frontal EEG, mPFC LFP, parietal EEG, dHC LFP) which was followed by post hoc paired sample *t*-tests, to specify significant differences between any two of the recording sites. For comparisons of mean power spectra, mean coherence, and mean EMG rms amplitude measures over time, nonparametric permutation tests were used with 2000 iterations [22]. A *p*-value of <0.05 was considered significant.

Results

Characterization of sleep stages from skull EEG and cortical and hippocampal LFP recordings

Sleep architecture was determined using the frontal EEG and EMG recordings. During the 12 hr recording period, the rats spent (mean ± SEM) 262.4 ± 14.0 min (corresponding to 36.3 ± 5.0% of the recording time) awake and 458.7 ± 13.8 min (63.7 ± 1.9%) asleep, with 364.1 ± 14.0 min (50.5 ± 5.0%) spent in SWS, 15.6 ± 2.1 min (2.2 ± 0.3%) in IS, and 79.0 ± 3.3 min (11.0 ± 0.5%) in REM sleep (Table 1). Figure 2A shows example recordings from the different recording sites for one animal. We took the frontal EEG signal as reference and determined the congruence (i.e. co-occurrence) of sleep stages between the frontal EEG and each of the three other recording sites (i.e. the parietal EEG and the LFP signals from mPFC and dHC). The congruence in wake and sleep stage occurrence during the total 12 hr period was high for time in wake (>92.0%) and SWS (>96.5%), somewhat lower for REM sleep (>87.0%), and distinctly lower for IS (<36.5%) where congruence was lowest for the mPFC LFP recordings (2.5 ± 1.6%, Figure 2B).

The time spent awake and in the different sleep stages for each of the recording sites was then subjected to ANOVA which revealed significant differences among the recording sites for time awake ($F(3, 12) = 4.02$, $p = 0.034$), time in IS ($F(3, 12) = 11.95$, $p = 0.001$), and in REM sleep ($F(3, 12) = 5.66$, $p = 0.012$), whereas time in SWS did not differ among recording sites ($F(3, 12) = 2.26$, $p = 0.134$; Figure 2C). Post hoc analyses of wake time indicated slightly longer wake times in mPFC than dHC LFP recordings ($t(4) = 2.91$, $p = 0.044$). Time in IS was longer in both frontal and parietal EEG signals compared with both mPFC and dHC LFP signals ($t \geq 5.8$, $p \leq 0.05$, for all comparisons, Figure 2C). IS was not detectable in mPFC recordings in three animals, and in dHC recordings in one animal. Time spent in REM sleep was longer in dHC than in mPFC LFP recordings, and also longer than in parietal EEG recordings ($t \geq 2.96$, $p \leq 0.041$, for all comparisons).

There were also distinct differences between the recording sites in the average duration of SWS periods ($F(2.81, 2930.4) = 60.2$, $p < 0.001$) and REM sleep periods ($F(3, 759) = 14.1$, $p < 0.001$, Figure 2D). SWS periods were generally longer in the EEG than LFP signals, and shortest in the mPFC LFP signal ($t \geq 13.3$, $p \leq 0.03$, for respective comparisons). REM sleep duration was also shortest in the mPFC signal ($t \geq 4.9$, $p \leq 0.001$, for all comparisons).

Table 1. Sleep architecture during the 12 hr recording period based on the frontal EEG recordings

Sleep architecture during the 12 hr recording				
Stage	Latency (min)	No. of episodes	Time in min	Time in %
Wake	0 ± 0	161.4 ± 15.1	262.4 ± 14.0	36.4 ± 5.0
SWS	34.7 ± 4.8	172.6 ± 15.0	364.1 ± 14.0	50.5 ± 5.0
IS	118.1 ± 18.6	49.8 ± 5.1	15.6 ± 2.1	2.2 ± 0.3
REM sleep	120.0 ± 17.0	47.8 ± 5.0	79.0 ± 3.3	11.0 ± 0.5

Latency is given with reference to start of the recording period. Average time spent in the different sleep stages is given in minutes and per cent of total 12 hr recording time. $n = 5$.
SWS = Slow-wave sleep; IS = Intermediate stage; REM = Rapid eye movement.

Wake–sleep transitions

Generally, the disparate appearance of sleep stages at the different recording sites concentrated on periods of transition between sleep stages. To examine whether the timing of wake-to-sleep transitions depended on the recording site, we analyzed in which of the four recording sites an ongoing wake epoch ended first (set to t = 0), and determined for each of the remaining recording sites the time interval it took to also finish the wake period and to enter sleep. The main result of this analysis was that the frontal EEG transited from wake into sleep significantly earlier than all other recording sites ($F(2.629, 1614.2) = 27.64$, $p < 0.001$, for ANOVA Site main effect, $t \geq 7.14$, $p \leq 0.001$ for respective pairwise comparisons, Figure 3A). However, although significant, the time differences were overall moderate (on average < 3.5 s) and below the 10 s resolution of visual sleep stage scoring. A corresponding analysis for sleep-to-wake transitions revealed that the frontal EEG was also the first to transit from sleep into wakefulness with this effect reaching significance for the comparisons with the mPFC LFP and parietal EEG signals ($F(3, 2022) = 9.09$, $p < 0.001$, for Site main effect, $t \geq 4.34$, $p \leq 0.001$, for pairwise comparisons).

Appearance of IS and REM sleep

IS episodes were overall rather short (0.31 ± 0.04 min) and most often identified in the frontal EEG recordings (Figure 2C). IS preceded REM sleep epochs in 71.9 ± 5.1% (frontal EEG), 3.45 ± 2.18% (mPFC LFP), 61.7 ± 7.5% (parietal EEG), and 18.6 ± 11.8% (dHC LFP) of all REM sleep epochs. We determined for the periods when the frontal EEG indicated IS, the occurrence of SWS and REM sleep at the other recording sites. During these periods (with the frontal EEG indicating IS), at the other recording sites, overall more SWS than REM sleep occurred, with no significant difference in SWS percentage among the recording sites ($p > 0.75$, for Site main effect, Figure 4B). On the other hand, the percentage of REM sleep during these periods was highest in the dHC recordings, and significantly higher when compared with the mPFC LFP and parietal EEG ($F(2, 8) = 10.20$, $p = 0.006$, for Site main effect, $t \geq 4.35$, $p \leq 0.012$ for respective pairwise comparisons).

To directly examine sleep stage dynamics at the transition into REM sleep, we identified REM sleep onsets in any of the four

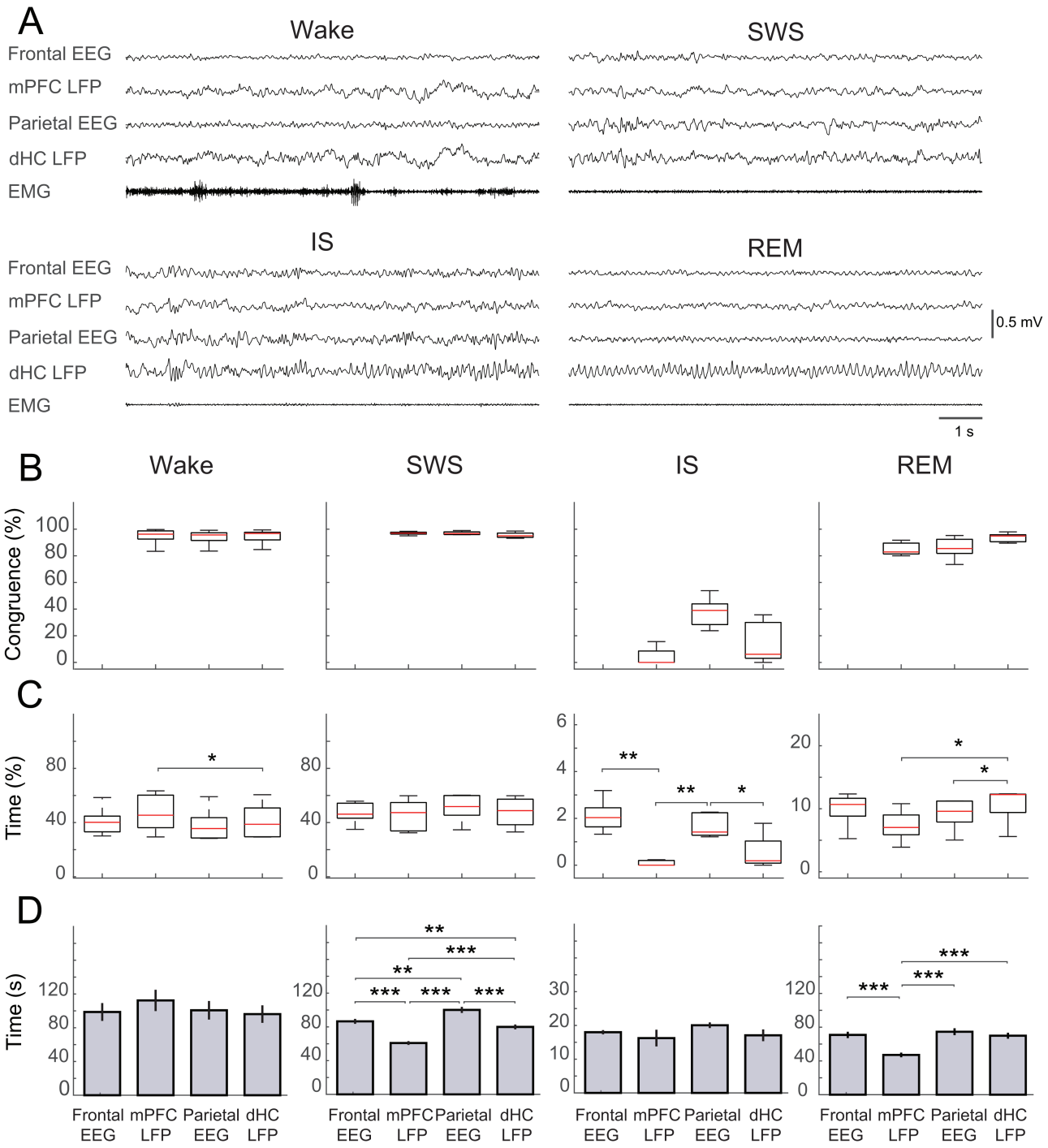

Figure 2. Sleep stage characterization in EEG and LFP recordings. (A) Examples of 10 s epoch recordings of (from top to bottom) frontal EEG, mPFC LFP, parietal EEG, and dHC LFP during wakefulness (top left), SWS (top right), IS (bottom left), and REM sleep (bottom right). (B) Comparison of sleep stage occurrence in the different recordings. Occurrence of sleep stages in mPFC LFP, parietal EEG, and dHC LFP signals is expressed as percentage of congruence with the occurrence of the sleep stages in the frontal EEG signal used as reference. (C) Distribution of time spent awake, in SWS, IS and REM sleep and (D) average duration of episodes awake, in SWS, IS, and REM sleep for the different recording sites. Box-whisker plots indicating median, upper quartile and lower quartile, top and bottom of the box, respectively. $^{*}p < 0.05$; $^{**}p < 0.01$; $^{***}p < 0.001$ for pairwise comparison. EEG = Electroencephalogram; LFP = Local field potential; EMG = Electromyogram; mPFC = Medial prefrontal cortex; dHC = Dorsal hippocampus; SWS = Slow-wave sleep; REM = Rapid eye movement; IS = Intermediate stage.

recording sites and assessed how long it took in the respective three other recording sites to enter REM sleep (Figure 3B). This analysis revealed that REM sleep started overall substantially earlier in the dHC recordings compared with all other recording sites, with the greatest difference between REM sleep occurrence in dHC and parietal EEG recordings where REM sleep occurred with an average delay of 17.2 ± 1.1 s (with reference to dHC REM onset; $F(2.53, 387.2) = 38.21$, $p < 0.001$, for ANOVA Site main effect, $t \geq 4.23$, $p \leq 0.001$, for all pairwise comparison with dHC recordings, see Supplementary Figure S2 for results from an analysis

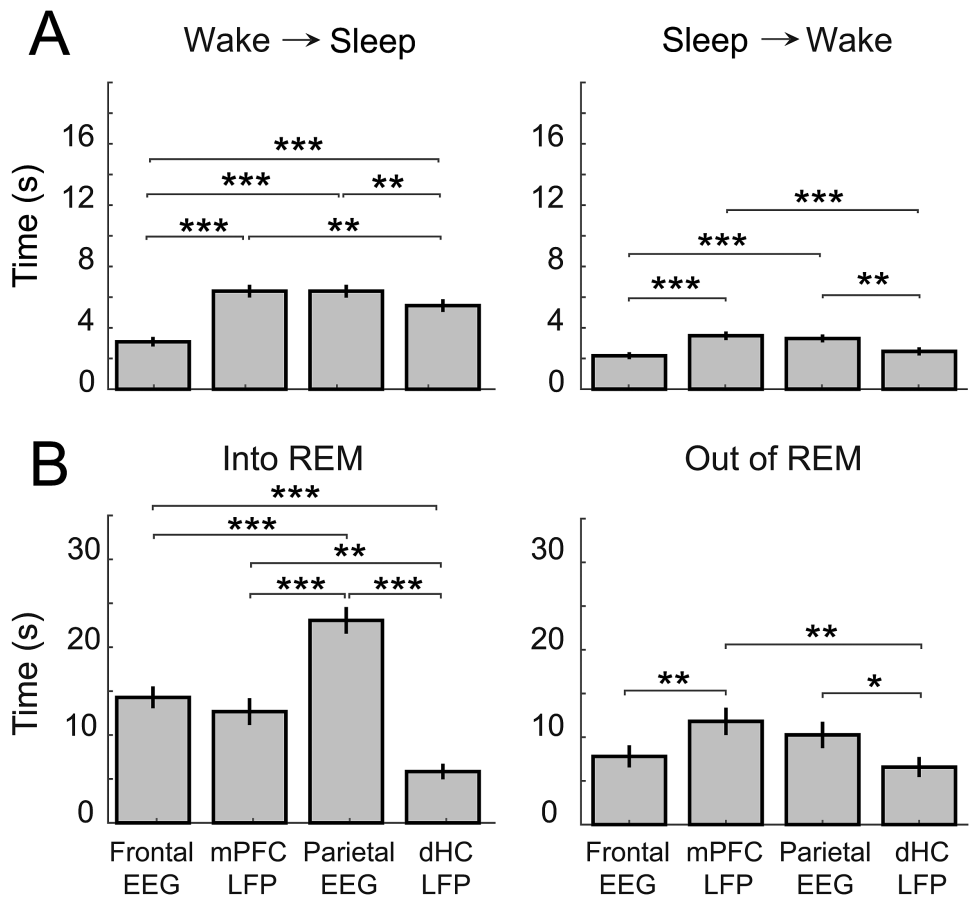

Figure 3. Transitions into and out of sleep and REM sleep. Timing of (A) wake-to-sleep (left) and sleep-to-wake transitions (right) and (B) of transitions into REM sleep (left) and out of REM sleep (right) at the different recording sites (frontal EEG, mPFC LFP, parietal EEG and dHC LFP). In these analyses, the earliest transitions into the specified brain state occurring at a certain recording site were set to 0 s and, then, the delay time was calculated till this transition occurred at each of the other recording sites. The y-axes indicate the mean (±SEM) delay time (across all detected transitions) for each recording site. Note, overall short delay times for wake-to-sleep transitions with the frontal EEG indicating first signs of sleep following a wake period. Note also that in dHC LFP recordings REM sleep is entered substantially earlier than at all other recording sites. $^{**}p < 0.05$; $^{**}p < 0.01$; $^{***}p < 0.001$ for pairwise comparisons. EEG = Electroencephalogram; LFP = Local field potential; mPFC = Medial prefrontal cortex; dHC = Dorsal hippocampus; REM = Rapid eye movement.

based on the more fine-grained scoring of 2 s epochs). In 36.6 per cent of all REM sleep episodes detected (53 cases of 145), REM sleep onset in dHC recordings preceded that at all other sites (whereas in only eight cases REM sleep started simultaneously at all sites) and in 16.5 per cent of all REM sleep episodes detected (24 cases of 145), REM sleep in the dHC LFP started later than in one of the other sites. In addition, REM sleep occurred significantly earlier (by on average 8.8 ± 1.3 s) in the frontal than in the parietal EEG ($t(153) = 6.81$, $p < 0.001$). A corresponding analysis of transitions out of REM sleep revealed that REM sleep, on average also ended earliest in dHC LFP recordings. Although the respective time difference was rather small (on average < 5 s), the effect reached significance in comparison with the mPFC LFP and parietal EEG signal ($F(2.74, 421.7) = 4.29$, $p = 0.007$, for Site main effect, $t \geq 2.05$, $p \leq 0.042$, for respective pairwise comparisons Figure 3B).

We further analyzed the sleep stages in the other recordings sites when REM sleep had started first in dHC recordings. The frontal EEG indicated IS during almost 80 per cent of this time, whereas the LFP from mPFC indicated SWS most of the time, and in the parietal EEG IS and SWS each covered about half of the time (see Figure 4C also for pairwise statistical comparisons). Finally, we examined the time course of the dissociation between REM sleep onset in cortical EEG and dHC LFP recordings across the 12 hr recording period (summarized in Supplementary Figure S1). These analyses revealed that the number of REM epochs increased across this period. However, the number of REM sleep epochs with an earlier onset in dHC LFP than cortical EEG recordings remained constant and, accordingly, the proportion of such epochs with an earlier onset in hippocampal LFP recordings decreased across this time ($H(2) = 6.36$, $p = 0.042$, for Kruskal–Wallis one-way ANOVA effect of time).

Theta activity and muscle atonia at early hippocampal REM sleep onsets

We further examined those transitions into REM sleep ($n = 53$) which occurred earlier in dHC LFP recordings than at the other recordings sites. For these cases, we calculated average power spectra for EEG and LFP signals, for 10 s intervals before and after REM sleep onset, respectively. Averaging was done either time-locked to REM onset as identified in the dHC LFP recordings or time-locked to REM onset as identified in each of the respective other three recording sites (Figure 5A–C). Comparing these two ways of time-locking revealed distinct differences for the frontal and parietal EEG, i.e. power was higher in a broad

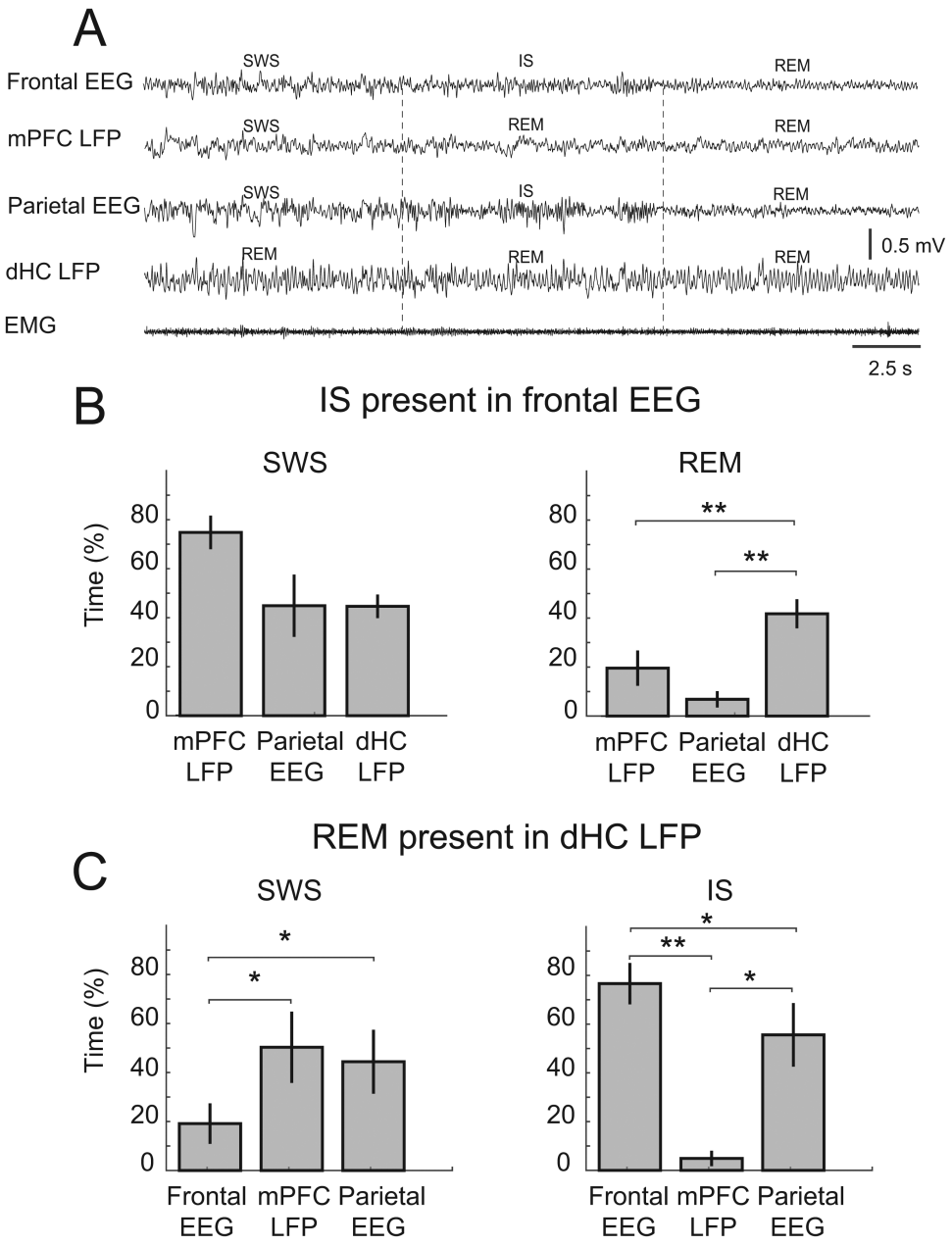

Figure 4. Appearance of REM sleep. (A) Example recordings of frontal EEG, mPFC LFP, parietal EEG, dHC LFP, and EMG signals over three consecutive 10 s intervals. Note, while REM sleep (as identified by high theta activity) is present in dHC LFP recordings already in the first 10 s interval, at the other sites consolidated REM sleep is reached not until the third 10 s interval. EMG activity decreases already during the first 10 s interval. (B) Percentages of SWS (left) and REM sleep (right) at the different recording sites, for intervals of IS in the frontal EEG. (C) Percentages of SWS (left) and IS (right) at the different recording sites, when REM sleep had started already in dHC LFP recordings. Means (±SEM) across all epochs are indicated. $^{*}p < 0.05$; $^{**}p < 0.01$ for pairwise comparison. EEG = Electroencephalogram; LFP = Local field potential; EMG = Electromyogram; mPFC = Medial prefrontal cortex; dHC = Dorsal hippocampus; SWS = Slow-wave sleep; REM = Rapid eye movement; IS = Intermediate stage.

frequency range including delta (1.0–4.0 Hz) and spindle (10–16 Hz) frequencies before and (though less consistently) also after the REM onsets when these REM onsets were determined in the respective EEG recordings in comparison to the spectra aligned to REM onset as defined in dHC LFP recordings. Notably this increase spared the 5.0–10.0 Hz theta band. Moreover, analyzing the coherence between recordings for cases where dHC LFP entered REM sleep first in the same way revealed a significantly reduced coherence in theta activity, particular between the dHC LFP and frontal EEG, when recordings were time-locked to the REM onset in the dHC recording (Figure 5D). Together these findings suggest that during the intervals of early local REM sleep in dHC recordings, there is also high theta activity in the cortical EEG activity that is synchronized to the hippocampal theta. However, the detection of REM sleep in the EEG signal is hampered by strong concurring SWS-related oscillatory activity.

For the cases where REM sleep onset in dHC recordings preceded REM onset in the three other recording sites, we also assessed the time course of muscle atonia as another hallmark of REM sleep. Generally, root mean square (rms) EMG activity, as expected, distinctly decreased from the 10 s interval before REM sleep onset to the 10 s interval after REM sleep onset. In the

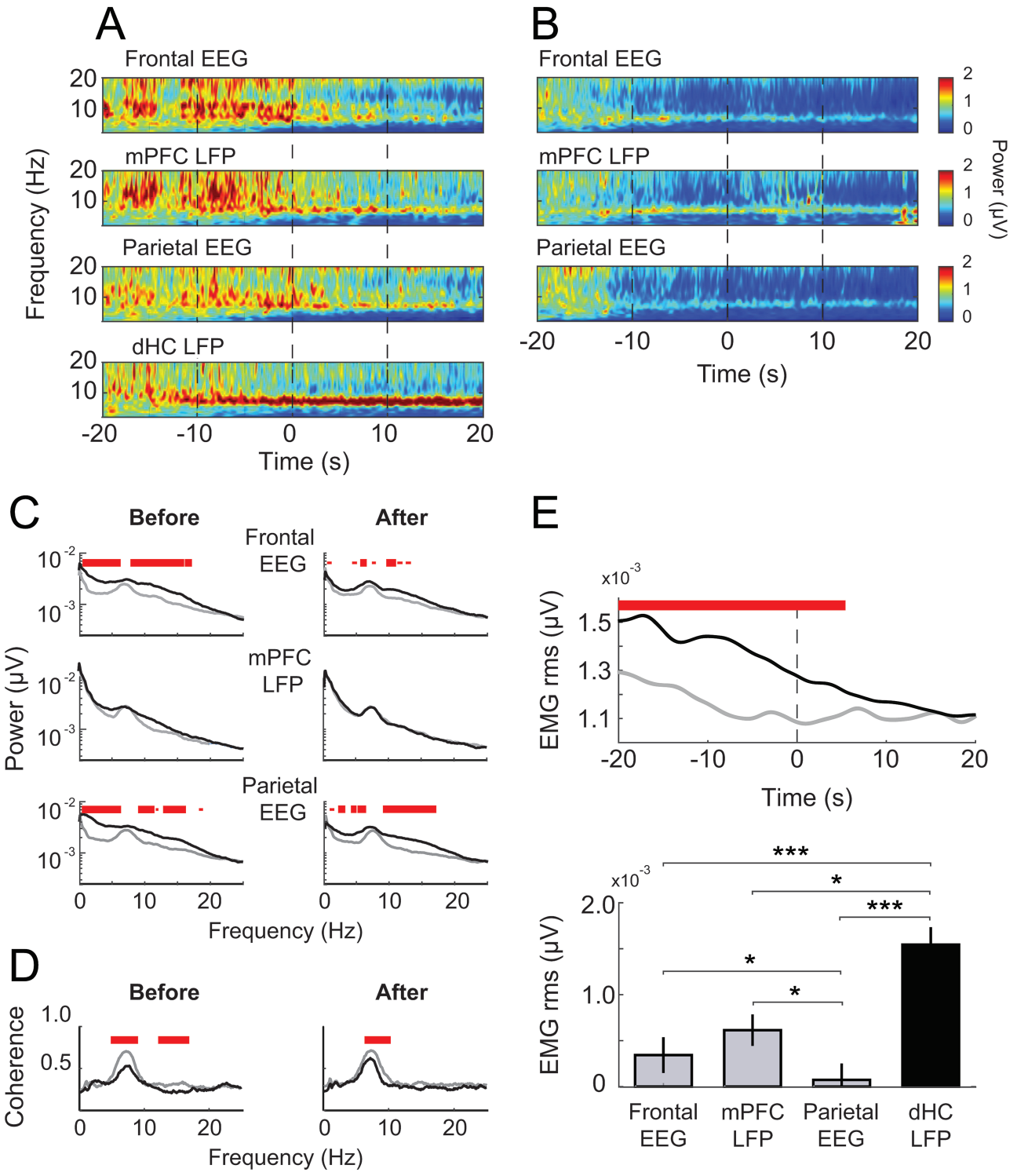

Figure 5. Early transitions into REM sleep at dHC LFP recordings. (A, B) Average time-frequency plots (power—color coded) in the different frequency bands for frontal EEG, mPFC LFP, parietal EEG, and dHC LFP signals, during a ±20 s interval around REM sleep onset ("0 s") for the cases when REM sleep started first in dHC LFP recordings ($n = 53$). Averages in (A) are time-locked to REM onset as identified in dHC LFP recordings, and in (B) to REM onset as identified in each of the other three recordings sites. (C) Power spectra for 10 s epochs before (left) and after (right) REM sleep onset for the cases when REM sleep started first in dHC LFP recordings, time-locked to REM onset as identified in dHC LFP recordings (black lines), and time-locked to REM onset as identified in each of the respective other three sites (frontal EEG, mPFC LFP, and parietal EEG; grey lines). (D) Coherence between the dHC LFP signal and the frontal EEG for 10-s epochs before (left) and after (right) REM sleep onset for the cases when REM sleep started first in dHC LFP recordings, time-locked to REM onset as identified in dHC LFP recordings (black line) and time-locked to REM onset as identified in the frontal EEG (grey). (E) Upper panel: Average EMG root mean square signal during a ±20 s interval around REM sleep onset ("0 s") for the cases when REM sleep started first in dHC LFP recordings ($n = 53$). Averages were either time-locked to the REM sleep onset as determined in dHC LFP recordings (black solid line) or to the REM sleep onset as determined in the parietal EEG (grey line). (C, D, and E) Significant differences in power, coherence, and EMG rms, respectively, are indicated by horizontal thin ($p < 0.05$) and thick ($p < 0.01$) red lines. Bar graph below shows mean differences in EMG rms activity between the 10 s intervals before minus after REM sleep onset for these cases, with REM sleep onset determined either in frontal EEG, mPFC LFP, parietal EEG, or dHC LFP recordings. Note, highest value, i.e. strongest decrease in EMG activity for defining REM sleep onset with reference to dHC LFP signal (black bar). $^{*}p < 0.05$; $^{***}p < 0.001$ for pairwise comparisons. EEG = Electroencephalogram; LFP = Local field potential; EMG = Electromyogram; mPFC = Medial prefrontal cortex; dHC = Dorsal hippocampus; rms = root mean square.

cases with an earlier REM sleep onset in dHC recordings, this decrease from before to after REM sleep onset was significantly higher when the rms EMG signal was time-locked to the onset as determined in the dHC recordings, compared with time-locking the signal to REM sleep onset as determined in any of the other recording sites ($F(2.2, 84) = 9.74$, $p < 0.001$, for Site main effect, $t \geq 6.6$, $p \leq 0.03$ for pairwise comparisons, Figure 5E). Thus, earlier REM onsets in dHC recordings were also accompanied by earlier muscle atonia. A complementary analysis on the cases where REM sleep occurred in dHC LFP recordings occurred later than at least one of the other three recording sites, did reveal hints that in these cases atonia is specifically coupled to REM occurrence in the hippocampal recording (Supplementary Figure S3).

Discussion

We compared in rats the expression of sleep stages in EEG recordings over frontal and parietal cortex and in LFP recordings from mPFC and dHC, and found distinct differences between cortical and hippocampal signals that mainly pertained to the timing of REM sleep. In dHC LFP recordings, REM sleep epochs in many cases started substantially earlier than at the other recording sites preferentially covering neocortical activity, which confirms recent findings by Emrick et al. [18]. The early start of REM sleep in hippocampal recordings, moreover, was accompanied by a REM sleep-typical decrease in muscle tone. We also found differences in the occurrence of SWS at the different recording sites. However, compared with those found for REM sleep, these were overall marginal. In fact, determination of SWS in neocortical and hippocampal signals was hallmarked by a very high congruence of greater than 95 per cent. Our findings underline that differences in the regional expression of sleep stages need to be considered when it comes to characterizing the function of sleep stages, especially of REM sleep.

The high congruence of SWS at the different recording sites with no differences in the time spent in SWS in neocortical and hippocampal signals suggests that SWS reflects a rather unitary phenomenon that catches widespread areas of the brain. Classification of SWS relies mainly on the occurrence of slow waves including the <1.0 Hz slow oscillation. These oscillations are generated in thalamo-cortical networks [23–26]. Beyond synchronizing activity in these regions, the oscillations are also known to synchronize activity in several other brain regions including the hippocampus, thereby allowing precisely timed interactions between these regions [19, 27–29]. However, despite the high congruence in the occurrence of SWS at the different sites, there were subtle differences. At a first glance, it appears surprising that in the mPFC LFP signal the mean duration of SWS epochs was on average slightly shorter than at the other sites, because the prefrontal cortex is thought to be a major source of slow waves [30]. However, an LFP recording from deep layers of the mPFC is expected to be most sensitive to and to pick up only locally generated slow potential changes, whereas the amplitude of slow wave potentials originating from other sites is comparatively low at this site. By contrast, skull EEG electrodes, although receiving an overall diminished potential, pick up slow-wave signals from rather broad cortical areas. Consistent with this explanation, we found that the prefrontal EEG signal was the first to indicate the occurrence of SWS. Again, it is to emphasize that these differences were marginal and appear to mainly reflect the different sensitivity of LFP and EEG recordings to the slow-wave signal.

Contrasting with the SWS-related findings, the observed differences in REM sleep occurrence appeared to reflect a disparate regulation of this sleep stage in neocortical and hippocampal networks, which were most obvious at the transition into this sleep stage. This was evident already in the analyses of IS which in rats is defined as a transition stage between SWS and REM sleep, mainly characterized by the simultaneous occurrence of spindle-like activity and theta activity. Apart from the fact that co-occurrence of IS at the different sites was quite low (<37%), we found that IS epochs mainly occurred in EEG recordings covering frontal cortical signal, and that while the frontal cortex was in IS, the hippocampal LFP signaled already the presence of REM sleep much more often than the other recording sites (Figure 4B). Conversely, during early REM sleep onsets in hippocampal LFP recordings, the frontal EEG signaled the presence of IS in almost 80 per cent of the cases (Figure 4C), altogether suggesting that the spread of hippocampal theta activity might contribute to classification of IS in the cortical signal. Indeed, due to its amalgamate nature and the resulting difficulties to determine this sleep stage, in many studies IS is not considered as a separate stage from SWS.

The view of a disparate regulation REM sleep in hippocampal and neocortical networks is corroborated by our finding that REM sleep onset in hippocampal LFP recordings on average substantially preceded REM onsets at the other recoding sites. This finding confirms and extends findings from a previous study [18], which overall reported an even stronger asynchrony in the occurrence of REM sleep comparing skull EEG recordings with dorsal hippocampal LFP recordings. Of note, in that study hippocampal LFP recordings were referenced to an electrode in neocortical deep white matter, which contrasts with the present recordings employing an occipital skull electrode. Although widely used in standard LFP recordings, such reference electrode might bias hippocampal LFP recordings due to EEG activity picked up from underlying cerebellum [31]. However, comparing our present dHC LFP recordings with those in other studies using different electrode montages did not reveal obvious alterations, e.g. with regard to the occurrence of spindles and theta activity. Also, theta activity (used as core signal for the determination of REM sleep) showed up in very much the same way when, for exploratory purposes, we re-referenced the dHC LFP signal to the medial prefrontal LFP electrode. Nevertheless, although a substantial bias seems unlikely, the precise contribution of cerebellar EEG activity during sleep to the dHC LFP signal using an occipital skull reference is presently unclear. It is hence the more important that the central findings of our study quite well agree with those of Emrick et al., despite their use of a rather different reference for LFP recordings. Note, our findings exclude an independent regulation of REM sleep in the hippocampus because in the hippocampus REM sleep much more often preceded that followed the occurrence of REM sleep in neocortex. The signal hallmarking REM sleep is 5.0–10.0 Hz theta activity which, however, also occurs during (active) wakefulness [32, 33]. Generation of the theta rhythm involves the medial septum along with the diagonal band of Broca which directly projects to the hippocampus, with the hippocampal network representing the major theta current generator [33, 34]. In this way, the first appearance of REM sleep in hippocampal networks and before the appearance in neocortex might partly be a consequence of

this direct innervation of the hippocampus from theta generating structures. However, the early appearance of REM sleep in hippocampal recordings, in our study, was also coupled to a distinct decrease in muscle tone (Figure 5E), another major feature of REM sleep, with this coupling pointing to the involvement of brainstem mechanisms in the disparate regulation of hippocampal REM sleep. The meso-pontine area of the brainstem, including *REM-off* and *REM-on* networks, has been proposed as a switch between REM sleep and SWS [35]. Different populations of the *REM-on* network project to the basal forebrain (including theta generating structures of the medial septum and diagonal band of Broca) and to medullary nuclei and the spinal cord where they contribute to establishing muscle atonia [35–37]. Thus, projections of these brainstem *REM-on* networks are likely capable of mediating a concurrent increase in hippocampal theta activity and muscle atonia.

Interestingly, in the cases where REM sleep occurred earlier in hippocampal networks, our spectral analyses of the EEG signal during this interval revealed enhanced power in wide frequency ranges including the 0.5–4.0 Hz slow wave activity and the 10–16 Hz spindle activity ranges characteristic for SWS, but sparing the 5.0–10.0 Hz theta range (Figure 5C). Notably, this increase spared the 5.0–10.0 Hz theta range reflecting that the EEG recordings at that time also expressed high theta activity which—as revealed by coherence analyses—appeared to be synchronized in phase with the hippocampal theta rhythm (Figure 5D). Thus, when REM sleep occurs earlier in the hippocampus than neocortex, this appears to be due to SWS-related activity still capturing neocortical networks, in the presence of REM-related theta activity that in the EEG, at that time, probably represents volume-conducted hippocampal activity [38, 39]. This conclusion is further supported by our analysis of the time course in dissociation of cortical and hippocampal REM sleep onset, indicating enhanced proportion of REM sleep epochs with earlier onset in hippocampal networks in the beginning of the recording (light) period when sleep and pressure were high. Thus, the expression of theta activity per se in the cortical EEG during this time of local hippocampal REM sleep appears not to be hindered by the simultaneous appearance of slow wave and spindle frequency activity [40]. The mechanisms that then, with some delay, make neocortical networks to ultimately synchronize to the hippocampal theta rhythm remain to be clarified.

In sum, our data are consistent with the concept that sleep and SWS for the most part present as global phenomena with a common impact on different brain regions. However, the occurrence of REM sleep underlies region-specific regulatory mechanisms, in as much this sleep stage in many cases begins substantially earlier in hippocampal than neocortical networks. Future studies need to characterize the mechanisms mediating this dissociation between hippocampal and neocortical networks, and the question to what extent this dissociation might become stronger with increased propensity of sleep and SWS. Whatever the case, the present findings might be also of relevance for the understanding of the functions (like memory formation) that have been associated with the stage of REM sleep and involve respective structures of interest [41, 42].

Supplementary Material

Supplementary material is available at *SLEEP* online.

Acknowledgments

We thank Dr. Hong-Viet Ngo and Ms. Ilona Sauter for help with data analyses and histology, respectively.

Funding

This work was supported by the Deutsche Forschungsgemeinschaft (TR-SFB 654 Plasticity and Sleep). E.D. was supported by a VRI Scholarship from the Pontificia Universidad Católica de Chile.

Notes

Conflict of interest statement. The authors declare that the research was conducted in the absence of any commercial or financial relationships that could be construed as a potential conflict of interest.

References

1. Rechtschaffen A, Kales A. *A Manual of Standardized Terminology, Techniques and Scoring System for Sleep Stages of Human Subjects*. Bethesda, MD: U. S. National Institute of Neurological Diseases and Blindness, Neurological Information Network; 1968.
2. Neckelmann D, *et al*. The reliability and functional validity of visual and semiautomatic sleep/wake scoring in the Møll-Wistar rat. *Sleep*. 1994;**17**(2):120–131.
3. Tobler I. Is sleep fundamentally different between mammalian species? *Behav Brain Res*. 1995;**69**(1-2):35–41.
4. Lesku JA, *et al*. A phylogenetic analysis of sleep architecture in mammals: the integration of anatomy, physiology, and ecology. *Am Nat*. 2006;**168**(4):441–453.
5. Gottesmann C, *et al*. Intermediate stage of sleep in the cat. *J Physiol (Paris)*. 1984;**79**(5):365–372.
6. Glin L, *et al*. The intermediate stage of sleep in mice. *Physiol Behav*. 1991;**50**(5):951–953.
7. Benington JH, *et al*. Scoring transitions to REM sleep in rats based on the EEG phenomena of pre-REM sleep: an improved analysis of sleep structure. *Sleep*. 1994;**17**(1):28–36.
8. Krueger JM, *et al*. Sleep as a fundamental property of neuronal assemblies. *Nat Rev Neurosci*. 2008;**9**(12):910–919.
9. Nobili L, *et al*. Dissociated wake-like and sleep-like electrocortical activity during sleep. *Neuroimage*. 2011;**58**(2):612–619.
10. Vyazovskiy VV, *et al*. Local sleep in awake rats. *Nature*. 2011;**472**(7344):443–447.
11. Vyazovskiy VV, *et al*. The dynamics of cortical neuronal activity in the first minutes after spontaneous awakening in rats and mice. *Sleep*. 2014;**37**(8):1337–1347.
12. Nir Y, *et al*. Regional slow waves and spindles in human sleep. *Neuron*. 2011;**70**(1):153–169.
13. Maquet P. The role of sleep in learning and memory. *Science*. 2001;**294**(5544):1048–1052.
14. Rasch B, *et al*. About sleep's role in memory. *Physiol Rev*. 2013;**93**(2):681–766.
15. Diekelmann S, *et al*. The memory function of sleep. *Nat Rev Neurosci*. 2010;**11**(2):114–126.
16. Watson BO, *et al*. Sleep, memory & brain rhythms. *Daedalus*. 2015;**144**(1):67–82.
17. Sarasso S, *et al*. Hippocampal sleep spindles preceding neocortical sleep onset in humans. *Neuroimage*. 2014;**86**:425–432.

18. Emrick JJ, *et al*. Different simultaneous sleep states in the hippocampus and neocortex. *Sleep*. 2016;**39**(12):2201–2209.
19. Mölle M, *et al*. Hippocampal sharp wave-ripples linked to slow oscillations in rat slow-wave sleep. *J Neurophysiol*. 2006;**96**(1):62–70.
20. Bjorvatn B, *et al*. EEG power densities (0.5-20 Hz) in different sleep-wake stages in rats. *Physiol Behav*. 1998;**63**(3):413–417.
21. Oostenveld R, *et al*. FieldTrip: open source software for advanced analysis of MEG, EEG, and invasive electrophysiological data. *Comput Intell Neurosci*. 2011;**2011**:156869.
22. Maris E, *et al*. Nonparametric statistical testing of EEG- and MEG-data. *J Neurosci Methods*. 2007;**164**(1):177–190.
23. Steriade M, *et al*. Thalamocortical oscillations in the sleeping and aroused brain. *Science*. 1993;**262**(5134):679–685.
24. Hughes SW, *et al*. Cellular mechanisms of the slow (<1 Hz) oscillation in thalamocortical neurons in vitro. *Neuron*. 2002;**33**(6):947–958.
25. Steriade M. Grouping of brain rhythms in corticothalamic systems. *Neuroscience*. 2006;**137**(4):1087–1106.
26. Crunelli V, *et al*. The slow (<1 Hz) rhythm of non-REM sleep: a dialogue between three cardinal oscillators. *Nat Neurosci*. 2010;**13**(1):9–17.
27. Siapas AG, *et al*. Coordinated interactions between hippocampal ripples and cortical spindles during slow-wave sleep. *Neuron*. 1998;**21**(5):1123–1128.
28. Wierzynski CM, *et al*. State-dependent spike-timing relationships between hippocampal and prefrontal circuits during sleep. *Neuron*. 2009;**61**(4):587–596.
29. Maingret N, *et al*. Hippocampo-cortical coupling mediates memory consolidation during sleep. *Nat Neurosci*. 2016;**19**(7):959–964.
30. Riedner BA, *et al*. Temporal dynamics of cortical sources underlying spontaneous and peripherally evoked slow waves. *Prog Brain Res*. 2011;**193**:201–218.
31. Canto CB, *et al*. The sleeping cerebellum. *Trends Neurosci*. 2017;**40**(5):309–323.
32. Bland BH. The physiology and pharmacology of hippocampal formation theta rhythms. *Prog Neurobiol*. 1986;**26**(1):1–54.
33. Buzsáki G. Theta oscillations in the hippocampus. *Neuron*. 2002;**33**(3):325–340.
34. Pignatelli M, *et al*. Neural circuits underlying the generation of theta oscillations. *J Physiol Paris*. 2012;**106**(3-4):81–92.
35. Lu J, *et al*. A putative flip-flop switch for control of REM sleep. *Nature*. 2006;**441**(7093):589–594.
36. Krenzer M, *et al*. Brainstem and spinal cord circuitry regulating REM sleep and muscle atonia. *PLoS One*. 2011;**6**(10):e24998.
37. Fraigne JJ, *et al*. REM sleep at its core – circuits, neurotransmitters, and pathophysiology. *Front Neurol*. 2015; **6**:1–9.
38. Scheffzük C, *et al*. Selective coupling between theta phase and neocortical fast gamma oscillations during REM-sleep in mice. *PLoS One*. 2011;**6**(12):e28489.
39. Scheffzük C, *et al*. Global slowing of network oscillations in mouse neocortex by diazepam. *Neuropharmacology*. 2013;**65**:123–133.
40. Lecci S, *et al*. Coordinated infraslow neural and cardiac oscillations mark fragility and offline periods in mammalian sleep. *Sci Adv*. 2017;**3**(2):e1602026.
41. Ribeiro S. Sleep and plasticity. *Pflugers Arch*. 2012;**463**(1):111–120.
42. Calais JB, *et al*. Experience-dependent upregulation of multiple plasticity factors in the hippocampus during early REM sleep. *Neurobiol Learn Mem*. 2015;**122**:19–27.

Temporal associations between sleep slow oscillations, spindles and ripples

Carlos N. Oyanedel[†1,2], Ernesto Durán[†1,2,3], Niels Niethard[1], Marion Inostroza[1], Jan Born[1,4*]

[1] Institute of Medical Psychology and Behavioral Neurobiology, University of Tübingen, 72076 Tübingen, Germany.

[2] Graduate School of Neural & Behavioural Science, International Max Planck Research School, 72074 Tübingen, Germany.

[3] Laboratorio de Circuitos Neuronales, Departamento de Psiquiatría, Centro Interdisciplinario de Neurociencias, Pontificia Universidad Católica de Chile, 8330024 Santiago de Chile, Chile.

[4] Centre for Integrative Neuroscience (CIN), University of Tübingen, 72076 Tübingen, Germany

† These authors contributed equally to this work

*** Corresponding author:** Jan Born. E-mail: jan.born@uni-tuebingen.de

Number of pages: 39

Number of figures: 8

Number of tables: 2

Number of supplementary figures: 7

Number of words: 10266 (whole manuscript); 242 (abstract)

Key words: rat, slow wave sleep, hippocampus, medial prefrontal cortex

Abstract

The systems consolidation of memory during slow wave-sleep (SWS) is thought to rely on a dialogue between hippocampus and neocortex that is regulated by an interaction between neocortical slow oscillations (SOs), thalamic spindles, and hippocampal ripples. Here, combining frontal and parietal surface EEG with local field potential (LFP) recordings in medial prefrontal cortex (mPFC) and dorsal hippocampus (dHC), we examined the temporal relationships between these oscillatory events in rats, to identify the possible direction of interaction between these events under natural conditions. Consistent with a top-down driving influence, EEG SO upstates are associated with an increase in spindles and hippocampal ripples. These associations were missing for SO upstates identified in mPFC LFP recordings. Ripples in dHC recordings always followed the onset of spindles consistent with spindles timing ripple occurrence. Moreover, comparing ripple activity during co-occurring SO-spindle events with that during isolated SOs or spindles, revealed that ripple dynamics during SO-spindle events are mainly determined by the spindle, with only the SO downstate providing a global inhibitory signal to both thalamus and hippocampus. As to bottom-up influences, we found an increase in hippocampal ripples ~200 ms before the SO downstate, but no similar increase preceding SO downstates for spindles. Overall, the temporal pattern is consistent with a loop-like scenario where, top-down, SOs can trigger thalamic spindles which, in turn, regulate in hippocampal networks the occurrence of ripples. Ripples, bottom-up, and independent from thalamic spindles, can contribute to the emergence of a neocortical SOs.

Introduction

Sleep has been identified as a state that supports the systems consolidation of hippocampal memory (Diekelmann & Born, 2010; Dudai et al. 2015; Sawangjit et al., 2018). In particular, during slow-wave sleep (SWS), the hippocampus and neocortex establish a dialog where the depolarizing upstates of the slow oscillations (SOs) coordinate the occurrence of thalamic spindles in synchrony with hippocampal ripples, the latter accompanying the reactivations of hippocampal memory representations during SWS (Rasch & Born, 2013; Watson & Buzsáki, 2015). Ripples nesting in spindle oscillations have been proposed as a mechanism promoting the hippocampo-to-neocortical transmission of reactivated memory information and the more gradual redistribution of representations towards neocortical networks (Siapas & Wilson, 1998, Sirota et al., 2003; Clemens et al., 2007, 2011; Staresina et al., 2015; Latchoumane et al. 2017). The SO (~1 Hz) is a global and synchronized cortical phenomenon that preferentially originates in prefrontal cortex, substantially involving subcortical structures like the thalamus (Steriade et al., 1993a; Hughes et al., 2002; Crunelli & Hughes, 2010; Neske, 2016), and typically travels towards posterior cortex, reaching also the hippocampus (Massimini et al., 2004; Staresina et al., 2015). The shorter downstate of the SO is associated with generalized hyperpolarization and reduced neuronal firing whereas the longer SO upstate goes along with synchronized membrane depolarization and increased neuronal firing, and also drives the generation of thalamic spindles (Steriade et al., 1993b; Destexhe et al., 1999; Neske, 2016; Niethard et al., 2018). Spindles (10–15 Hz), originating from GABAergic networks of the reticular thalamic nucleus, spread via thalamo-cortical fibers to the entire neocortex, but they also reach the hippocampus where they are phase-locking ripples (Steriade et al., 1993a; Kim et al., 2015; Clemens et al., 2007, 2011; Staresina et al., 2015). Ripples are high-frequency bursts (100 – 200 Hz) that occur in the CA1 subregion in conjunction with a

CA3-generated sharp wave, and typically accompany the reactivation of neuronal ensembles that are activated and used for encoding the representation during prior wake phases (Buzsaki et al., 1992; Khodagholy et al., 2017; Diba and Buzsaki, 2007).

Although there is a continuing controversy about the role SOs, spindles and ripples play in memory consolidation (e.g., Ackermann et al., 2015; Kim et al., 2019; Ngo and Born, 2019), a large body of evidence supports the view that these oscillatory events are involved in memory formation (summarized in Klinzing et al., 2019; Inostroza & Born, 2013). Indeed, several studies consistently revealed an association of memory formation with an increased co-occurrence of these oscillatory events, where ripples tend to nest in the excitable phases of the spindle, and such spindle-ripples events tend to nest into the upstate of the SO (Sirota et al., 2003; Mölle et al., 2006, 2009; Staresina et al., 2015; Maingret et al., 2016; Latchoumane et al., 2017; Helfrich et al., 2018). In light of the strong implications of these findings for memory processing during SWS, here we aimed at a characterization of the dialogue between neocortex and hippocampus during SWS in terms of SO, spindle, and ripple events, under natural conditions. Of special interest was the temporal relationship between these events - what comes first – which in connection with the spatial distribution of the events across the different brain regions allows to specify the direction of the interaction between these events. For this purpose, we recorded in rats EEG signals via skull electrodes over the frontal and parietal cortex and, local field potentials (LFPs) from medial prefrontal cortex (mPFC) and dorsal hippocampus (dHC). Our results are consistent with the view that top-down, the SO downstate provides a suppressive signal that synchronizes thalamic spindles and hippocampal ripples, whereas the SO upstate drives mainly thalamic spindles which, in turn, regulate hippocampal ripple occurrence. Hippocampal ripples might, bottom-up, contribute to the

occurrence of neocortical SO events. Differing from previous findings, we do not find, under natural conditions, hints for a contribution of spindles to the generation of SO events.

Materials and Methods

Animals

Five male Long Evans rats (Janvier, Le Genes-Saint-Isle, France, 280-340 g, 14-18 weeks old) were used. The rats were kept in temperature (22 ± 2 °C) and humidity (45 – 65 %) controlled cages, on a 12-h light/dark cycle with the lights off at 19:00 h. Water and food were available *ad libitum*. All experimental procedures were approved by the University of Tübingen and the local institutions in charge of animal welfare (Regierungspräsidium Tübingen, Germany). The animals had been used in a previous study (Duran et al., 2018).

Surgeries

Animals were anesthetized with an intraperitoneal injection of fentanyl (0.005 mg/kg of body weight), midazolam (2.0 mg/kg), and medetomidin (0.15 mg/kg). They were placed into a stereotaxic frame and were supplemented with isoflurane (0.5%) if necessary. The scalp was exposed and five holes were drilled into the skull. Three EEG screw electrodes were implanted: one frontal electrode (AP: +2.6 mm, ML: -1.5 mm, relative to Bregma), one parietal electrode (AP: -2.0 mm, ML: -2.5 mm, relative to Bregma), and one occipital reference electrode (AP: -10.0 mm, ML: 0.0 mm, relative to Bregma). Additionally, two platinum electrodes were implanted to record LFP signals (also referenced to the occipital skull electrode): one into the right medial prefrontal cortex (mPFC; AP: +3.0 mm, ML: +0.5 mm, DV: -3.6 mm), and one into the left dorsal hippocampus (dHC; AP: -3.1 mm, ML: +3.0 mm, DV: -3.6 mm). Electrode positions were

confirmed by histological analysis (supplementary Fig. 1). For EMG recordings, in all animals a stainless steel wire was implanted in the neck muscle. Electrodes were connected to a six-channel electrode pedestal (PlasticsOne, USA) and fixed with cold polymerizing dental resin, and the wound was sutured. Rats had at least 5 days for recovery.

Recordings

Rats were habituated to the recording box (dark grey PVC, 30 x 30 cm, height: 40 cm) for two days, twelve hours per day. On the third day, animals were recorded for twelve hours, during the light phase. The animal's behaviour was continuously tracked using a video camera mounted on the recording box. EEG, LFP and EMG signals were continuously recorded and digitalized using a CED Power 1401 converter and Spike2 software (Cambridge Electronic Design, Cambridge, UK). During the recordings, the electrodes were connected through a swiveling commutator to an amplifier (Model 15A54, Grass Technologies, USA). EEG signals were amplified and filtered between 0.1 – 300 Hz. LFP signals were amplified and filtered between 0.1 – 1000 Hz. EMG signals filtered between 30 – 300 Hz. The signals were sampled at 1 kHz.

Sleep stage determination

Sleep stages and wakefulness were determined off-line based on EEG and EMG recordings, using standard visual scoring procedures for consecutive 10-s epochs as previously described (Neckelmann et al., 1994; Durán et al., 2018; Table 1). Three sleep stages were discriminated: slow wave sleep (SWS), intermediate stage (IS) and REM sleep. Wakefulness was identified by mixed-frequency EEG and sustained EMG activity, SWS by the presence of high amplitude low activity (delta activity: < 4.0 Hz) and reduced EMG tone, REM sleep by low-amplitude EEG

activity with predominant theta activity (5.0 – 10.0 Hz), phasic muscle twitches and decrease of EMG tone. IS was identified by a decreased delta activity, progressive increase of theta activity and presence of sleep spindles. Recordings were scored by two experienced experimenters (interrater agreement >89.9 %). Afterward consensus was achieved for epochs with divergent scoring.

Event detections

To identify SOs, standard procedures were used as described in detail previously (Mölle et al. 2006; Sawangjit et al., 2018). In brief: EEG and LFP signals were filtered between 0.3 and 4.5 Hz, and an SO event was selected in the EEG if the following criteria were fulfilled: *(i)* two consecutive negative-to-positive zero crossings of the signal occurred at an interval between 0.4 and 2.0 s, *(ii)* of these events in an individual rat and channel, the 35% with the highest negative peak amplitude between both zero crossings were selected, and *(iii)* of these events the 45% with the highest negative-to-positive peak-to-peak amplitude were selected. Because in the LFP the SO shows up in opposite polarity, LFP signals were inverted (multiplied by -1) before applying the detection algorithm. The criteria resulted in the detection of SOs with downstate peak amplitudes exceeding -80 μV in the EEG and 110 μV in LFP recordings, and peak-to-peak amplitudes exceeding 120 μV in the EEG and 160 μV in LFP recordings.

Spindle detection was also based on procedures described previously (e.g. Mölle et al. 2009). The EEG signal was filtered between 10.0 and 16.0 Hz. Then, the envelope was extracted via the absolute value, i.e., the instantaneous amplitude, of the Hilbert transform on the filtered signal, followed by an additional smoothing (moving average with 200-ms window size). A spindle was identified when the absolute value of the transformed signal exceeded 1.5 standard

deviations (SD) of the mean signal in the respective channel, during the animal's SWS epochs, for at least 0.4 s and not more than 2.0 s. Spindle onset was defined by the time when the signal the first time exceeded the 1.5-SD threshold. The spindle power was calculated as the integral of the envelope of the Hilbert-transformed signal between spindle onset and end. For calculating Hilbert transformations the MATLAB function *Hilbert* was used. The envelope was extracted using the MATLAB function *abs*, which returns the absolute value (modulus), i.e., the "instantaneous amplitude" of the transformed signal.

Ripples were identified only in dorsal hippocampal (dHC) LFP recordings (as described in Mölle et al. 2009). The signal was filtered between 150.0 – 250.0 Hz. As for spindle detection, the Hilbert transform was calculated and the signal was smoothed using a moving average (window size 200 ms). A ripple event was identified when the Hilbert transform value exceeded a threshold of 2.5 SDs from the mean signal during an animal's SWS epochs, for at least 25 ms (including at least 3 cycles) and for not more than 500 ms.

Co-occurrence of events

For analyzing the temporal relationships between SOs, spindles, and ripples we calculated event correlation histograms, with one of the event types used as reference (e.g., SOs) and one of the respective other two event types (spindles or ripples) used as target event. For calculating event correlation histograms only epochs were considered in which a target event occurred within a ±1.5–s window around the reference event. Table 2 summarizes the proportion of reference events co-occurring (in this interval) with one of the respective target events, separately for the three types of events of interest (SOs, spindles, ripples). To analyze the occurrence of spindle and ripple events with reference to the SO, the respective target events were time-locked to the SO downstate peak

(t = 0 s) representing the most distinct and optimal time reference for scaling the SO cycle. The SO upstate peak is typically much flatter and more variable and has been proven to provide only a very imprecise reference for averaging and event time-locking (Mölle et al., 2002; Buszaki, 2006). For the analogous analyses with spindles and ripples as reference events, the spindle onset and the maximum trough of a ripple, respectively, were used for time-locking target events. Window sizes (around t = 0 s) was always 3 s (±1.5 s), and bin size was 100 ms. To calculate the event rate for SOs, the downstate peaks of all detected events were taken. For spindle and ripple activity, all detected spindle and ripple peaks and troughs were taken. (Exploratory analyses on spindles revealed basically identical results when counting one event per spindle). The counts in every bin were divided by the number of the reference events (used for time-locking one of the respective other two event types), and then divided by the bin width to give event rate per second (Hz).

Phase-locking analyses

Supplementing event correlation histograms, we calculated the "preferred cycle phase", for the temporal association of spindles and hippocampal ripples, respectively, with the SO, as well as for the temporal association of ripples with the spindle oscillation. For determining the temporal associations with the SO cycle, each detected SO associated with a spindle and ripple, respectively, was filtered between 0.3 and 4.5 Hz and the Hilbert transform was calculated. Then, the instantaneous phase of the SO at spindle onset and ripple maximum, respectively, was extracted. Correspondingly, for determining the temporal associations of ripples with the spindle cycle, each spindle that co-occurred with a ripple was first filtered between 10.0 and 16.0 Hz, then the Hilbert transform was calculated, and the instantaneous phase of the spindle at the time of a ripple was extracted. For calculating the average preferred phase, we used the function *CircHist* of the CircStat toolbox (Zittrell, 2009; Berens, 2009).

Power spectral analyses

In addition to event-based analyses, we calculated time-frequency plots of LFP power (in dHC recordings) to analyze the co-occurrence of SO-spindle events with ripples. For this purpose time-frequency analysis was performed per SO and spindle event. The function *mtmconvol* of the FieldTrip toolbox (Oostenveld et al., 2011) was used for frequencies from 150.0 to 250.0 Hz in steps of 1 Hz using a sliding Hanning tapered window with a variable, frequency-dependent length that always comprised ten cycles. Time-locked time-frequency analysis of all events were normalized by dividing the values with the average power during the baseline between -2.0 to -1.0 s before the event (using the FieldTrip function *ft_freqbaseline, baselinetype: 'relative'*), and then averaged across all events (using the FieldTrip function *ft_freqgrandaverage*).

Statistical analyses

Kolmogorov–Smirnov tests were used to assure normality of the distribution for each parameter. Differences in SOs and spindles among the different recording sites were assessed using repeated measures analyses of variance (ANOVA) with "recording site" as factor (frontal EEG, mPFC LFP, parietal EEG, dHC LFP), followed by *post hoc* paired sample *t*-tests, to specify significant differences between any two of the recording sites. For the evaluation of event correlation histograms each bin was compared to a baseline interval which was the 1-s interval form -2.0 s to -1.0 s prior to the reference event at 0 s. For LFP recordings, these analyses were restricted to a ±0.8-s interval around the reference event. Additionally, we tested the significance of the event correlation histograms against a randomized event distribution using procedures as described by Mölle et al. (2006). These analyses revealed essentially similar results and, hence, are not reported

here. For statistical evaluation of ripple-related power spectra, the normalized power values were averaged across the 150-250 Hz frequency band and for subsequent 100-ms bins of the event-locked time-frequency plot, and compared to baseline values (-2.0 to -1.0 s prior to the reference event) using paired-sample *t-tests.*

Histology

After the last recording session, rats were terminally anesthetized with fentanyl (0.01 mg/kg of body weight), midazolam (4.0 mg/kg), and medetomidin (0.3 mg/kg). The electrodes positions were marked by electrolytic lesion (10 µA, 30 s; supplementary Fig. 1). Rats were perfused with physiological saline (200 – 300 mL) followed by 4 % paraformaldehyde (PFA, 200 – 300 mL). After decapitation, the brains were removed and post-fixed in 4 % PFA for one day. Coronal sections of 60 µm were cut using a vibratome, stained with 0.5 % toluidine blue and examined under a light microscope.

Results

Event detection during SWS in the EEG, and cortical and hippocampal LFP

We analyzed brain oscillations during all SWS epochs recorded for each rat in a 12-hour session during the light phase. Supplementary Fig. 1 shows examples of parietal EEG and dHC LFP recordings during these SWS epochs for individual rats. The rats spent on average 364.1 min in SWS (Table 1). Table 2 summarizes occurrence (absolute numbers, densities) of SO, spindle, and ripple events and their co-occurrence in the different recording channels. SO density was highest in the parietal EEG and distinctly lower in the frontal EEG and dHC LFP ($F(3, 12) = 3.7$, $p = 0.043$, see Fig. 1 for pairwise comparisons). SO duration was shorter in LFP than EEG recordings, and shortest in the mPFC LFP ($F(3, 12) = 26.9$, $p < 0.001$). SO amplitude was higher in the parietal than frontal EEG and higher in the dHC than mPFC LFP ($F(3,12) = 7.0$, $p = 0.006$, Fig. 1).

The number of spindles identified ranged between 399.6 ± 109.2 in the frontal EEG and 176.2 ± 43.2 in the mPFC LFP (Table 2). Both spindle density and duration were higher in the frontal EEG than all other sites ($F(3,12) = 13.9$, $p < 0.001$ and $F(3,12) = 26.7$, $p < 0.001$, respectively, Fig. 2). Spindle power was lowest in mPFC and highest and most variable in dHC LFP recordings ($F(3,12) = 6.0$, $p < 0.009$). Spindle frequency was generally higher in EEG than LFP recordings ($F(3,12) = 19.6$, $p < 0.001$). In dHC LFP recordings, we detected 1498.6 ± 298.5 ripples with an average density of 10.5 ± 0.9 ripples per minute, duration of 101.4 ± 4.2 ms, and power of 1.1 ± 0.2 mV^2s^{-1}.

Temporal association between SOs and spindles

The percentage (of the total number) of SOs that co-occurred, in an interval ±1.5 s around the SO downstate peak, with a spindle was between 14.8 ± 1.1 % in the frontal EEG and 6.1 ± 0.3 % in

mPFC LFP recordings (Table 2). Event correlation histograms of spindle events time-locked to the SO downstate peak confirmed a clear relationship in both frontal and parietal EEG recordings such that spindle occurrence was diminished for a more or less extended interval around the SO downstate peak, and distinctly increased during the subsequent SO upstate, reaching a maximum ~500 ms after the SO downstate peak (see Fig. 3, also for statistical comparisons). The SO-upstate related increase in spindle occurrence was likewise demonstrated in phase-locking analyses (Fig. 3, right panels). Surprisingly, there was no distinct temporal association between SOs and spindles in the mPFC LFP (Fig. 3C), or dHC LFP (Fig. 3D). Extended analyses showed that mPFC SOs also did not modulate spindle occurrence in the other recordings, except for a slight increase in spindles in the parietal EEG during the SO upstate (supplementary Fig. 2).

A complementing pattern with an increase in the occurrence of SO downstates preceding spindle onset in the EEG, was revealed when, conversely, spindles were taken as reference of events correlation histograms for SO events. However, with the alignment to spindle onset the temporal relationships between SOs and spindles generally appeared to be more variable (supplementary Fig. 3). Additional exploratory analyses revealed overall similar relationships to the SO for slow spindles determined in the 7-10 Hz band.

Temporal association between SOs and ripples

The percentage of SOs co-occurring with hippocampal ripples was comparable for all channels: 39.3 ± 2.3 % in frontal EEG, 40.1 ± 2.5 % in parietal EEG, 36.7 ± 2.6 % in mPFC LFP, and 38.3 ± 2.6 % in dHC LFP recordings (Table 2). Event correlation histograms of ripple events, referenced to the SO downstate peak, indicated a suppression of hippocampal ripples around the downstate peak of SOs in the frontal and parietal EEG, followed by an increased ripple occurrence during

the SO upstate (Fig. 4A). These upstate-related increases in ripple occurrence were also revealed in phase-locking analyses of SO-ripple co-occurrence (Fig. 4A, right panels). The parallel downstate-related decrease and upstate-related increase in ripples in mPFC recordings did not reach significance. Instead, there was a slight but significant increase in ripples preceding (by ~400 ms) the SO downstate in mPFC recordings.

SOs identified in dHC recordings displayed a distinct dynamic of accompanying ripple activity (Fig. 4A). While showing the typical upstate-related increase in ripple events, hippocampal SOs were accompanied by a second increase in ripples that preceded the SO downstate peak and was even more pronounced than the upstate-related increase. This ripple increase preceding the SO did not reflect an upstate-related ripple increase of a foregoing SO, because a comparison of isolated SOs with SOs occurring in a train of several succeeding SOs revealed the ripple increase preceding the SO downstate to be even more distinct for SOs occurring in isolation (supplementary Fig. 4). Moreover, the number of SOs with ripples preceding and following the downstate was significantly lower than the number of SOs with either a preceding ripple or a following upstate-related ripple (supplementary Fig. 4B), indicating that the two types of ripples were independently occurring during the hippocampal SO cycle.

Event correlation histograms of SO events referenced to dHC ripples, confirmed that ripples were preceded by an increase in SO events as defined by the downstate peak, in the frontal and parietal EEG and dHC LFP, and there was also a suppression of such SO events in the EEG and mPFC LFP during an ongoing ripple (Fig. 4B). In addition, in these histograms, hippocampal ripples were followed, with a delay of 200-500 ms, by an increase in SO events in the frontal and parietal EEG consistent with a bottom-up influence of ripples on SO occurrence.

Temporal dynamic between spindles and ripples

The percentage of spindles co-occurring (±1.5-s around spindle onset) with hippocampal ripples averaged between 45.0 ± 4.0 % (mPFC LFP) and 51.7 ± 5.9 % (dHC LFP, Table 2). Conversely, the percentage of ripples in dHC co-occurring with spindles averaged between 7.2 ± 0.6 % (mPFC LFP) and 17.4 ± 2.6% (frontal EEG). Fig. 5A shows event correlation histograms for ripple events time-locked to (the onset of) spindles identified in the four different recordings. A distinct relationship was observed only for spindles in the parietal EEG such that here spindle onsets were followed, with a delay of ~300 ms, by an increased occurrence of ripples. There was a parallel increase in ripples for spindles in the dHC LFP which approached significance. No consistent patterns occurred in frontal EEG and mPFC LFP recordings. A supplementary phase-coupling analysis confirmed in 4 of the 5 rats significant spindle-ripple nesting such that the occurrence of ripples concentrated on the excitable phase of the spindle oscillation, particularly for spindles identified in dHC recordings (Staresina et al., 2015; Latchoumane et al., 2017). Histograms of spindle occurrence time-locked to ripples confirmed that ripples were preceded by an increase in spindle events starting 300-100 ms before, in all the recordings (Fig. 5B). The pattern is overall consistent with a driving influence of spindles on ripple occurrence in hippocampal networks.

Triple co-occurrence of slow oscillations, spindles and hippocampal ripples

We finally examined the co-occurrence of SOs with spindles *and* hippocampal ripples which has been proposed as a mechanism regulating information flow during the systems consolidation of memories (Latchoumane et al., 2017; Staresina et al., 2015). Spindles, in these analyses, were detected in dHC LFP recordings, because analyses accounting for spindles detected in other channels did not reveal channel specific differences in associated ripple activity, and because

evidence from foregoing studies suggested that coupling between spindles and hippocampal ripples is strongest for spindles detected in the hippocampus, in comparison with spindles identified in cortical LFP or EEG recordings (e.g., Clemens et al., 2011; Latchoumane et al., 2017). An event-based analysis indicated that the number of SO events co-occurring with spindle and ripple events was overall low, reaching a maximum of 3.6 ± 0.4 % in dHC recordings, and thus did not provide sufficient statistical power for a fine-grained analysis of temporal relationships. Given that the determination of the three kinds of events of interest was based on more or less arbitrary amplitude criteria, we therefore decided, with regard to hippocampal ripples, to shift the focus of analysis to the signal power in the respective 150-250 Hz frequency band.

In a first analysis focussing on the role of SOs, we compared average power spectra of the dHC LFP in a ±0.3-s interval around the maximum trough of the spindle (identified in the dHC), between spindles that did and did not co-occur with an SO event. With respect to SOs, analyses were performed collapsed across events identified in all four channels. The spectra indicated an increase in 150-250 Hz ripple power oscillating around the maximum trough of the spindle ($p < 0.01$) which did not differ between spindles occurring in isolation and spindles co-occurring with an SO (Fig. 6), suggesting that the presence of an SO does not substantially add to the spindle-related modulation of ripple power. Spindles co-occurring with SOs and isolated spindles did not differ in terms of duration, frequency or power (all $p > 0.1$).

In a second analysis concentrating on the role of spindles, we compared average power spectra of the dHC LFP in a ±0.8 s-interval around the SO downstate peak, between SOs that did and did not co-occur with a spindle (identified in the dHC LFP). Figure 7 summarizes results of this analysis (see supplementary Fig. 7 for an exploratory analysis where ripple activity was related to spindle activity in the respective channel of SO detection). The spectra indicated a suppression

of ripple power around the SO downstate peak that was most distinct for isolated SOs (Fig. 7). Importantly, ripple power was distinctly higher during SOs that co-occurred with spindles than during SOs occurring in isolation, with this difference being restricted ($p < 0.05$) to a 100-ms bin around the downstate peak in the analyses across all channels, as well as in a separate analysis of SOs identified in the dHC LFP (Fig. 7). SOs co-occurring with spindles and isolated SOs did not consistently differ in terms of amplitude and duration ($p > 0.1$). Together, these findings go beyond our event-based approach (above) in indicating that the spindle oscillation is the primary factor driving hippocampal ripple activity even in the presence of a SO upstate, whereas the direct hippocampal influence of the SO appears to be restricted to its suppression of ripple activity during the hyperpolarizing downstate.

Discussion

We examined the communication between neocortex and hippocampus as established during SWS in rats through the interaction of neocortical SOs, spindles, and hippocampal ripples. Combining concurrent LFP recordings from mPFC and dHC and EEG recordings from frontal and parietal sites we aimed at an integrative assessment of the oscillatory events of interest and their temporal relationships in natural conditions. As to top-down modulations, we found that SO downstates in the EEG are associated with a parallel decrease in spindles and hippocampal ripple activity whereas the SO upstate was associated with increases in spindle and ripple activity. Notably, this dynamic was not obtained in mPFC LFP recordings. Spindle onsets were followed by an increase in hippocampal ripple activity with, this increase not depending on whether or not the spindle co-occurred with a SO suggesting that, once a spindle is released and reaches the hippocampus, it dominates the regulation of hippocampal ripple activity. As to bottom-up influences, we found an

increase in hippocampal ripples preceding (~200 ms) the SO downstate, whereas no similar increase preceding SO downstates was found for spindles, which in combination suggests that ripples directly contribute to the occurrence of neocortical SOs. Overall, in comparison with foregoing studies, our approach revealed a more complete picture of the temporal relationships between the three oscillatory events of interest, i.e., a picture suggesting a loop-like scenario where top-down, the SO-downstate sets the frame for a global time-window for processing memory information (Fig. 8). In this window, the transition into the SO upstate drives thalamic spindles which, in turn, time the occurrence of ripples and associated replay of memory information in hippocampal networks. Bottom-up, ripples might contribute to the emergence of a neocortical SO.

By determining the precise temporal relationships we aimed to reveal hints about the direction of information flow between neocortex and hippocampus during memory processing in SWS. Focussing on the oscillatory configuration under natural conditions, we refrained from experimentally manipulating one of the oscillations. This approach comes with the price that our data do not allow for strictly causal inferences between the rhythms, although the identified temporal relationships allow to exclude certain causal interactions. Importantly, we here deliberately supplemented our LFP recordings by surface EEG recordings, in order to support the translation of our findings to the conditions in healthy humans only allowing for EEG recordings. Indeed, relevant electrophysiological results from rodent sleep studies are often ignored in human research simply because of the lack of precise knowledge about how an intracortical LFP event appears in the surface EEG recording. Generally, the comparison of EEG signals, e.g., over frontal cortex, with LFP signals from mPFC in the present study revealed that SOs and spindles as picked up in the EEG are not necessarily related to corresponding oscillations of the LFP in underlying cortex. Thus, LFP recordings reflect the much more localized generation of these oscillations,

particularly of spindles, which agrees with previous work (Adrillon et al., 2011; Nir et al., 2011; Ayoub et al., 2012). Indeed, also human studies revealed that many sleep spindles have an extremely small spatial extent and are thus picked up only by methods with extremely small receptive fields, like MEG and intracortical LFP recordings (Dehghani et al., 2010a, b, 2011a, b; Hagler et al., 2018; Ujma et al., 2019).

In keeping with the majority of studies in the field, we concentrated on an event-based analysis of SOs, spindles and ripples, with the numbers of events detected during SWS closely comparable to those in previous studies (Siapas and Wilson, 1998; Sirota et al., 2003; Mölle et al., 2006; Rasch & Born, 2013). Of note, whereas the proportion of spindles co-occurring with an SO was generally >65 %, conversely, the proportion of SOs co-occurring with a spindle was generally rather low (<15 %; Table 2) which may be taken to question the concept of a strong driving influence of SOs on the thalamic generation of spindles. However, spindle generating mechanisms undergo fast refractoriness which prevents that each SO can trigger a spindle event (Destexhe et al., 1998; Ngo et al., 2015). In addition, methodological factors play a role: The localized nature of spindle events might have prevented detection of events co-occurring with an SO and, also, events might have been missed due to too high detection criteria. In the case of spindles, the commonly used detection procedures have indeed been found to lack convergent validity and to differ in how they extract the EEG events contributing to spectral peaks (Ujma et al., 2015; Cox et al., 2017; Bódizs et al., 2009). Event detection criteria mainly based on amplitude-thresholds, are thus arbitrary to a certain extent and difficult to compare between event types like SOs and spindles. Implicating an all-or-none conceptualization of the event of interest, such event-detection approach may not sufficiently reflect that SO and spindle generation can capture and synchronize more or less extended networks resulting in LFP and EEG oscillations of smaller or greater

amplitude. Generally, for these reasons, it seems justified to supplement an event-based analysis by power spectral analyses, which we did here to examine the triple-co-occurrence of SOs, spindles and ripples.

Our EEG recordings confirmed previous findings of a robust increase in spindle activity accompanying the early upstate of SOs (Mölle et al., 2009, 2011; Nir et al., 2011) which supports the view that membrane depolarization of cortico-thalamic projections during the SO upstate are driving the generation of spindle activity in thalamic networks (Steriade et al., 1993a; 1993b). A clear coupling of spindles to SO upstates was not observed in hippocampal LFP recordings, which is likewise compatible with the notion that such coupling originates in cortico-thalamic feedback loops. SO and spindles in hippocampal LFP recordings likely represent travelling waves that reach these networks via thalamic and cortical projections (Vertes et al., 2007; Wolansky et al., 2006; Varela et al., 2014). The hippocampus itself is not capable of generating SOs (Isomura et al., 2006).

Interestingly, a coupling of spindles to SO upstates was also entirely absent in mPFC recordings. This finding might surprise at a first glance, as the majority of SOs arise from prefrontal cortical networks (Massimini et al., 2004). However, the observation well agrees with intracranial recordings in humans where such SO-spindle coupling was similarly weakened or even completely absent specifically in recordings from prefrontal regions (Andrillon et al., 2011). It might reflect anatomical conditions with only weak cortico-thalamic projections conveying frontal depolarization to thalamic spindle generators (Carman et al., 1964). SOs arising from medial prefrontal cortex may primarily propagate intracortically towards posterior areas, which is consistent with our observation that SO upstates in mPFC recordings were associated with an increased spindle activity in the parietal EEG.

Not only spindles but also hippocampal ripples nested into the SO upstates, with this upstate-related increase being preceded by a dip in ripple activity during the prior SO downstate. Ripple occurrence distinctly increased also following the onset of spindles in the parietal EEG and hippocampal LFP, and hippocampal ripples were preceded by increased spindle activity in all channels. Moreover, hippocampal ripple power was increased during spindles regardless of whether the spindles co-occurred with an SO or not. On the other side, ripple activity was significantly higher when a spindle identified in hippocampal recordings co-occurred with a SO than during an isolated SO. Altogether these observations suggest that spindles reaching the hippocampus are the primary regulator of ripple activity in these networks, even in the presence of an SO. The influence of the SO, in this constellation, appears to be mainly restricted to a downstate-related suppression of ripples, indicating that the downstates of these global SOs also effectively inactivate hippocampal circuitry (Behrens et al., 2005). Consistent with a spindle-mediated regulation of hippocampal ripples, mPFC recordings in which an SO upstate-related modulation of spindle activity was missing, did also not reveal any upstate-associated modulation of hippocampal ripple activity. Moreover, in a previous study, optogenetically induced spindles identified in hippocampal LFP recordings synchronized hippocampal ripple activity regardless of whether or not the spindle was induced during an SO upstate (Latchoumane et al., 2017). The pathways of hippocampal spindle effects on ripple activity are unclear, but likely involve the nucleus reuniens of the thalamus (Vertes et al., 2006; Cassel et al., 2013; Varela et al., 2014).

Our data also provide cues about possible bottom-up contributions of hippocampal ripples to neocortical SOs. Hippocampal ripples were consistently followed by an increased occurrence of SO downstates. This relationship was likewise evidenced when ripples were aligned to SO downstates in dHC recordings, and such increase in ripples also preceded the SO downstates

identified in mPFC recordings. These findings concur with previous studies suggesting that hippocampal ripples can directly prime the occurrence of cortical downstates by activating inhibitory cortical networks, especially in prefrontal cortex (Logothetis et al., 2012; Maingret et al., 2016; Xia et al., 2017). Interestingly, immediately during a hippocampal ripple the occurrence of cortical SO downstates was suppressed, suggesting a rebound mechanism that produces the increase in SOs with a delay of about 200 ms. Such mechanism would also be consistent with the fact that during the SO downstate, cortical inhibitory interneurons themselves are inactive (Niethard et al., 2018).

Surprisingly, we did not find clear hints at increases in spindle events that preceded increases in cortical SO events. In previous studies, the stimulation of thalamic spindle activity consistently induced neocortical SOs (Lewis et al., 2015; Latchoumane et al., 2017). In combination, these data suggest that thalamic spindles, in principle, can contribute to SO generation, although this rarely happens in natural "unstimulated" conditions as examined here. This conclusion fits with evidence that spindle-generating networks appear to go into refractoriness distinctly faster than SO-generating networks (Ngo et al., 2015; Antony et al., 2018). It highlights the importance to examine the oscillatory interactions of interest in natural conditions. In sum, the temporal relationships revealed here suggest the presence of a loop-like scenario with a top-down global inactivation of the loop during the SO downstate, followed by a spindle regulated increase in ripples (and associated memory processing) in hippocampal circuitry during the SO upstate (Fig. 8). Bottom-up, hippocampal ripple can trigger SOs and this influence appears to bypass spindle-generating thalamic networks.

Acknowledgments

We thank Dr. Hong-Viet Ngo and Ms. Ilona Sauter for help with data analysis and histology, respectively. This study was supported by a grant from the Deutsche Forschungsgemeinschaft (TR-SFB 654: Plasticity and Sleep). ED was supported by a VRI Scholarship from the Pontificia Universidad Católica de Chile.

Conflict of Interest Statement

The authors declare that the research was conducted in the absence of any commercial or financial relationships that could be construed as a potential conflict of interest.

Author Contribution

C.N.O., E.D., M.I. and J.B. planned and designed the experiments. C.N.O. and E.D. performed the experiments and performed the histology. C.N.O, E.D. and N.N. analysed the data. C.N.O., E.D., and J.B. wrote the manuscript. All authors approved the final version of the paper.

Data Accessibility Statement

The data that support the findings of this study are available from corresponding authors on reasonable request.

Abbreviations

ANOVA	analysis of variance
AP	anteroposterior
dHC	dorsal hippocampus

DV	dorsoventral
EEG	electroencephalography
EMG	electromyography
IS	intermediate stage
LFP	local field potential
ML	mediolateral
mPFC	medial prefrontal cortex
PFA	paraformaldehyde
REM	rapid-eye-movement
SD	standard deviations
SEM	standard error of the mean
SO	slow oscillation
SWS	slow wave sleep

References

Ackermann S, Hartmann F, Papassotiropoulos A, de Quervain DJ, Rasch B (2015) No associations between interindividual differences in sleep parameters and episodic memory consolidation. *Sleep* **38**, 951-959.

Andrillon T, Nir Y, Staba RJ, Ferrarelli F, Cirelli C, Tononi G, Fried I (2011) Sleep spindles in humans: insights from intracranial EEG and unit recordings. *J. Neurosci.* **31**, 17821-17834.

Antony JW, Piloto L, Wang M, Pacheco P, Norman KA, Paller KA (2018) Sleep spindle refractoriness segregates periods of memory reactivation. *Curr. Biol.* **28**, 1736-1743.

Ayoub A, Mölle M, Preissl H, Born J (2012) Grouping of MEG gamma oscillations by EEG sleep spindles. *Neuroimage* **59**, 1491-1500.

Behrens CJ, Van den Boom LP, De Hoz L, Friedman A, Heinemann U (2005) Induction of sharp wave–ripple complexes in vitro and reorganization of hippocampal networks. *Nat. Neurosci.* **8**, 1560-1567.

Bódizs R, Körmendi J, Rigó P, Lázár AS (2009) The individual adjustment method of sleep spindle analysis: Methodological improvements and roots in the fingerprint paradigm. *J. Neurosci. Methods* **178**, 205-213.

Berens P (2009) CircStat: A MATLAB Toolbox for Circular Statistics. *J. Stat. Softw.* **31**, doi: 10.18637/jss.v031.i10.

Buzsáki, G. (2006). Rhythms of the brain. New York: Oxford University Press.

Buzsaki G, Horvath Z, Urioste R, Hetke J, Wise K (1992) High-frequency network oscillation in the hippocampus. *Science* **256**, 1025-1027.

Carman JB, Cowan WM, Powell TPS (1964) Cortical connexions of the thalamic reticular nucleus. *J. Anat.* **98**, 587598.

Cassel JC, Pereira de Vasconcelos A, Loureiro M, Cholvin T, Dalrymple-Alford JC, Vertes RP (2013) The reuniens and rhomboid nuclei: neuroanatomy, electrophysiological characteristics and behavioral implications. *Prog. Neurobiol.* **111**, 34-52.

Clemens Z, Mölle M, Erőss L, Barsi P, Halász P, Born J (2007) Temporal coupling of parahippocampal ripples, sleep spindles and slow oscillations in humans. *Brain* **130**, 2868-2878.

Clemens Z, Mölle M, Erőss L, Jakus R, Rásonyi G, Halász P, Born J (2011) Fine-tuned coupling between human parahippocampal ripples and sleep spindles. *Eur. J. Neurosci.* **33**, 511-520.

Cox R, Schapiro AC, Manoach DS, Stickgold R (2017) Individual Differences in Frequency and Topography of Slow and Fast Sleep Spindles. *Front. Hum. Neurosci.* **11**, 433.

Crunelli V, Hughes SW (2010) The slow (<1 Hz) rhythm of non-REM sleep: a dialogue between three cardinal oscillators. *Nat. Neurosci.* **13**, 9-17.

Dehghani N, Cash SS, Chen CC, Hagler DJ Jr, Huang M, Dale AM, Halgren E (2010b) Divergent cortical generators of MEG and EEG during human sleep spindles suggested by distributed source modeling. *PLoS One* **5**, e11454.

Dehghani N, Cash SS, Halgren E (2011a) Emergence of synchronous EEG spindles from asynchronous MEG spindles. *Hum. Brain Mapp.* **32**, 2217-2227.

Dehghani N, Cash SS, Halgren E (2011b) Topographical frequency dynamics within EEG and MEG sleep spindles. *Clin. Neurophysiol.* **122**, 229-235.

Dehghani N, Cash SS, Rossetti AO, Chen CC, Halgren E (2010a) Magnetoencephalography demonstrates multiple asynchronous generators during human sleep spindles. *J. Neurophysiol.* **104**, 179-188.

Destexhe A, Contreras D, Steriade M (1999) Spatiotemporal analysis of local field potentials and unit discharges in cat cerebral cortex during natural wake and sleep states. *J. Neurosci.* **19**, 4595-4608.

Destexhe A, Contreras D, Steriade M (1998) Mechanisms underlying the synchronizing action of corticothalamic feedback through inhibition of thalamic relay cells. *J. Neurophysiol.* **79**, 999-1016.

Diba K, Buszáki G (2007) Forward and reverse hippocampal place-cell sequences during ripples. *Nat. Neurosci.* **10**, 1241-1242.

Diekelmann S, Born J (2010) The memory function of sleep. *Nat. Rev. Neurosci.* **11**, 114–126.

Dudai Y, Karni A, Born J (2015) The consolidation and transformation of memory. *Neuron* **88**, 20-32.

Durán E, Oyanedel CN, Niethard N, Inostroza M, Born J (2018) Sleep stage dynamics in neocortex and hippocampus. *Sleep* **41**, zsy060.

Hagler DJ Jr, Ulbert I, Wittner L, Erőss L, Madsen JR, Devinsky O, Doyle W, Fabo D, Cash SS, Halgren E (2018) Heterogeneous origins of human sleep spindles in different cortical layers. *J. Neurosci.* **38**, 3013-3025.

Helfrich F, Mander, BA, Jagust WJ, Knight RT, Walker MP (2018) Old brains come uncoupled in sleep: Slow wave-spindle synchrony, brain atrophy, and forgetting. *Neuron* **97**, 221-230.

Hughes SW, Cope DW, Blethyn KL, Crunelli V (2002) Cellular mechanisms of the slow (< 1 Hz) oscillation in thalamocortical neurons in vitro. *Neuron* **33**, 947-958.

Isomura Y, Sirota A, Özen S, Montgomery S, Mizuseki K, Henze DA, Buzsáki G (2006) Integration and segregation of activity in entorhinal-hippocampal subregions by neocortical slow oscillations. *Neuron* **52**, 871-882.

Khodagholy D, Gelinas JN, Buzsáki G (2017) Learning-enhanced coupling between ripple oscillations in association cortices and hippocampus. *Science* **358**, 369-372.

Kim D, Hwang E, Lee M, Sung H, Choi JH (2015) Characterization of topographically specific sleep spindles in mice. *Sleep* **38**, 85-96.

Kim J, Gulati T, Ganguly K (2019) Vompeting roles of slow oscillations and delta waves in memory consolidation versus forgetting. *Cell* **179**, 514-526.

Latchoumane CF, Ngo HV, Born J, Shin HS (2017) Thalamic spindles promote memory formation during sleep through triple phase-locking of cortical, thalamic, and hippocampal rhythms. *Neuron* **95**, 424-435.

Lewis LD, Voigts J, Flores FJ, Schmitt LI, Wilson MA, Halassa MM, Brown EN (2015) Thalamic reticular nucleus induces fast and local modulation of arousal state. *Elife* **4**, e08760.

Logothetis NK, Eschenko O, Murayama Y, Augath M, Steudel T, Evrard HC, Besserve M, Oeltermann A (2012) Hippocampal-cortical interaction during periods of subcortical silence. *Nature* **491**, 547-553.

Maingret N, Girardeau G, Todorova R, Goutierre M, Zugaro M (2016) Hippocampo-cortical coupling mediates memory consolidation during sleep. *Nature Neurosci.* **19**, 959-964.

Massimini M, Huber R, Ferrarelli F, Hill S, Tononi G (2004) The sleep slow oscillation as a traveling wave. *J. Neurosci.* **24**, 6862-6870.

Mölle M, Bergmann TO, Marshall L, Born J (2011) Fast and slow spindles during the sleep slow oscillation: disparate coalescence and engagement in memory processing. *Sleep* **34**, 1411-1421.

Mölle M, Eschenko O, Gais S, Sara SJ, Born J (2009) The influence of learning on sleep slow oscillations and associated spindles and ripples in humans and rats. *Eur. J. Neurosci.* **29**, 1071-1081.

Mölle M, Marshall L, Gais S, Born J (2002) Grouping of spindle activity during slow oscillations in human non-rapid eye movement sleep. *J. Neurosci.* **22**, 10941-10947.

Mölle M, Yeshenko O, Marshall L, Sara SJ, Born J (2006) Hippocampal sharp wave-ripples linked to slow oscillations in rat slow-wave sleep. *J. Neurophysiol.* **96**, 62-70.

Neckelmann D, Olsen OE, Fagerland S, Ursin R (1994) The reliability and functional validity and semiautomatic sleep/wake scoring in the Moll-Wister rat. *Sleep* **17**, 120-131.

Neske GT (2016) The slow oscillation in cortical and thalamic networks: mechanisms and functions. *Front. Neural Circuits* **9**, 88.

Ngo HVV, Born J (2019) Sleep and the balance between memory and forgetting. *Cell* **179**, 289-291.

Ngo HVV, Miedema A, Faude I, Martinetz T, Mölle M, Born J (2015) Driving sleep slow oscillations by auditory closed-loop stimulation-a self-limiting process. *J. Neurosci.* **35**, 6630-6638.

Niethard N, Ngo HV, Ehrlich I, Born J (2018) Cortical circuit activity underlying sleep slow oscillations and spindles. *Proc. Natl. Acad. Sci. U. S. A.* **115**, E9220-E9229.

Nir Y, Staba RJ, Andrillon T, Vyazovskiy VV, Cirelli C, Fried I, Tononi G (2011) Regional slow waves and spindles in human sleep. *Neuron* **70**, 153-169.

Oostenveld R, Fries P, Maris E, Schoffelen JM (2011) FieldTrip: Open sourse software for advanced analysis of MEG, EEG and invasive electrophysiological data. *Comput. Intell. Neurosci.* **2011**, 156869.

Rasch B, Born J (2013) About sleep's role in memory. *Physiol. Rev.* **93**, 681-766.

Sawangjit A, Oyanedel CN, Niethard N, Salazar C, Born J, Inostroza M (2018) The hippocampus is crucial for forming non-hippocampal long-term memory during sleep. *Nature* **564**, 109-113.

Siapas AG, Wilson MA (1998) Coordinated interactions between hippocampal ripples and cortical spindles during slow-wave sleep. *Neuron* **21**, 1123-1128.

Sirota A, Csicsvari J, Buhl D, Buzsáki G (2003) Communication between neocortex and hippocampus during sleep in rodents. *Proc. Natl. Acad. Sci. U. S. A.* **100**, 2065-2069.

Staresina BP, Bergmann TO, Bonnefond M, Van Der Meij R, Jensen O, Deuker L, Elger CE, Axmacher N, Fell J (2015) Hierarchical nesting of slow oscillations, spindles and ripples in the human hippocampus during sleep. *Nature Neurosci.* **18**, 1679-1686.

Steriade M, Contreras D, Curró Dossi R, Nuñez A (1993a) The slow (< 1 Hz) oscillation in reticular thalamic and thalamocortical neurons: scenario of sleep rhythm generation in interacting thalamic and neocortical networks. *J. Neurosci.* **13**, 3284-3299.

Steriade M, McCormick DA, Sejnowski TJ (1993b) Thalamocortical oscillations in the sleeping and aroused brain. *Science* **262**, 679-685.

Ujma PP, Gombos F, Genzel L, Konrad BN, Simor P, Steiger A, Dresler M, Bódizs R (2015) A comparison of two sleep spindle detection methods based on all night averages: individually adjusted versus fixed frequencies. *Front. Hum. Neurosci.* **9**, 52.

Ujma PP, Hajnal B, Bodizs R, Gombos F, Eross L, Wittner L, Halgren E, Cash S, Ulbert I, Fabo D (2019) The laminar profile of sleep spindles in humans. *bioRxiv,* 563221.

Varela C, Kumar S, Yang JY, Wilson MA (2014) Anatomical substrates for direct interactions between hippocampus, medial prefrontal cortex, and the thalamic nucleus reuniens. *Brain Struct. Funct.* **219**, 911-929.

Vertes RP, Hoover WB, Szigeti-Buck K, Leranth C (2007) Nucleus reuniens of the midline thalamus: link between the medial prefrontal cortex and the hippocampus. *Brain Res. Bull.* **71**, 601-609.

Vertes RP, Hoover WB, Do Valle AC, Sherman A, Rodriguez JJ (2006) Efferent projections of reuniens and rhomboid nuclei of the thalamus in the rat. *J. Comp. Neurol.* **499**, 768-796.

Watson BO, Buzsáki G (2015) Sleep, memory & brain rhythms. *Daedalus* **144**, 67-82.

Wolansky T, Clement EA, Peters SR, Palczak MA, Dickson CT (2006) Hippocampal slow oscillation: a novel EEG state and its coordination with ongoing neocortical activity. *J. Neurosci.* **26**, 6213-6229.

Xia F, Richards BA, Tran MM, Josselyn SA, Takehara-Nishiuchi K, Frankland PW (2017) Parvalbumin-positive interneurons mediate neocortical-hippocampal interactions that are necessary for memory consolidation. *Elife* **6**, e27868.

Zittrell F (2019) CircHist: Circular histogram in MATLAB. *GitHub,* doi: 10.5281/zenodo.3445084.

Table 1

Stage	Latency (min)	Number of episodes	Time (min)	Time (%)
Wake	-	161.4 ± 15.1	262.4 ± 14.0	36.4 ± 5.0
SWS	34.7 ± 4.8	172.6 ± 15.0	364.1 ± 14.0	50.5 ± 5.0
IS sleep	118.1 ± 18.6	49.8 ± 5.1	15.6 ± 2.1	2.2 ± 0.3
REM sleep	120.0 ± 17.0	47.8 ± 5.0	79.0 ± 3.3	11.0 ± 0.5

Table 1. Sleep architecture during the 12-h recording period in the light phase. Latency is given with reference to start of the recording period; time spent in the different sleep stages in minutes and percent of the total 12-h period. *n* = 5. SWS = Slow wave sleep; IS = Intermediate stage; REM = Rapid eye movement.

Table 2 Absolute numbers and co-occurrence of oscillatory events – slow oscillations, spindles, ripples during slow wave sleep.

	Frontal EEG		Parietal EEG		mPFC LFP		dHC LFP	
	Absolute number of slow oscillations (SOs)							
	3175.4 ± 810.6		3507.6 ± 920.8		3252.2 ± 850.6		3128.6 ± 809.8	
	SO density (#/min)							
	20.9 ± 0.5		22.9 ± 0.5		21.0 ± 0.7		20.6 ± 0,5	
	% SOs co-occuring with spindles							
	Mean	*SEM*	*Mean*	*SEM*	*Mean*	*SEM*	*Mean*	*SEM*
Frontal EEG	14.80	1.06	14.76	1.07	11.44	0.68	12.29	0.47
Parietal EEG	11.46	0.80	11.19	0.91	8.53	0.78	10.27	0.51
mPFC LFP	7.04	0.46	6.95	0.52	6.14	0.34	5.69	0.46
dHC LFP	8.40	1.06	8.75	1.06	7.20	0.95	7.68	1.45
	% SOs co-occuring with ripples							
	Mean	*SEM*	*Mean*	*SEM*	*Mean*	*SEM*	*Mean*	*SEM*
dHC LFP	39.27	2.28	40.09	2.52	36.71	2.63	38.32	2.61

	Frontal EEG		Parietal EEG		mPFC LFP		dHC LFP	
	Absolute number of spindles							
	399.6 ± 109.2		317.4 ± 85.0		176.2 ± 43.2		226.4 ± 70.3	
	Spindle density (#/min)							
	2.7 ± 0.1		2.0 ± 0.1		1.2 ± 0.1		1.5 ± 0.2	
	% Spindles co-occuring with SOs							
	Mean	*SEM*	*Mean*	*SEM*	*Mean*	*SEM*	*Mean*	*SEM*
Frontal EEG	81.20	2.09	80.05	1.94	80.05	1.17	78.05	2.14
Parietal EEG	81.35	2.24	80.80	2.42	79.58	1.82	81.11	1.30
mPFC LFP	69.55	0.92	66.70	3.37	74.76	4.59	72.38	1.75
dHC LFP	75.01	1.55	77.02	2.43	68.12	4.13	71.81	2.16
	% Spindles co-occuring with ripples							
	Mean	*SEM*	*Mean*	*SEM*	*Mean*	*SEM*	*Mean*	*SEM*
dHC LFP	47.7	4.4	46.3	4.9	45.0	4.0	51.7	5.9

	dHC LFP			
	Absolute number of ripples		**Ripple density (#/min)**	
	1498.6 ± 298.5		10.5 ± 0.9	
	% Ripples co-occuring with spindles		**% Ripples co-occuring with SOs**	
	Mean	*SEM*	*Mean*	*SEM*
Frontal EEG	17.4	2.6	70.1	2.4
Parietal EEG	13.4	2.6	71.4	2.9
mPFC LFP	7.2	0.6	70.7	1.9
dHC LFP	10.4	1.0	74.1	2.4

Figure Captions

Figure 1. **Characterization of slow oscillations (SOs)**. (A) Grand mean (±SEM) SO in the unfiltered signal from all recording sites time-locked to SO downstate peak (for n see Table 2). (B) *Top left,* SO density (events/min) calculated as the number of SO detected in each recording site divided by the time in SWS. *Top right,* SO duration (in s) measured as the time between two succeeding negative-to-positive zero crossings of the SO cycle. *Bottom left,* SO amplitude (in mV) measured as the downstate-to-upstate peak-to-peak amplitude. Box-whisker plots indicate median, upper (top) and lower (bottom) quartiles. * $p < 0.05$; ** $p < 0.01$; *** $p < 0.001$ for pairwise comparison, n = 5.

Figure 2. **Characterization of spindles.** (A) Grand mean (± SEM) spindles in the unfiltered signal from all recording sites time-locked to the maximum trough of a spindle (for n see Table 2). (B) *Top* left, spindle density (events/min), i.e., the number of spindles in each channel divided by the time in SWS. *Top right,* spindle duration (in s), i.e., time between onset and end of a spindle. *Bottom left*, spindle power (in mV^2s^{-1}), i.e., the integral of the Hilbert-transformed signal between spindle onset and end. *Bottom right,* spindle frequency (in Hz). Box-whisker plots indicate median, upper (top) and lower (bottom) quartiles. * $p < 0.05$; ** $p < 0.01$; *** $p < 0.001$ for pairwise comparison, n =5.

Figure 3. Temporal association between SOs and spindles. Left panels: Event correlation histogram of spindle events time-locked to the SO downstate peak (0 s, vertical dashed lines) in (A) frontal EEG, (B) parietal EEG, (C) mPFC LFP, and (D) dHC LFP signals. Event rate (in Hz) refers to spindle events quantified by all peaks and troughs of an identified spindle. Mean (±SEM)

rates across all SO epochs with co-occurring spindles from 5 rats are shown. Bin size: 100 ms. Graphs above the histograms show means (±SEM) for the respective reference SOs, time-locked to the SO downstate peak. Significant increases (red) or decreases (blue) in event rates are indicated (thin lines: $p < 0.05$; and thick lines: $p < 0.001$, for pairwise comparison with a 1-s baseline interval (-2.0 to -1.0 s)). Right panels: Results from complementary phase-locking analyses. Circular histogram of preferred phase for spindle onsets during SO cycle (12 bins, 30° each, SO downstate peak is at 180^0 in EEG and at 0^0 in LFP recordings). Red dashed line and red range of the circle represent average phase and 95% confidence interval. ** $p < 0.01$; *** $p < 0.001$ for Rayleigh test which solely tests for deviance from an overall uniform phase distribution of spindle onsets. Note, event correlation histograms and phase-locking analyses indicate clear modulation of spindle occurrence during SO downstate and upstate in frontal and parietal EEG signals. This modulation is absent (and not significant) in the event-correlation histograms of the LFP signal, especially from mPFC.

Figure 4. Temporal association between slow oscillations (SOs) and hippocampal ripples. (A) Left panels: Event correlation histograms of ripple events time-locked to the SO downstate peak (0 s, vertical dashed lines) in (top, left) frontal EEG, (top right) parietal EEG, (bottom left) mPFC LFP, and (bottom right) dHC LFP signals. Event rate (in Hz) refers to ripple events quantified by all ripple troughs and peaks. Mean (±SEM) rates across all SO epochs with co-occurring ripples from 5 rats are shown. Graphs above the histograms show means (±SEM) for the respective reference SOs, time-locked to the SO downstate peak. Right panels: Results from complementary phase-locking analyses. Circular histogram of preferred phase for ripple occurrence during SO cycle (12 bins, 30° each, SO downstate peak is at 180^0 in EEG and at 0^0 in LFP recordings). Red

dashed line and red range of the circle represent average phase and 95% confidence interval. ** $p < 0.01$; *** $p < 0.001$ for Rayleigh test of deviance from an overall uniform phase distribution of ripples. Note, event correlation histograms and phase-locking analyses indicate a decrease in ripple occurrence around the SO downstate peak followed by an increase in ripple activity, for SOs in both EEG channels. Also, note increase in ripple activity before the SO downstate peak in both LFP channels. (B) Event correlation histograms of SO events time-locked to (the maximum trough) of hippocampal ripples (0 s, vertical dashed lines). SO events were identified in (top, left) frontal EEG, (top right) parietal EEG, (bottom, left) mPFC LFP, and (bottom right) dHC LFP signals. Event rate (in Hz) refers to SO events quantified by their downstate peak. Mean (±SEM) rates across all ripple epochs with co-occurring SOs from 5 rats are shown. Graphs above the histograms show mean (±SEM) for the respective reference ripples, time-locked to the maximum ripple troughs. Bin size for event correlation histograms: 100 ms. Significant increases (red) and decreases (blue) in event rates are indicated (thin lines: $p < 0.05$; and thick lines: $p < 0.01$, for pairwise comparison with a 1-s baseline interval (-2.0 to -1.0 s)).

Figure 5. Temporal association between spindles and hippocampal ripples. (A) Event correlation histograms of ripple events time-locked to the onset of spindles (0 s, vertical dashed lines) identified in (top, left) frontal EEG, (top right) parietal EEG, (bottom, left) mPFC LFP, and (bottom right) dHC LFP signals. Event rate (in Hz) refers to ripple events quantified by all ripple troughs and peaks. Mean (±SEM) rates across all spindle epochs with co-occurring ripples from 5 rats are shown. Graphs above the histograms show mean (±SEM) root mean square amplitude of the respective reference spindles, time-locked to the spindle onset. (B) Event correlation histograms of spindle events time-locked to the maximum trough of ripples identified in dHC

recordings (0 s, vertical dashed lines). Spindle events were identified in (top, left) frontal EEG, (top right) parietal EEG, (bottom, left) mPFC LFP, and (bottom right) dHC LFP signals. Event rate (in Hz) refers to spindle events quantified by all spindle troughs and peaks. Mean (±SEM) event rates across all ripple epochs with co-occurring spindle events from 5 rats are shown. Graphs above the histograms show dHC LFP grand averages (±SEM) time-locked to the maximum ripple troughs. Bin size for histograms is 100 ms. Significant increases (red) and decreases (blue) in event rates are indicated (t: $p < 0.1$; thin lines: $p < 0.05$; and thick lines: $p < 0.001$, for pairwise comparison with a 1-s baseline interval (-2.0 to -1.0 s)).

Figure 6. Hippocampal ripple power during spindles. Top panels: Grand average (±SEM) spindle from unfiltered dHC LFP signal during a ±0.3-s interval around the maximum trough of the spindle (0 s) for spindles co-occurring with an SO (left, n = 658) and isolated spindles occurring in the absence of an SO event (right, n = 1770). Spindles were detected in dHC LFP recordings. SOs were detected in all four channels (i.e., frontal and parietal EEG, mPFC and dHC LFP recordings). Please, refer to supplementary Figure 5 for a separate analysis on SOs only identified in dHC LFP recordings). Co-occurrence of an SO was indicated when an SO downstate occurred within the ±1.5-s interval around the spindle maximum trough. Bottom panels: Time-frequency plots of power in the 150 – 250 Hz frequency band of the dHC LFP signal time-locked to the maximum trough of reference spindle (0 s). Power is color-coded and given as normalized value, i.e., divided by the average power during a baseline interval (-2.0 to -1.0 s). Significant differences (increases) from baseline values are indicated underneath (p-values for paired-sample t-test, uncorrected). There were no differences in power between spindles co-occurring with SOs and spindle occurring alone.

Figure 7: Hippocampal ripple power during slow oscillations (SOs). Top panels: Grand average (±SEM) SOs from unfiltered signals during a ±0.8 s-interval around the downstate peak of the SO (0 s) for SOs co-occurring with a spindle (left) and SOs occurring in the absence of a spindle event (right). SOs were detected in all four channels (frontal EEG: dark green, parietal EEG: light green, mPFC LFP: dark purple and dHC LFP: light purple. Please, refer to supplementary Figure 6 for a separate analysis on SOs only identified in dHC LFP recordings). Spindles were always detected in dHC LFP recordings. The co-occurrence of a spindle was indicated when a spindle onset occurred within the ±1.8 s-interval around the SO downstate peak. Middle panels: root mean square amplitude for the dHC LFP signal filtered in the spindle frequency band (10.0 – 16.0 Hz). Bottom panels: Time-frequency plot of power in the 150.0-250.0 Hz frequency band of the dHC LFP signal time-locked to the downstate peak of reference SO (0 s). Power is color-coded and given as normalized value, i.e., divided by the average power during a baseline interval (-2.0 to -1.0 s). Significant differences (increases: red, decreases; blue) from baseline values are indicated underneath (p-values for paired-sample t-test, uncorrected). Additional comparison (not shown) between SOs co-occurring with spindles and SOs occurring alone indicated significantly increased ripple power ($p < 0.05$) in a 100-ms bin around the downstate peak. Note, ripple power was persistently increased during SOs co-occurring with spindles, but shows only a brief transient increase during upstates of SOs occurring alone.

Figure 8. Loop-like interaction of oscillatory events regulating the information flow between hippocampus and neocortex during slow wave sleep. Top-down, the neocortical slow oscillation (SO, blue) by its hyperpolarizing downstate provides a global signal inactivating the

whole loop thereby setting the temporal frame for memory processing that starts with the transition into the subsequent SO upstate. The SO upstate primarily acts on thalamic networks (blue arrow) to drive spindle activity in thalamo-cortical networks (with a peak ~500 ms following the downstate peak). Thalamic spindles that reach the hippocampus in turn act on these networks (green arrow) to increase ripples and associated memory replay, with this effect starting ~100 ms after spindle onset. Bottom-up, hippocampal ripples increase the occurrence of SO, especially in prefrontal cortex, as indicated by increased occurrence of SO downstates ~200 ms following a ripple. Note, the present data about temporal relationships between SOs, spindles and ripples, can only be used to exclude directions of causality, but not to infer causality in the interaction between these oscillatory events. Against this backdrop, the model represents an attempt to integrate the present findings about temporal relationships with findings in the literature about underlying causal mechanisms.

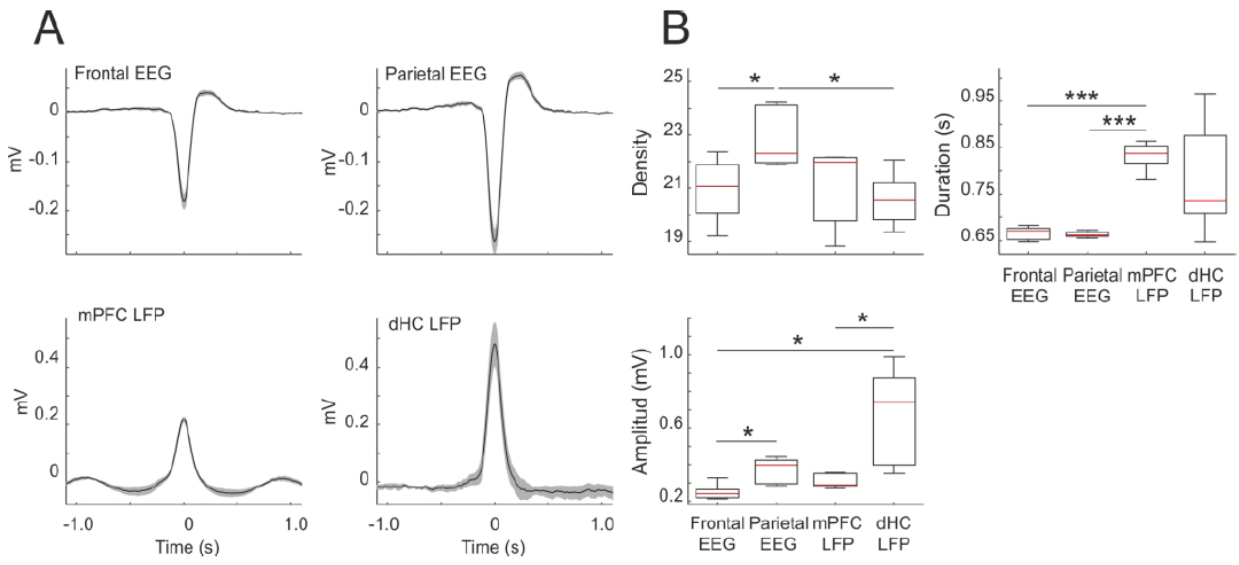

Figure 1. Characterization of slow oscillations (SOs).

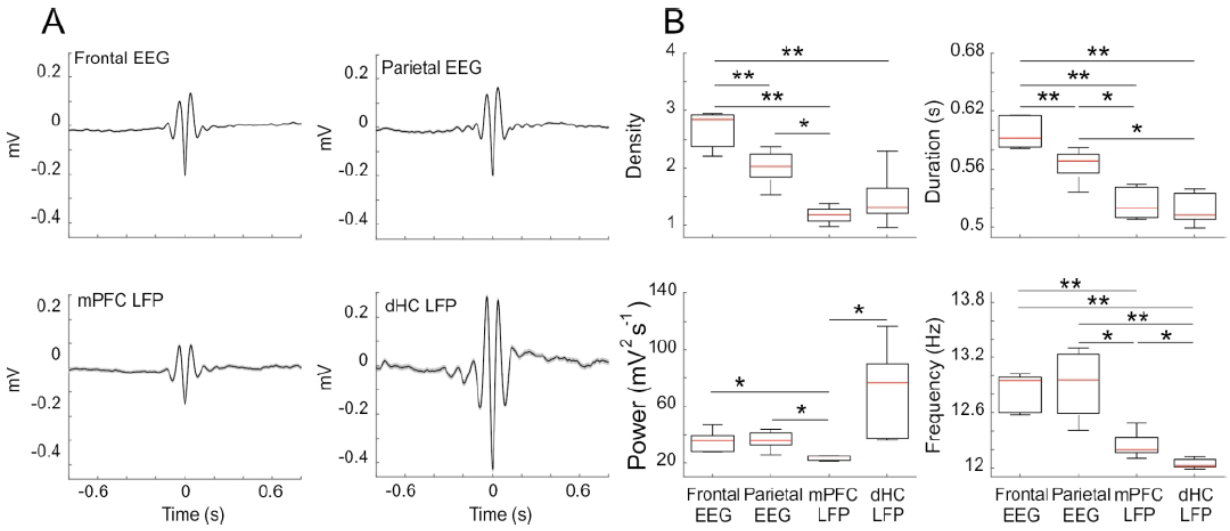

Figure 2. Characterization of spindles

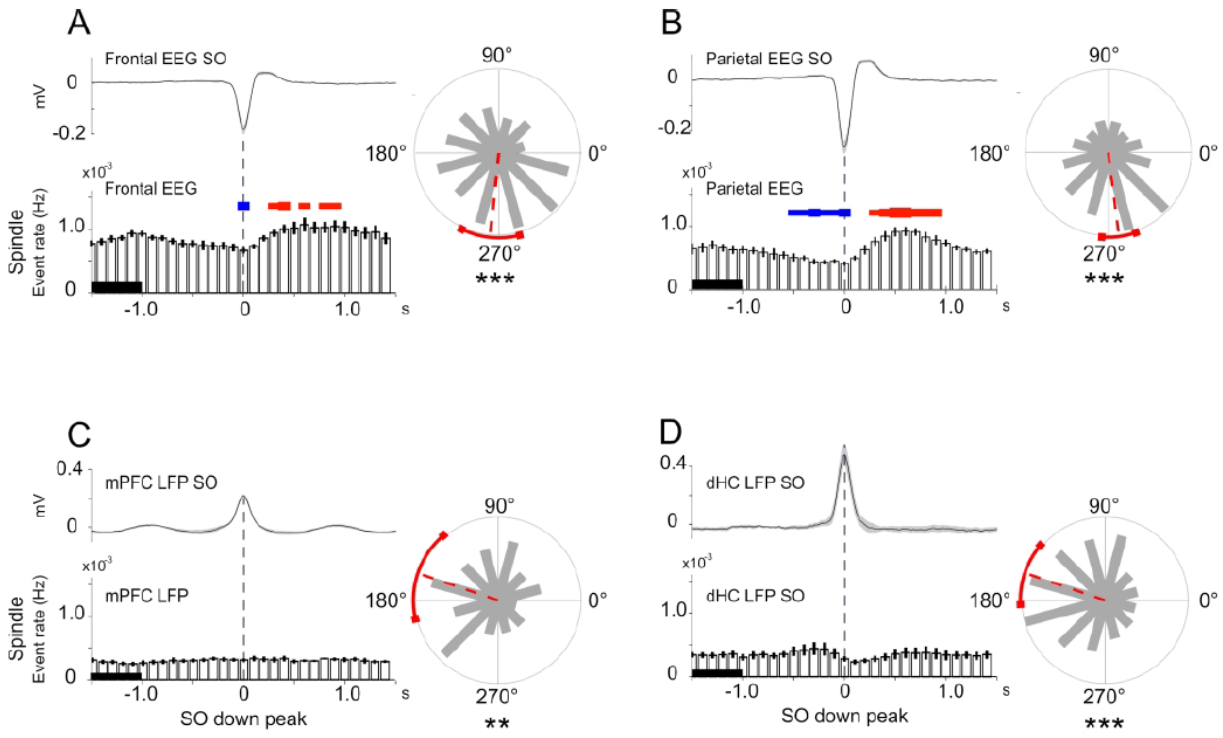

Figure 3. Temporal association between SOs and spindles.

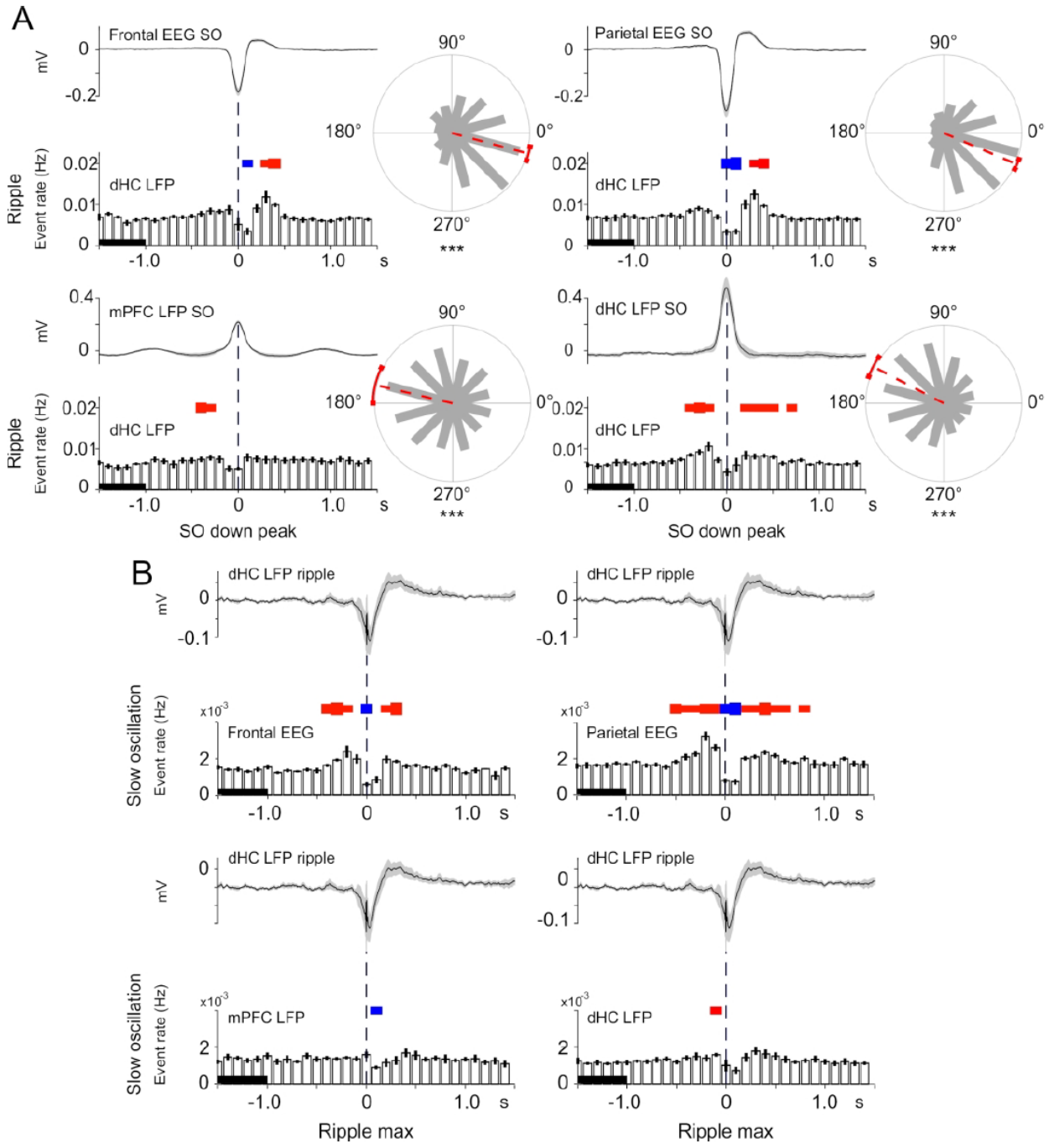

Figure 4. Temporal association between slow oscillations (SOs) and hippocampal ripples.

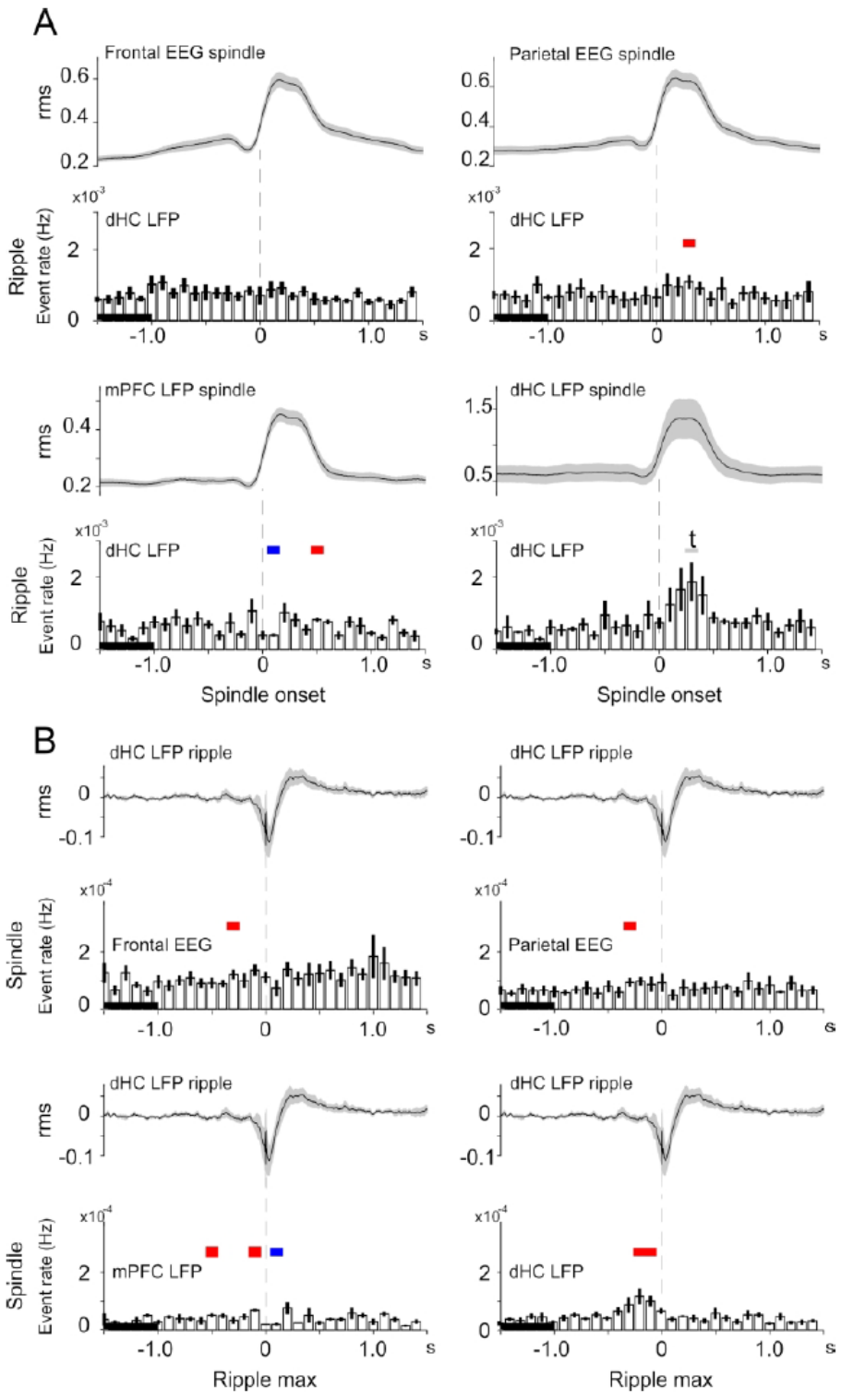

Figure 5. Temporal association between spindles and hippocampal ripples

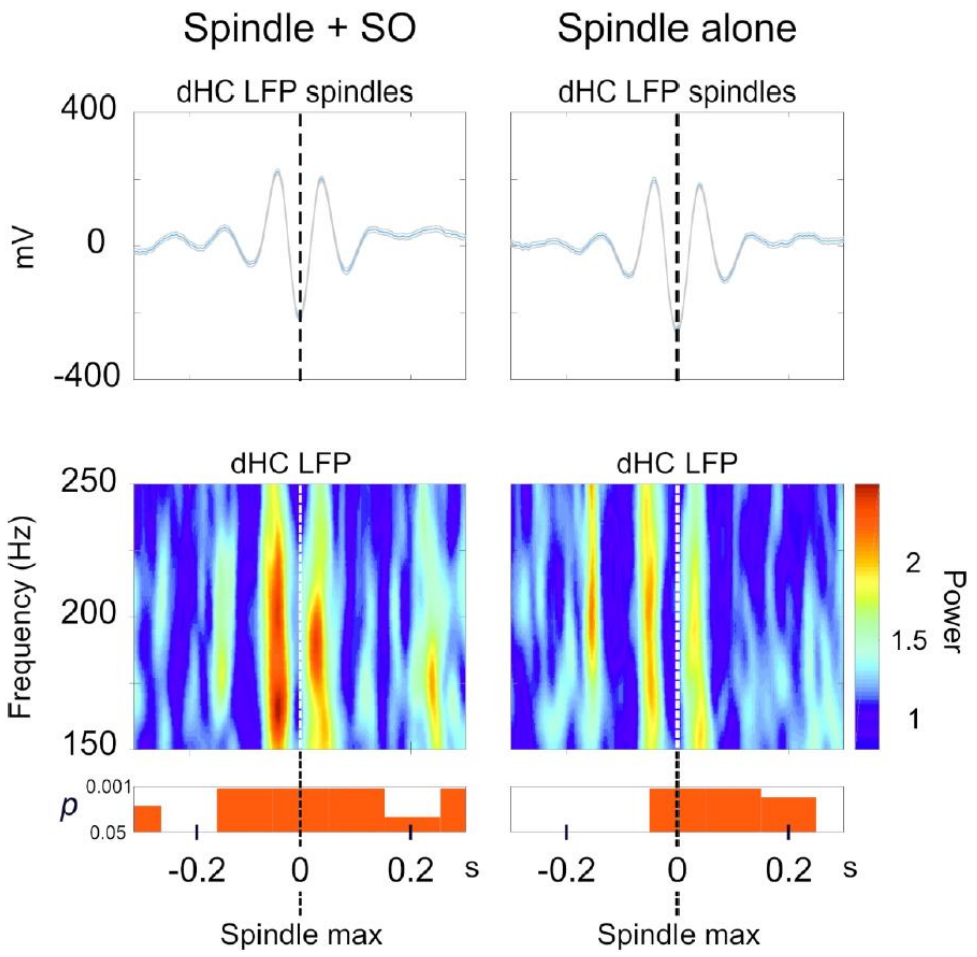

Figure 6. Hippocampal ripple power during spindles.

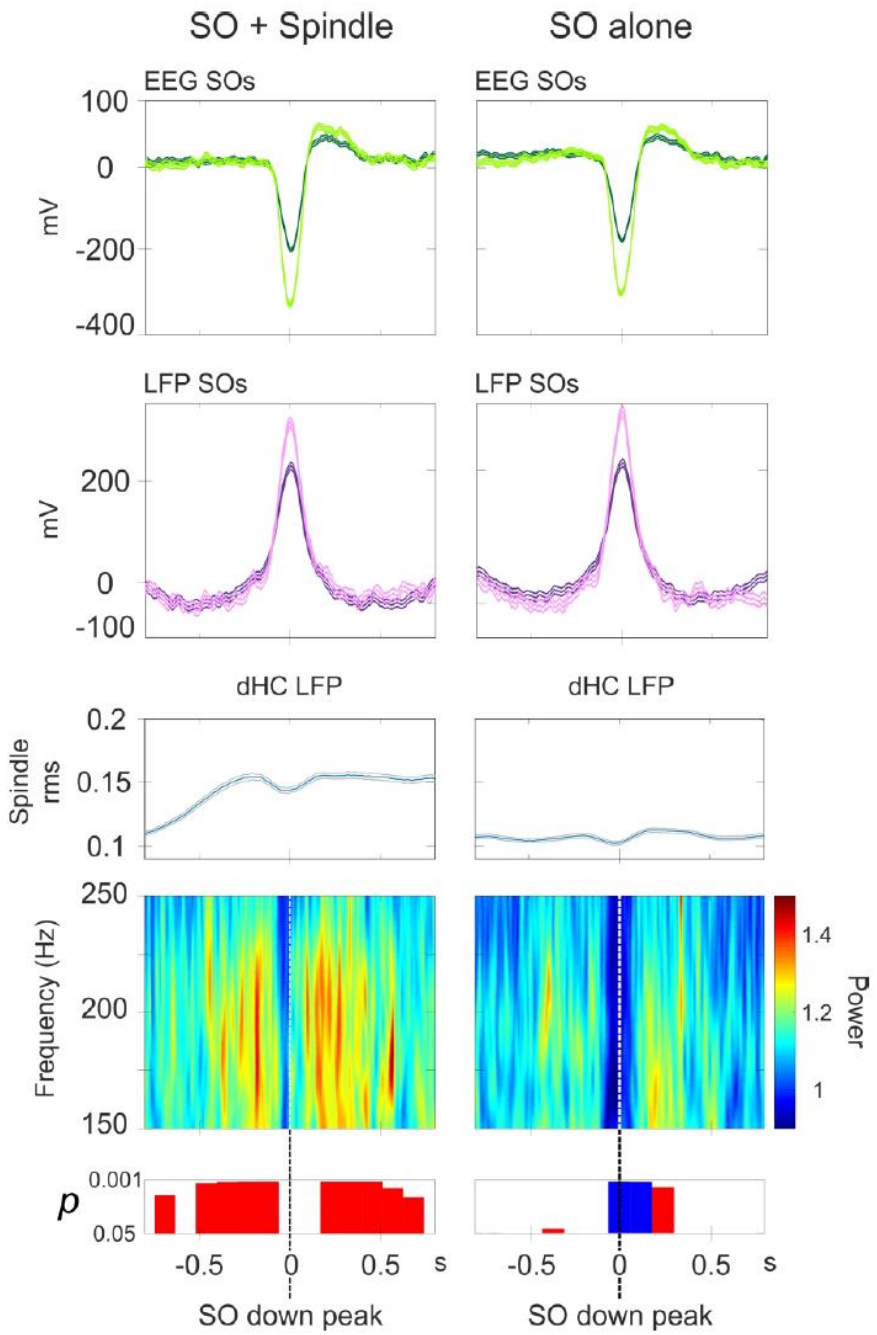

Figure 7: Hippocampal ripple power during slow oscillations (SOs).

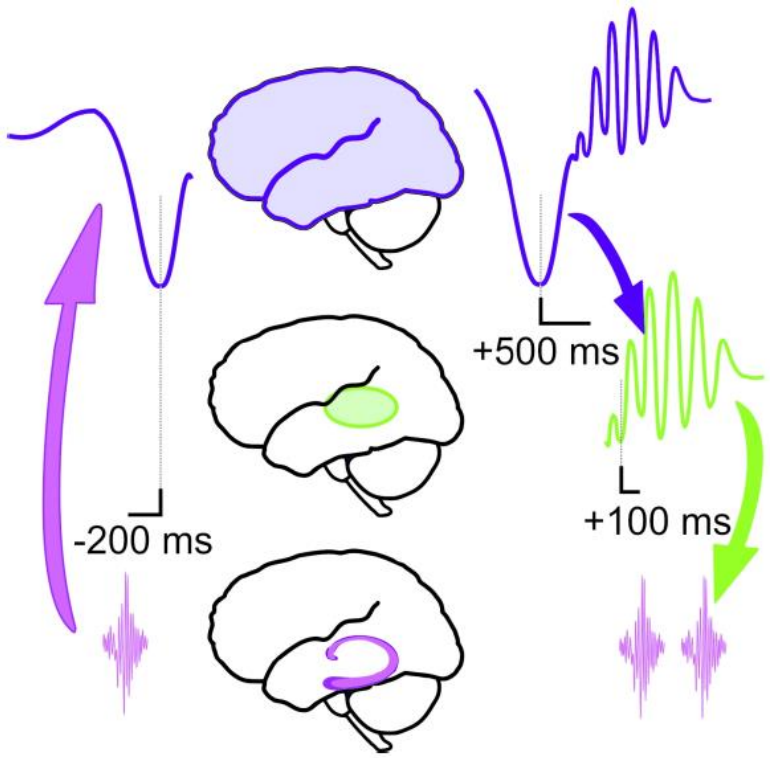

Figure 8. Loop-like interaction of oscillatory events regulating the information flow between hippocampus and neocortex during slow wave sleep.

Supporting information

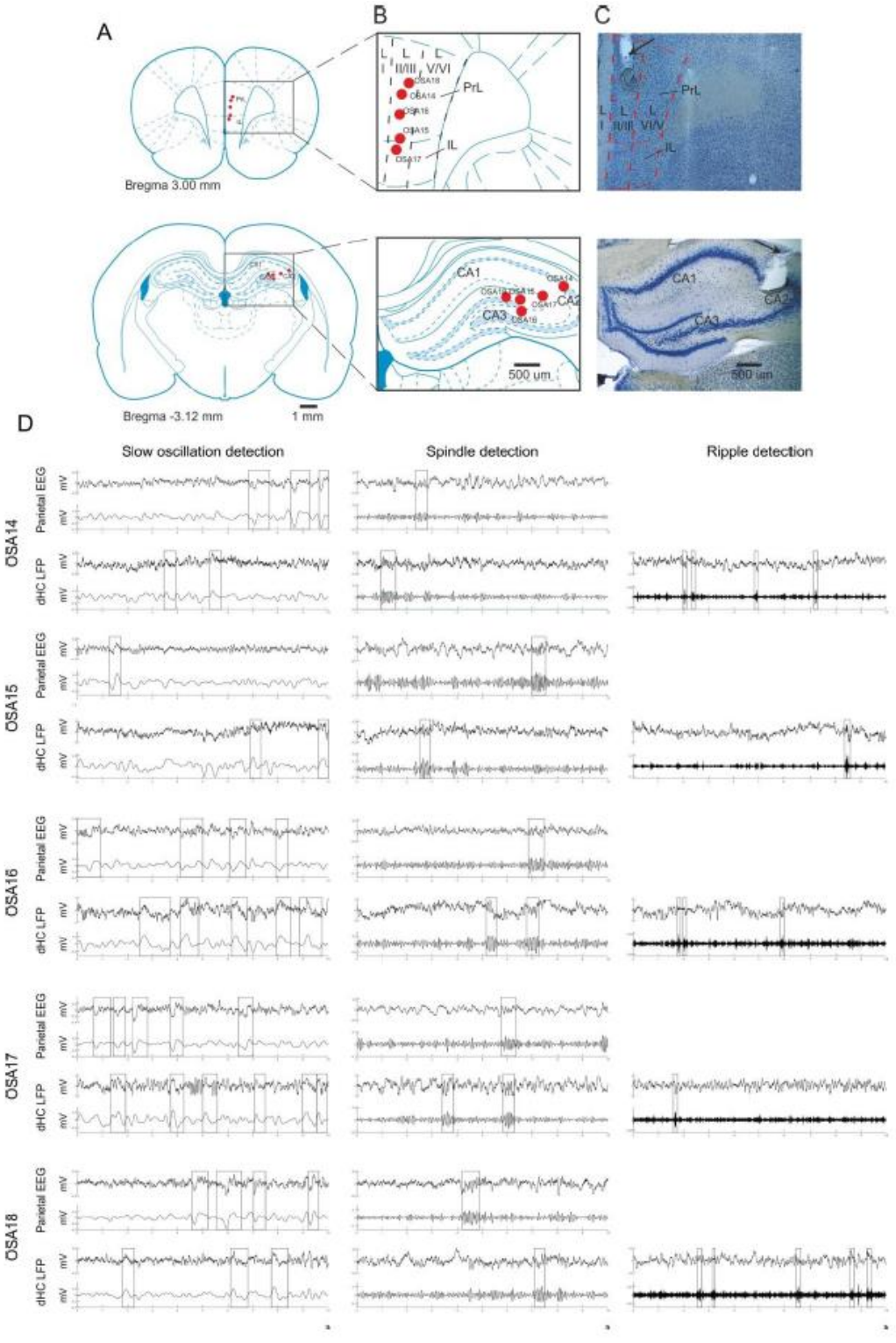

Supplementary Figure 1. Histological verification and reconstruction of the electrode placement in mPFC and dHC. (A) Coronal rat brain atlas diagrams adapted from Paxinos and Watson (1998) indicating the electrode position for mPFC (top) and dHC (bottom) LFP recordings. (B) Maps of electrode positions for mPFC (top) and dHC (bottom) LFP recordings (red dots). (C) Coronal view of an example methylene blue-stained section of the mPFC (top), with parcellation of layers I, II/III, and V/VI and electrode position indicated (arrow). Bottom, example section from same animal of dHC. (D) Example traces of LFP recordings from dHC and simultaneous parietal EEG recordings from individual animals (OSA14-OSA18). Unfiltered signals (upper trace) and signals filtered in the frequency band for identifying SOs, spindles, and ripples (lower trace) are shown (identified oscillatory events framed). Note, for example SOs (left panels) can occur in parietal recordings in the absence of any similar SO in dHC recordings excluding strong volume conductance of signal between channels. Recording polarity was determined based on wave shape characteristics of SOs. LFP = Local field potential; mPFC = Medial prefrontal cortex; dHC = Dorsal hippocampus.

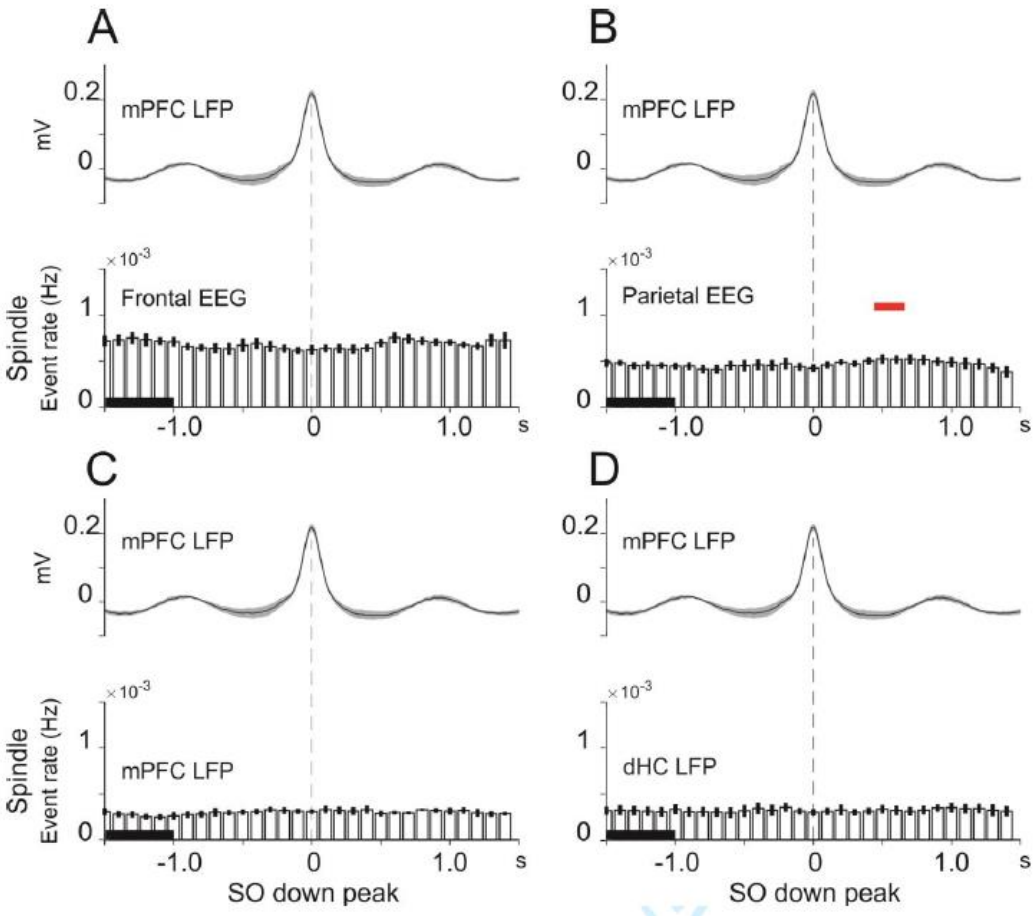

Supplementary Figure 2. **Temporal association between SO events in mPFC and spindles in EEG and LFP recordings.** Event correlation histogram of spindle events time-locked to the downstate peak (0 s, vertical dashed lines) of SOs identified in mPFC LFP recordings. Spindle events were identified in (A) frontal EEG, (B) parietal EEG, (C) mPFC LFP, and (D) dHC LFP signals. Event rate (in Hz) refers to spindle events quantified by all peaks and troughs of an identified spindle. Means (±SEM) rates across all SO epochs with co-occurring spindles (in one of the four channels) from 5 rats are shown. Bin size: 100 ms. Graphs above the histograms show the mean (±SEM) reference SO in mPFC recordings, time-locked to the SO downstate peak. Significant increases in event rates are indicated (red lines: $p < 0.05$, for pairwise comparison with a 1-s baseline interval (-2.0 to -1.0 s)).

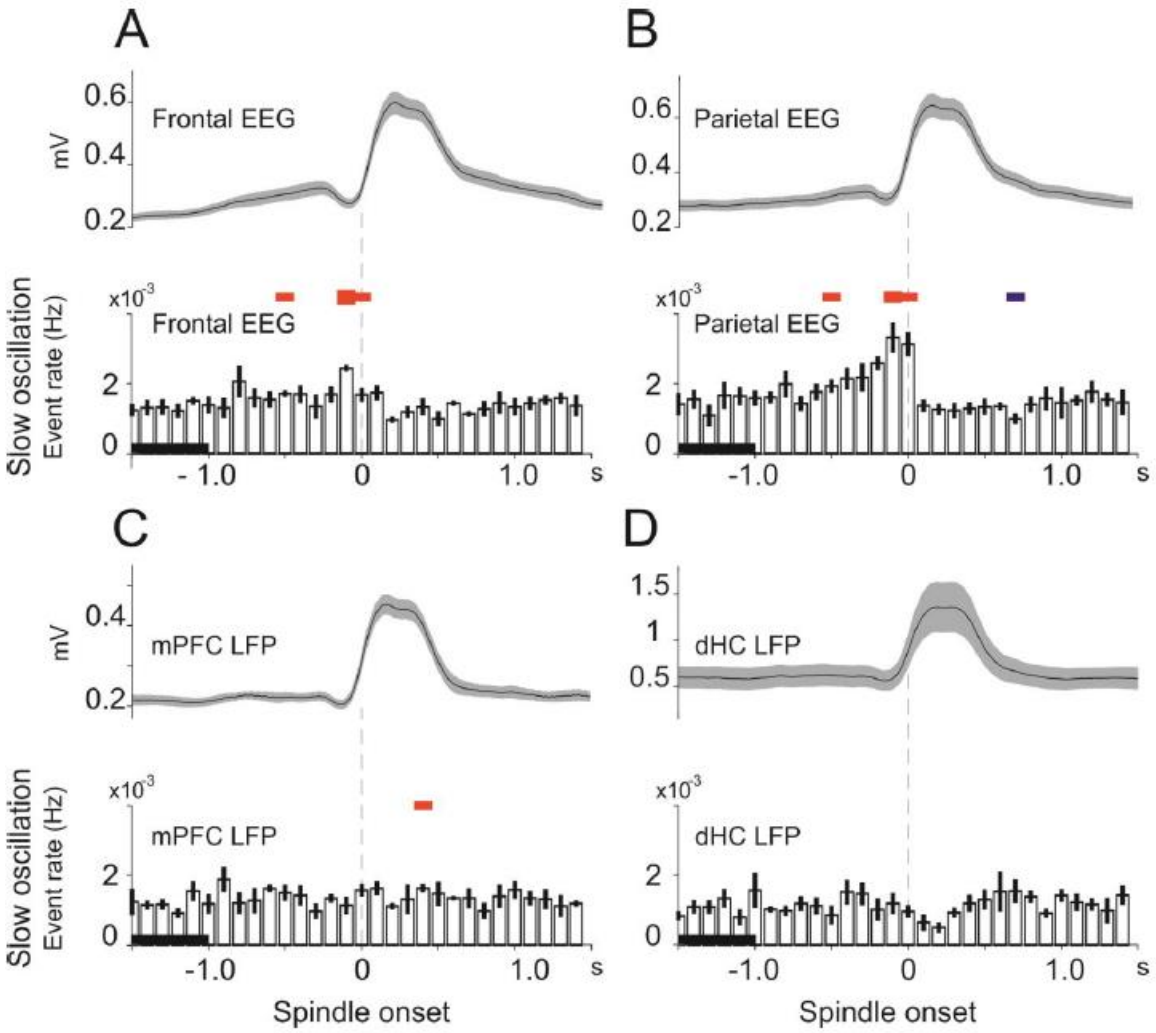

Supplementary Figure 3. **Temporal association between spindles and SOs.** Event correlation histogram of SO events time-locked to the onset of spindles (0 s, vertical dashed lines) in (A) frontal EEG, (B) parietal EEG, (C) mPFC LFP, and (D) dHC LFP signals. Event rate (in Hz) refers to SO events identified by their downstate peak. Mean (±SEM) rates across all spindle epochs with co-occurring SOs from 5 rats are shown. Bin size: 100 ms. Graphs above the histograms show mean (±SEM) root mean square amplitude of the respective reference spindles, time-locked to the spindle onset. Significant increases (red) or decreases (blue) in spindle occurrence are indicated (thin lines: $p < 0.05$; and thick lines: $p < 0.001$, for pairwise comparison

with a 1-s baseline interval (-2.0 to -1.0 s)).

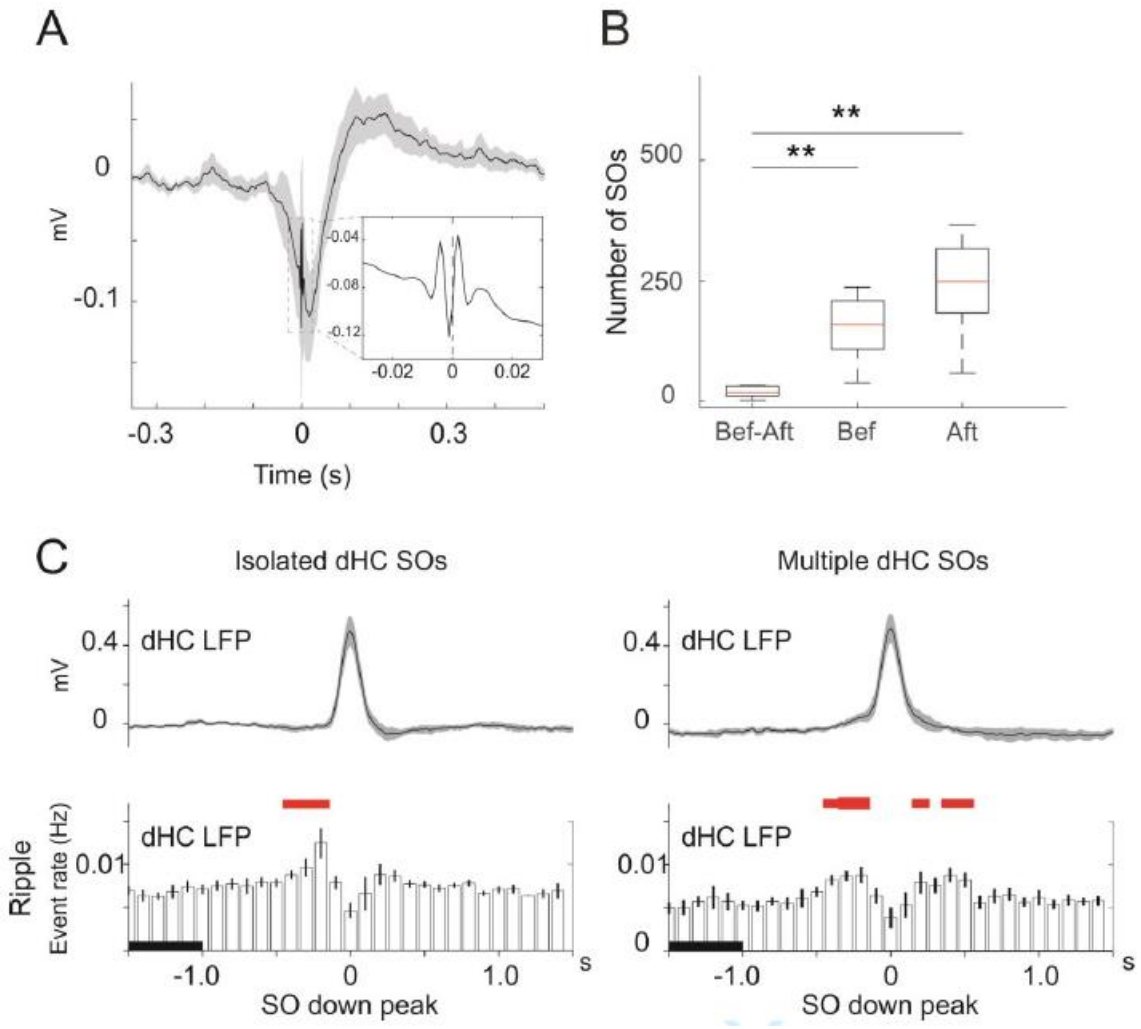

Supplementary Figure 4. **Hippocampal ripples before and after SO downstate peaks.** (A) Grand average (±SEM) of ripple from the unfiltered dHC LFP signal time-locked to the maximum ripple trough. Insert illustrates a single ripple. (B) Number of SO events with ripple events before and after the downstate peak (Bef—After), and with ripple event either before (Bef) or after (Aft) the downstate peak. Box-whisker plots indicate median, upper (top) and lower (bottom) quartiles. * $p < 0.05$; ** $p < 0.01$ for pairwise comparison. (C) Event correlation histograms of ripple events time-locked to the SO downstate peak (0 s, vertical dashed lines) for SO events in dHC LFP recordings that (left) either occurred in isolation (n = 1753.6 ± 495.7), or (right) were preceded or followed (within ± 1.5 ms) by another SO event, i.e., downstate peak (n = 1375.0 ± 343.0). Event

rate (in Hz) refers to events quantified by all troughs and peaks of an identified ripple. Mean (±SEM) rates across all respective SO epochs with co-occurring ripples from 5 rats are shown. Graphs above the histograms show means (±SEM) for the respective reference SOs, time-locked to the SO downstate peak. Bin size 100 ms. Significant increases (red) or decreases (blue) in ripple occurrence are indicated (thin lines: $p < 0.05$; and thick lines: $p < 0.001$, for pairwise comparison with a 1-s baseline interval (-2.0 to -1.0 s)). Note, on average stronger increase in ripple activity before the downstate peak of SOs occurring in isolation than before SOs followed by another SO.

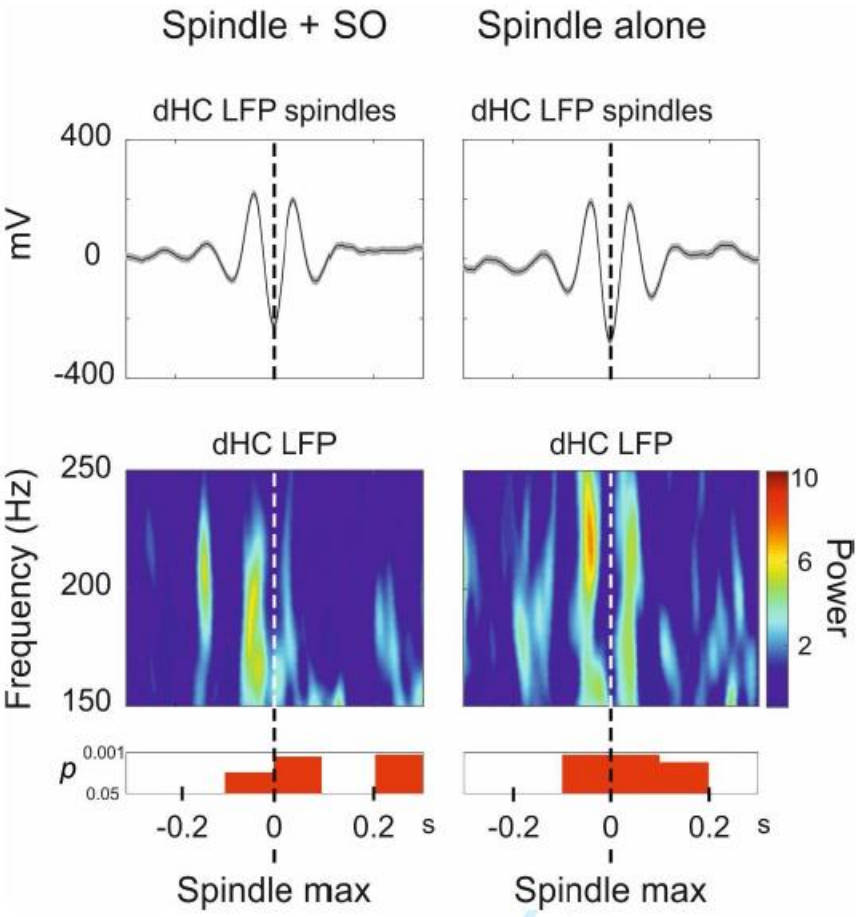

Supplementary Figure 5. Hippocampal ripple power during spindles. Top panels: Grand average (±SEM) spindle from unfiltered dHC LFP signal during a ±0.3-s interval around the maximum trough of the spindle (0 s) for spindles co-occurring with an SO (left, n = 138) and isolated spindles occurring in the absence of an SO event (right, n = 469). Unlike in Fig. 6 of the main text, here both spindles as well as SOs were detected in dHC LFP recordings. Co- occurrence of an SO was indicated when an SO downstate occurred within the ±1.5-s interval around the spindle maximum trough. Bottom panels: Time-frequency plots of power in the 150–250 Hz frequency band of the dHC LFP signal time-locked to the maximum trough of reference spindle (0 s). Power is color-coded and given as normalized value, i.e., divided by the average power during a baseline interval (-2.0 to -1.0 s). Significant differences (increases) from baseline values are indicated underneath (p-values for paired-sample t-test, uncorrected).

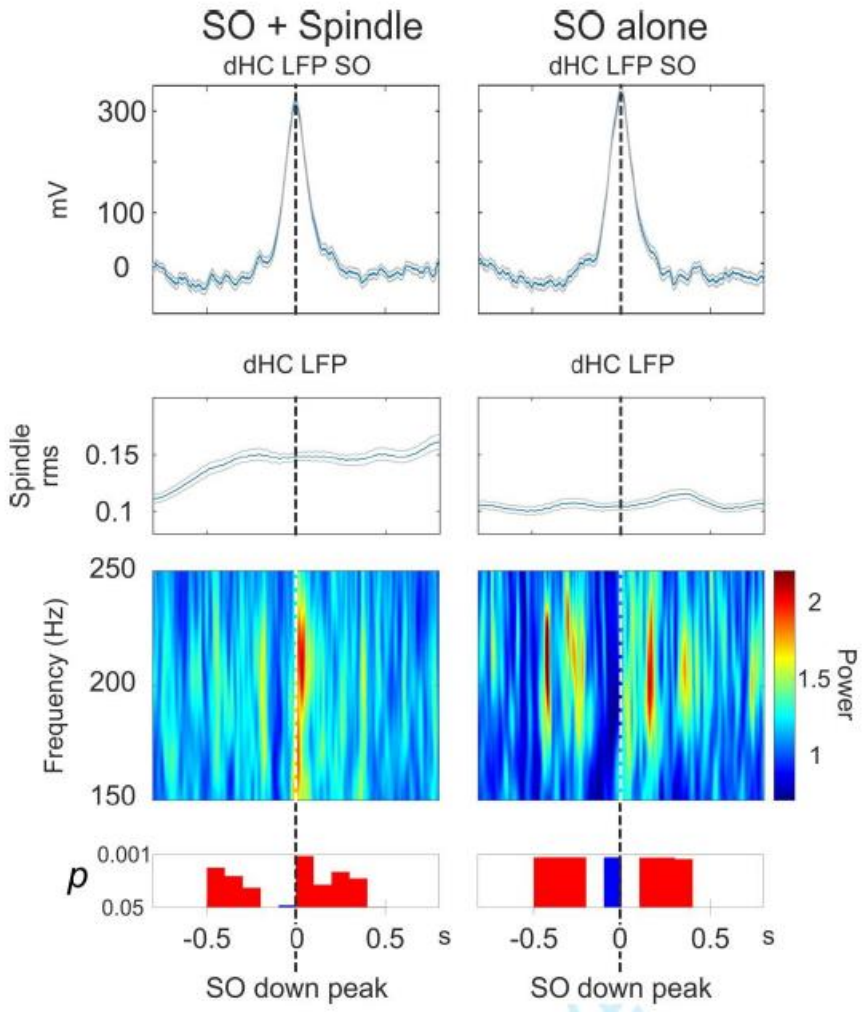

Supplementary Figure 6. **Hippocampal ripple power during slow oscillations (SOs).** Top panels: Grand average (±SEM) SOs from unfiltered signals during a ±0.8 s-interval around the downstate peak of the SO (0 s) for SOs co-occurring with a spindle (left) and SOs occurring in the absence of a spindle event (right). Unlike in Fig. 7 of the main text, here, both SOs and spindles were only detected in dHC LFP recordings. The co-occurrence of a spindle was indicated when a spindle onset occurred within the ±1.8 s-interval around the SO downstate peak. Middle panels: root mean square amplitude for the dHC LFP signal filtered in the spindle frequency band (10.0 – 16.0 Hz). Bottom panels: Time-frequency plot of power in the 150.0- 250.0 Hz frequency band of

the dHC LFP signal time-locked to the downstate peak of reference SO (0 s). Power is color-coded and given as normalized value, i.e., divided by the average power during a baseline interval (-2.0 to -1.0 s). Significant differences (increases: red, decreases; blue) from baseline values are indicated underneath (p-values for paired-sample t-test, uncorrected). Note, consistent with the analyses in Fig. 7 of the main text (collapsing SOs across all recording sites), upstates of SOs selectively identified in dHC recordings are associated with increased ripple power, whereas ripple power is decreased around the downstate of these SOs, particularly when they occur in the absence of a spindle. As a result, ripple power ~100 ms around the SO downstate peak is significantly lower ($p < 0.05$) for isolated SOs than SOs co-occurring with a spindle (not shown). Different from the analysis in Fig. 7, the upstate-related increase in ripple power during SOs occurring alone in the dHC LFP signal appears to be more persistent, likely reflecting that once a SO has reached the hippocampus, the upstate per se can effectively contribute to increasing ripple activity.

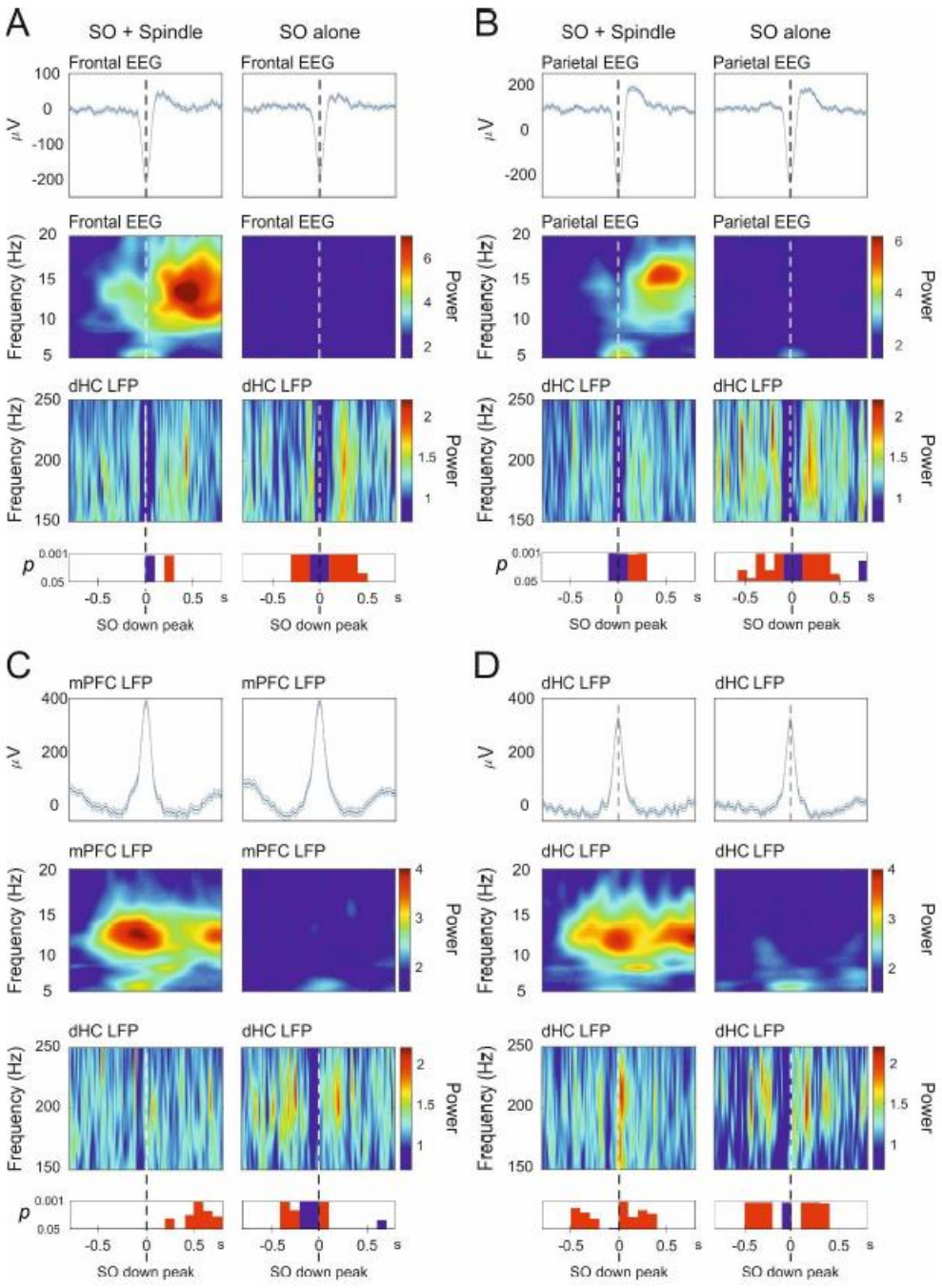

Supplementary Figure 7. Hippocampal ripple power during slow oscillations (SOs). Top panels: Grand average (±SEM) SOs from unfiltered signals from (A) frontal EEG, (B) parietal EEG, (C) mPFC LFP, and (D) dHC LFP, during a ±0.8 s-interval around the downstate peak of the SO (0 s) for SOs co-occurring with a spindle (left) and SOs occurring in the absence of a spindle event

(right) with the spindle identified in the same channel as the SO. The co- occurrence of a spindle was indicated when a spindle onset occurred within the ±1.8 s-interval around the SO downstate peak. Middle panels: Time-frequency plot of power in the 5.0-20.0 Hz band (covering the spindle band) time-locked to the downstate peak of the reference SO (0 s). Bottom panels: Time-frequency plot of power in the 150.0-250.0 Hz frequency band of the dHC LFP signal time-locked to the downstate peak of reference SO (0 s). Power is color-coded and given as normalized value, i.e., divided by the average power during a baseline interval (-2.0 to - 1.0 s). Significant differences in ripple band power (increases: red, decreases: blue) from baseline values are indicated underneath (p-values for paired-sample t-test, uncorrected). Except that ripple power around the downstate peak (0 s) of SOs co-occurring with spindles was higher with event detection in the dHC LFP than in EEG recordings ($p < 0.05$), there were no significant differences in ripple power depending on the site of SO/spindle detection.

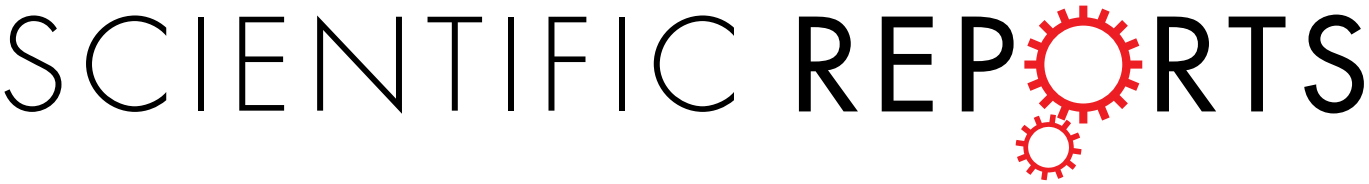

OPEN

Midline thalamic neurons are differentially engaged during hippocampus network oscillations

Received: 08 March 2016
Accepted: 20 June 2016
Published: 14 July 2016

Ariel Lara-Vásquez, Nelson Espinosa, Ernesto Durán, Marcelo Stockle & Pablo Fuentealba

The midline thalamus is reciprocally connected with the medial temporal lobe, where neural circuitry essential for spatial navigation and memory formation resides. Yet, little information is available on the dynamic relationship between activity patterns in the midline thalamus and medial temporal lobe. Here, we report on the functional heterogeneity of anatomically-identified thalamic neurons and the differential modulation of their activity with respect to dorsal hippocampal rhythms in the anesthetized mouse. Midline thalamic neurons expressing the calcium-binding protein calretinin, irrespective of their selective co-expression of calbindin, discharged at overall low levels, did not increase their activity during hippocampal theta oscillations, and their firing rates were inhibited during hippocampal sharp wave-ripples. Conversely, thalamic neurons lacking calretinin discharged at higher rates, increased their activity during hippocampal theta waves, but remained unaffected during sharp wave-ripples. Our results indicate that the midline thalamic system comprises at least two different classes of thalamic projection neuron, which can be partly defined by their differential engagement by hippocampal pathways during specific network oscillations that accompany distinct behavioral contexts. Thus, different midline thalamic neuronal populations might be selectively recruited to support distinct stages of memory processing, consistent with the thalamus being pivotal in the dialogue of cortical circuits.

The thalamus is a heterogeneous region with topographical projections covering most of the cortical mantle[1]. Historically, lateral thalamic nuclei and their sensorimotor function have been studied in great detail[1–3]. Conversely, less explored is the so-called "limbic thalamus", comprising structures located along the midline; including medial, anterior, intralaminar, and midline nuclei[4]. These structures encompass a narrow band of small nuclei distributed over the entire dorso-ventral extension of the thalamus[5]. A particular anatomical feature of the midline thalamus is its enriched expression of calcium-binding proteins. Indeed, mapping studies have revealed abundant calretinin (CR)- and calbindin (CB)-expressing somata along the midline thalamus[6–8]. These proteins are fundamental to regulate Ca^{2+} homeostasis and are implicated in the fine control and timing of synaptic Ca^{2+} signals[9,10]. In several brain regions, particularly the neocortex and hippocampus, CB and CR are robust molecular markers of discrete GABAergic neuronal populations[11–14]. However, similar insight has not been provided for the thalamus, where it is currently not known if calcium-binding proteins, such as CR or CB, can dissect specific cell types.

On the other hand, the functional role of the midline thalamus is just beginning to be understood. Initially, it was proposed that the main role of the midline thalamus is to adjust activity levels in target structures[5]. Nonetheless, in recent years insight has emerged on the relevance of several midline thalamic nuclei in regulating cognitive function. Indeed, it is now known that the paraventricular nucleus, part of the dorsal midline thalamic group, is necessary for fear memory[15]. In addition, the reuniens nucleus, from the ventral midline thalamic group, is required for some forms of goal-directed behaviour[16] and memory specificity[17]. Moreover, the reuniens nucleus is implicated in system consolidation of memory[18,19] and strategy shifting[20], and recent experiments have demonstrated that is contains head-direction cells[21]. Such cognitive and executive functions are implemented by the coordinated action of the frontal and medial temporal lobes[22,23]; suggesting that the midline thalamus is probably important to sustain cortical interactions underlying memory processing[5,24,25]. In fact, the hippocampus is directly targeted by ventral midline thalamic nuclei, particularly by the reuniens and rhomboidal nuclei[26–28], whereas most of the midline thalamus receives reciprocal afferents from the hippocampus via the subiculum[29–32].

Laboratorio de Circuitos Neuronales, Departamento de Psiquiatria, Centro Interdisciplinario de Neurociencia, Pontificia Universidad Catolica de Chile, Marcoleta 391, 8330024 Santiago, Chile. Correspondence and requests for materials should be addressed to P.F. (email: pjfuentealba@gmail.com)

Nucleus	CB+CR+ cells	CB−CR+ cells	CB+CR− cells	CB−CR− cells	Total
MD	0	1	2	2	5
PV	8	3	0	0	11
PC	1	1	1	3	6
PT	0	0	0	1	1
CM	2	2	3	1	8
AM	2	4	3	4	13
Rh	2	4	0	2	8
Re	5	3	3	6	17
Sub	0	0	1	6	7
VM	1	0	2	0	3
Total	21	18	15	25	79

Table 1. Selective expression of the neurochemical markers calbindin (CB) and calretinin (CR) in neurons recorded from midline thalamic nuclei. Abbreviations: MD, mediodorsal nucleus; PV, paraventricular nucleus; PC, paracentral nucleus; PT, paratenial nucleus; CM, centro medial nucleus; AM, anteromedial nucleus; Rh, rhomboidal nucleus; Re, reuniens nucleus; Sub, submedial nucleus; VM, ventromedial nucleus.

These anatomical and physiological evidence support the idea that the midline thalamus contributes to the coordination of temporal and frontal lobes in the implementation of cognitive function[4].

The hippocampus constitutes a central hub of the medial temporal lobe, which synchronizes neuronal activity along the temporal cortical axis, and also establishes coherent activity with the frontal lobe, which is required for learning and memory[33–35]. Two very characteristic oscillatory patterns of activity are present in the hippocampus, namely theta oscillations and sharp wave-ripples, which define particular brain states in behaving animals[33]. Each of these activity patterns seems to be associated with a specific phase of memory formation. Accordingly, theta waves (4–8 Hz oscillations in the local field potential) are prominent during exploratory states, and have been proposed to reflect memory encoding[36]; whereas ripple episodes (100–200 Hz oscillations in the local field potential) take place during quiet states (including slow wave sleep) and are believed to participate selectively in memory consolidation[37]. Given the global cortical effects of both theta and ripple oscillations, and the anatomical pathways linking the hippocampus and midline thalamus (i.e., subiculum and entorhinal cortex[4,27,29,31,32]), it becomes relevant to account for the functional connectivity between these networks during oscillatory activity.

Accordingly, here we recorded single-neuron and network activity in identified thalamic nuclei during hippocampal network oscillations. Our results indicate that the midline thalamic system comprises at least two sets of thalamic projection neuron defined by the expression of calcium-binding proteins, which are differentially engaged by hippocampal pathways during distinct network oscillations. These data establish a previously unidentified functional connection between the midline thalamus and hippocampus. Thus, diverse midline thalamic neuronal populations might be selectively recruited to support particular stages of memory processing.

Results

Calretinin and calbindin expression in midline thalamic neurons. We sampled the action potential firing of individual neurons from thalamic nuclei across the midline (Table 1). After recording, neurons were individually labeled with the juxtacellular filling method[38] and classified by their expression of neurochemical markers (Supplementary Table 1). In order to map the location of recorded neurons on the thalamus, we projected all labelled neurons on the neuroanatomical atlas of the mouse brain[39]. Neurons were recovered from most midline thalamic nuclei (Fig. 1a). The somatodendritic distributions of midline thalamic neurons were relatively uniform, with no obvious distinct morphological types. However, we could identify cells conforming to the distinct branching patterns of dendrites described in thalamic relay cells, such as "bushy" and "radiate" neurons[1,40]. Indeed, some cells had more angular and multipolar cell bodies, with dendritic trees branching dichotomously, characteristic of "radiate" cells (Fig. 1c). Conversely, other cells had elongated somata, with dendrites longer and branching less frequently, particularly in regions proximal to the soma, and followed a "bushy" organization (Fig. 1c). We were not able to fill the entire extension of axonal arborizations, even in cases where intense somatic labeling was achieved. In fact, most labelled cells did not show evidence of axonal labelling. When labelled, axons arose in all cases from the soma and rarely branched locally (Supplementary Figure 1). Given the above mentioned dendritic branching patterns, as well as axonal branching patterns, with little or no local collaterals, we considered our sample to be entirely comprised of thalamic projection neurons, which are known to be glutamatergic and typically reach the cortical mantle[1]. In order to characterize the neurochemical profiles of thalamic neurons, we tested the neurobiotin-labelled cells for expression of immunoreactivity for two calcium-binding proteins that have been reported to be abundantly expressed in the midline thalamus namely, calretinin (CR) and calbindin (CB)[6–8]. Nearly half of the labelled neurons expressed calbindin (CB+, 45.6%, n = 36) or calretinin (CR+, 49.4%, n = 39), showing that such neurochemical markers detect a large fraction of midline thalamic neurons (Supplementary Table 1). Neurons expressing combinations of CB and CR could be found in most nuclei across the midline thalamus (Fig. 1, Table 1). The expression of CR and CB largely overlapped in our neuronal sample. Indeed, nearly half of labelled neurons co-expressed both markers (47.7%, Table 1). Furthermore, neither the expression of CB nor CR was associated with distinct morphological somatodendritic distributions (i.e., "radiate" or "bushy") in thalamic midline neurons (Supplementary Figure 2).

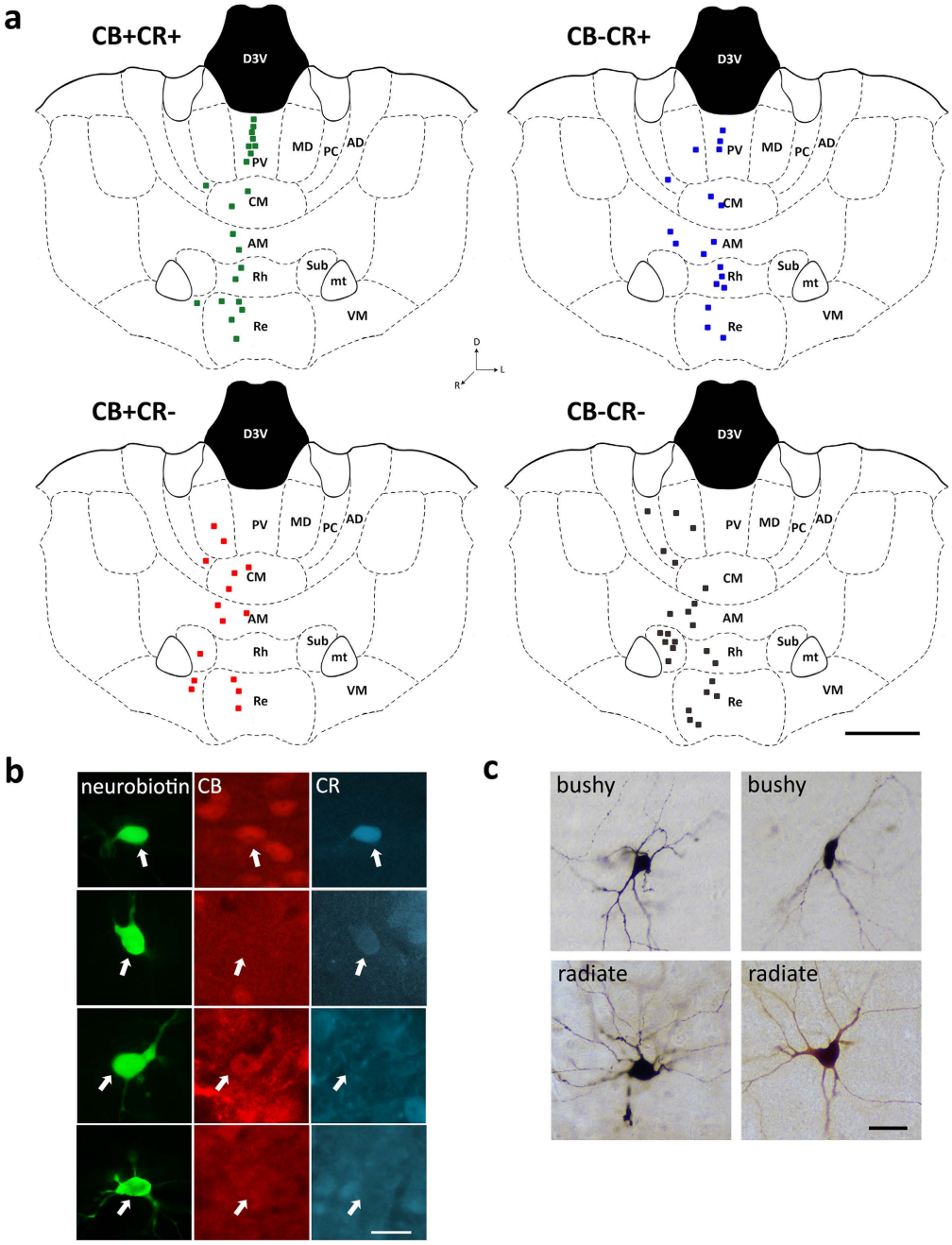

Figure 1. Anatomical location, neurochemical profile, and somatodendritic distribution of recorded midline thalamic neurons. (**a**) Coronal views of four identical plates containing the sample of identified neurons (n = 79), separated according to the expression of CB and CR (plus (+) and minus (−) symbols depict immunopositive and immunonegative cells, respectively). Shown is the anatomical location and molecular markers expressed in midline thalamic neurons based on the mouse brain atlas (adapted from plate 39[39]). CR+CB+, n = 21 cells; CR+CB−, n = 18 cells; CR−CB+, n = 15 cells; CR−CB−, n = 25 cells. One labelled cell (ED14c2, recorded in PT; CB−CR−) is not shown in this figure for it was located in distant anteroposterior coordinates (plate 34). AD, anterodorsal nucleus; AM, anteromedial nucleus; CM, centromedial nucleus; MD, mediodorsal nucleus; mt, mammillothalamic tract; PC, paracentral nucleus; PT, paratenial nucleus; PV, paraventricular nucleus; Re, reuniens nucleus; Rh, rhomboidal nucleus; Sub, submedial nucleus; VM, ventromedial nucleus. (**b**) Examples of diverse neurochemical profiles for the recorded and labelled thalamic neurons (arrows). Note top cell is CB+CR− (RC20c3, recorded in CM), middle cells are CB−CR+ (AL58c3, recorded in PV) and CB+CR+ (AL63c2, recorded in VM), bottom cell is CB−CR− (RC20c2, recorded in Sub). (**c**) Examples of somatodendritic distributions of DAB horseradish peroxidase product-labeled thalamic cells that were recorded and labelled *in vivo* (Supplementary Figure 2). Top panels; examples of "bushy" cells (left; AL53c7, recorded in AM; and right; AL35c2, recorded in MD). Bottom panels, examples of "radiate" cells (left; AL19c1, recorded in AM; and right; ED01c3, recorded in Re). Scale bars: (**a**) 1 mm; (**b,c**) 25 μm.

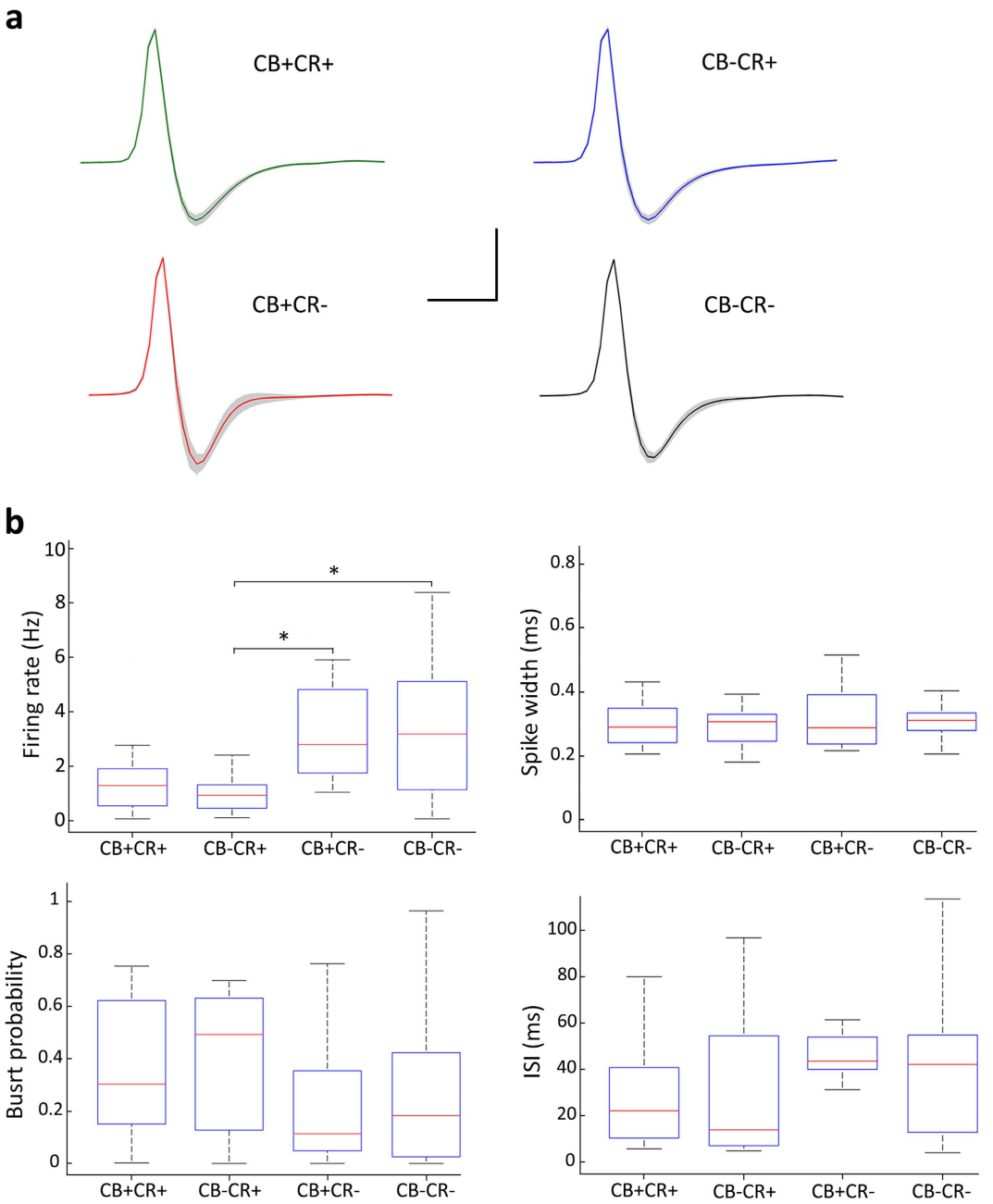

Figure 2. Basic action potential parameters of identified neurons in the midline thalamus. (**a**) Average action potential waveforms from thalamic neuronal populations as defined by their expression of neurochemical markers. Note that spike waveforms are consistently similar between neuronal populations. (**b**) Box plot representations of activity parameters from midline thalamic neurons calculated from the entire recording session. Note differences between CR+ and CR− cells only for spontaneous firing rates. Other parameters were not significantly different. CR+CB+, n = 21 cells; CR+CB−, n = 18 cells; CR−CB+, n = 15 cells; CR−CB−, n = 25 cells. One way ANOVA was used to assess for significant effects between cell populations, and significant differences (asterisks (*), $p < 0.05$) were then identified post hoc using Tukey's test (CR+CB− and CR−CB+, $p = 0.031$; CR+CB− and CR−CB−, $p = 0.046$). Scale bar: horizontal 1 ms, vertical 0.5 mV.

Hence, both proteins CB and CR were widely represented in the midline thalamus, and their combinatorial expression defined four neurochemical populations (Table 1).

Calretinin-expressing neurons exhibit low levels of spontaneous activity. We next quantitatively compared basic physiological parameters of the recorded neurons *in vivo*. Action potential waveforms were similar among the diverse neurochemically defined cell populations (Fig. 2a). We also compared the firing patterns based on the inter-spike intervals that neurons discharged, and found no apparent differences. Thalamic neurons operate in complementary functionally distinct firing modes; namely, tonic or bursting[41,42]. Consequently, we

		CB+ cells	CB− cells	P	CR+ cells	CR− cells	P
Firing rate	mean (Hz)	2.63 ± 0.43	2.57 ± 0.35	0.7453	1.64 ± 0.29	3.52 ± 0.41	***0.00009***
	n	*36*	*43*		*39*	*40*	
	theta oscillations (Hz)	3.31 ± 0.68	4.49 ± 0.87	0.4722	1.68 ± 0.40	6.05 ± 0.87	***0.00026***
	n	*28*	*32*		*29*	*31*	
	non-theta episodes (Hz)	2.56 ± 0.42	2.46 ± 0.33	0.8171	1.67 ± 0.30	3.32 ± 0.38	***0.00012***
	n	*36*	*43*		*39*	*40*	
Burst discharge	burst probability	0.29 ± 0.04	0.32 ± 0.04	0.7330	0.39 ± 0.04	0.24 ± 0.04	***0.0122***
	spikes/burst	2.71 ± 0.09	2.61 ± 0.09	0.3578	2.58 ± 0.09	2.72 ± 0.09	0.3357
	burst ISI (ms)	3.93 ± 0.15	3.95 ± 0.16	0.6585	4.15 ± 0.14	3.77 ± 0.16	***0.0466***
	n	*33*	*37*		*32*	*38*	

Table 2. Discharge parameters of identified neurons in the midline thalamus. Exact Mann–Whitney *U* test was used for statistical comparisons between populations. Significant differences were accepted at $p < 0.05$. Values are mean ± SEM.

sought to compare bursting discharge modes between the neurochemically defined cell populations, and found that the proportion of action potentials discharged in bursts (i.e.; burst probability) was not significantly different between the neuronal populations defined by neurochemical profile, during the entire recording session. We then evaluated neuronal activity in the midline thalamus by comparing the mean firing rate between neuronal populations during the entire recording session. Thus, we observed a difference in spontaneous activity levels. Indeed, on average, CR+ neurons had significantly lower firing rates than CR− cells (Fig. 2b). Given the fact that the expression profile of CB was seemingly uncorrelated with differences in baseline activity levels of midline thalamic neurons, we decided to perform further analysis focusing on the expression profiles of a single calcium-binding protein at a time (i.e.; CR or CB). Consequently, by sorting cells based solely on their expression of CB, we could define two populations with similar number of neurons (Table 2). In that case, we detected no significant differences in the mean firing rate of cells for both groups in CB+ and CB− neurons (Fig. 3a,c). In contrast, by reanalyzing the same neuronal pool, we confirmed a significantly lower mean firing rate of CR+ neurons when compared with CR− cells (Fig. 3b,c). The differences in firing rate were consistent over time, as they could be detected for the entire duration of physiological recordings (Fig. 3d). Importantly, differences detected in the population were cot found locally in the different midline thalamic nuclei, possibly due to the sample size (Supplementary Figure 3). We then compared the structure of burst discharges in midline thalamic neurons (Table 2). We found that CR+ neurons exhibited an overall higher proportion of burst discharges than CR− neurons (Table 2). This is consistent with the tendency seen in Fig. 2b for burst probability. Hence, our results suggest that there are consistent physiological differences associated to the expression profile of CR in midline thalamic neurons, with CR+ cells being less active, but more "bursty", than CR− cells.

Calretinin-expressing neurons are not robustly recruited during hippocampal theta oscillations. To obtain further insight in and provide context to the different levels of activity in midline thalamic neurons, we next focused on distinct brain states and their associated cortical network oscillations (Table 3). To study correlated patterns of activity between the hippocampus and thalamus, we recorded simultaneously the LFP from the dorsal CA1 and single cell activity from the midline thalamus. Most hippocampal recordings in our experimental conditions (75.9%, n = 60; Supplementary Table 2) presented non-theta periods with spontaneous transitions to theta oscillations (Fig. 4). During hippocampal theta oscillations, nearly half of midline thalamic neurons (53.3%, n = 32) increased their firing rate (121 ± 128% increase, range: 12–694%). Accordingly, we examined if the expression of CR or CB was related to changes in the spike timing of thalamic cells during theta oscillations. There were examples of individual cells dramatically increasing their activity during theta oscillations, and those neurons could be either CB+ (Fig. 4a) or CB− (Fig. 4b). As a population, both CB+ and CB− cells seemed to have the tendency to discharge more during theta oscillations. However, that trend was not statistically significant (Fig. 4e). Hence, the expression of CB held no apparent relation with the spike timing of midline thalamic cells during theta oscillations. Interestingly, when the same neuronal pool was sorted based on the expression of CR, a clear pattern emerged. Indeed, only the activity of CR− neurons was significantly modulated by hippocampal theta oscillations, as transitions between network states were associated with changes in their discharge rate (Fig. 4d,f). Conversely, CR+ neurons did not change their firing rate during theta oscillations (Fig. 4c,e). Furthermore, the firing rates of CR+ and CR− were significantly different during both theta ($p = 2.57 \times 10^{-4}$) and non-theta ($p = 1.19 \times 10^{-4}$) oscillations, with CR− cells being more active in both network states (Fig. 4f), consistent with their overall higher activity levels described above (Fig. 3). The apparent absence of brain state dependency in the activity levels of CR+ neurons (i.e., during theta and non-theta epochs) could be due to differences in the global network states during which the different neuronal populations (i.e., CR+ vs. CR− cells) were recorded. In order to assess this possibility, we compared basic parameters (i.e., frequency and power) of the brain states associated to the different neuronal populations that we characterized. Our analysis did not reveal any significant difference between brain states, suggesting that differences in neuronal activity were likely related to properties intrinsic to the neuronal populations, rather than global differences in network states (Table 3).

Since many thalamic neurons were active during hippocampal theta waves, we sought to establish if thalamic cells exhibited any phase preference to the oscillation. Even though CR− cells significantly increased their activity

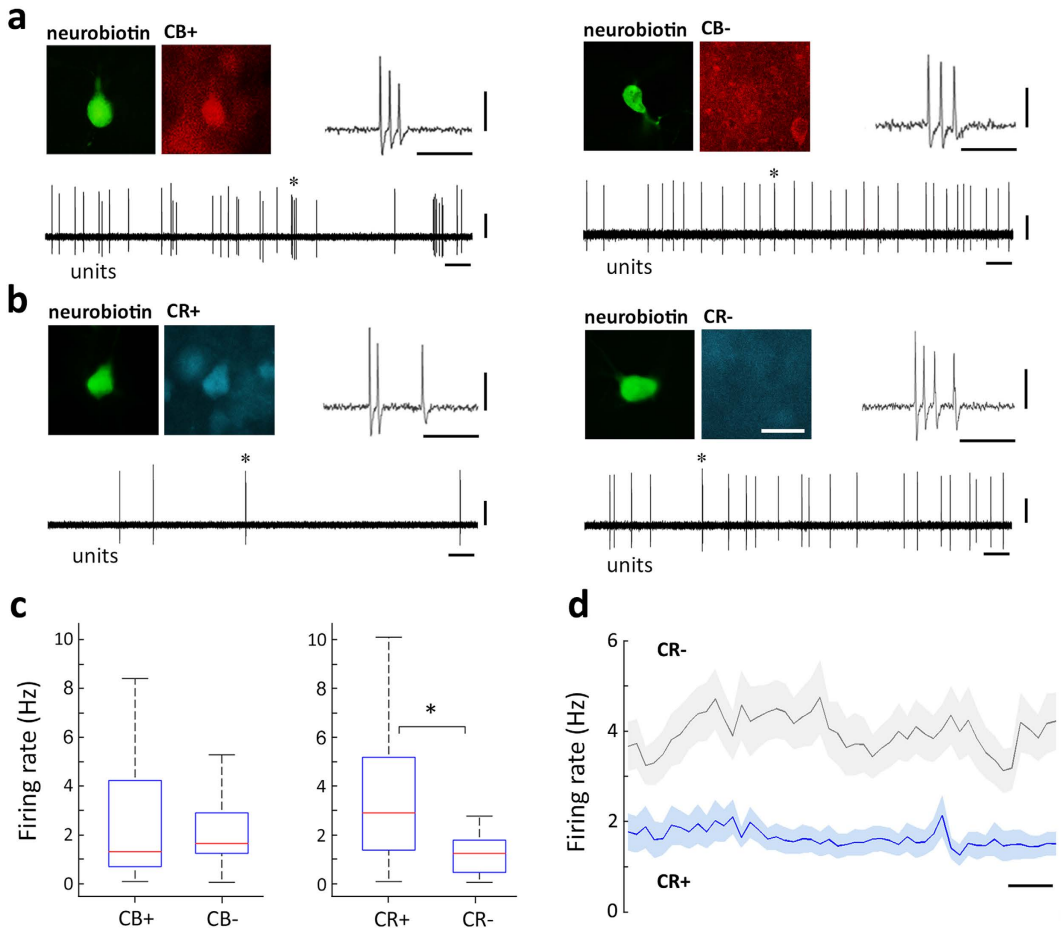

Figure 3. Spontaneous firing patterns of identified neurons in the midline thalamus. (**a**,**b**) Firing patterns and fluorescent micrographs showing immunoreactivity for CB (**a**) or CR (**b**) in four identified midline thalamic neurons, recorded in Re (AL24c1, left) and PC (AL40c2, right) for (**a**) and PV (ED22c7, left) and CM (AL58c5, right) for (**b**). Immunoreactivity for CB and CR is not shown in all cases for clarity; yet AL24c1 and AL40c2 were CR−; whereas AL58c5 and ED22c7 were CB+ (Supplementary Figure 6). Asterisks (*) depict example spike burst, expanded in the inset. (**c**) Box plot representations of the population data show no statistically significant difference in the spontaneous overall mean firing rates of cells when they were separated on the basis of the expression of CB (Mann-Whitney U test, $p = 0.745$; CB+, n = 36 cells; CB−, n = 43 cells); however, there was a statistically significant difference in the spontaneous mean firing rates when cells from the same pool were sorted according to the expression of CR (Mann-Whitney U test, $p = 8.94 \times 10^{-5}$, CR+, n = 39 cells, CR−, n = 40 cells). (**d**) Time resolved spontaneous discharge of thalamic neurons recorded in different sessions and animals sorted by their expression of CR. Time zero marks the onset of recording session for each neuron. Note consistent difference in firing rates between CR+ and CR− cells over time. Average ± SEM. CR+, n = 37 cells; CR−, n = 39 cells. Binsize, 10 s. Scale bars: (**a**) micrographs 25 μm; burst insets, horizontal 25 ms, vertical 0.5 mV; units, horizontal 1 s, vertical 0.5 mV; (**d**) 50 s.

during theta episodes, only a fraction of them was phase coupled to the oscillatory cycles (Fig. 5). Indeed, the spike timing of one third of CR− neurons (35.5%, n = 11) was significantly phase-modulated during theta oscillations (Rayleigh test, $p < 0.05$). To quantify the depth of modulation, we computed a normalized vector sum of the theta phase angles of all spike times for each cell, where the vector length and angle represent depth of modulation and preferred phase, respectively. Our analysis revealed that, on average, CR− cells were weakly modulated and did not exhibit a marked phase preference during theta oscillations ($r = 0.13 \pm 0.08$, phase = 68 ± 66.3°, n = 11). In fact, the discharge of a significantly smaller fraction (binomial test, $p = 0.026$) of CR+ neurons (21%, n = 6) was also modestly modulated during theta oscillations (Rayleigh test, $p < 0.05$), with similar characteristics to CR− cells ($r = 0.15 \pm 0.07$, phase = 81.1 ± 70.6°, n = 6). Theta-modulated cells did not exhibit any particular anatomical location (Supplementary Figure 4). Finally, we examined the neuroanatomical location of the theta-modulated neurons and established that they were widely distributed along the dorsoventral axis of the midline thalamus, and thus, were not associated to any specific nucleus or region (Fig. 5f). Thus, our results suggest that CR− midline thalamic neurons are actively engaged during hippocampal theta waves, whereas CR+ neurons, with lower baseline activity levels, are not strongly recruited by the oscillatory episodes. Overall, the

		CB+ cells	CB− cells	p	CR+ cells	CR− cells	p
Theta oscillations	Frequency (Hz)	5.03 ± 0.06	5.21 ± 0.08	0.1846	5.15 ± 0.09	5.11 ± 0.07	0.8014
	Power (mV/Hz)	7.35E-6 ± 1.13E-6	7.04E-6 ± 1.24E-6	0.5937	7.51E-6 ± 1.34E-6	6.88E-6 ± 1.06E-6	0.7786
	n	*28*	*32*		*29*	*31*	
Non-theta epochs	Frequency (Hz)	1.64 ± 0.11	1.69 ± 0.10	0.7941	1.74 ± 0.11	1.60 ± 0.09	0.3076
	Power (mV/Hz)	1.39E-4 ± 2.70E-5	1.41E-4 ± 2.60E-5	0.9372	1.27E-4 ± 2.47E-5	1.53E-4 ± 2.80E-5	0.3465
	n	*36*	*43*		*39*	*40*	
Sharp wave-ripples	Frequency (Hz)	102.28 ± 2.62	97.59 ± 2.37	0.2556	100.45 ± 2.66	99.03 ± 2.37	0.7799
	Power (z-score)	3.30 ± 0.18	3.53 ± 0.12	0.5190	3.65 ± 0.16	3.60 ± 0.13	0.9180
	n	*36*	*43*		*39*	*40*	

Table 3. Characteristics of brain states as defined by network oscillations in the hippocampus. Exact Mann–Whitney *U* test was used for statistical comparisons between populations. Significant differences were accepted at $p < 0.05$. Values are mean ± SEM.

spike timing of a sizable fraction of midline thalamic neurons (28.3%, n = 17) was significantly modulated by hippocampal theta oscillations, yet neither the strength of modulation or phase preference were robust (Fig. 5e).

Calretinin-expressing neurons are inhibited during hippocampal sharp wave-ripples. In our recordings, hippocampal ripples were reflected as short periods of high-frequency activity, taking place exclusively during non-theta epochs. In order to assess the spike timing of individual thalamic neurons with respect to ripple oscillations, we computed the normalized cross-correlation function between simultaneously recorded hippocampal ripples and the action potentials of individual neurons in the midline thalamus, considering the onset of ripple episodes as time reference (Fig. 6). All midline thalamic neurons seemed to slightly increase their discharge probability just before the onset of sharp wave-ripples (Fig. 6a–c). We then reanalyzed the same neuronal pool, but distinguished neurons based on their expression of CR. Hence, we found that CR− neurons did not exhibit major changes in their discharge probability during sharp wave-ripples. In contrast, the spike timing of CR+ neurons was significantly modulated by sharp wave-ripples (Fig. 6d–f). Indeed, the firing rate of CR+ cells was significantly inhibited during ripple episodes; and slightly activated immediately before and after the high frequency episodes (Fig. 6f). Importantly, the temporal correlation between thalamic discharge and hippocampal ripples was not the result of co-modulation by slow oscillatory activity characteristic of non-theta epochs[43,44], as spurious contributions were controlled by shuffling and subtracting surrogate data (see Methods). Hence, these results show that the discharge probability of CR+ neurons in the midline thalamus is selectively modulated during sharp wave-ripples.

Discussion

By recording and labeling individual neurons in anesthetized mice, we show here evidence for functionally distinct neuronal populations in the midline thalamus. Indeed, our anatomical and physiological characterization leads us to propose that at least two different populations of midline thalamic projection cell deliver differential synaptic output to cortical targets according to ongoing brain states as defined by hippocampal activity. Our data show that rather than anatomical location, a major defining feature in the physiological properties of midline thalamic neurons is the expression of CR, a calcium-binding protein. Hence, distinct thalamic neuronal populations, identified by the somatic expression of CR, are differentially regulated by hippocampal pathways during network rhythms associated to behavioural contexts, likely supporting different stages of memory processing.

Midline thalamic nuclei give rise to large glutamatergic axon terminals that densely distribute within frontal and temporal cortical lobes[27,45]. It has been reported that a dense fiber plexus located in the entorhinal cortex contains both CR and vesicular glutamate transporter 2 in the same axons. Complementary retrograde tracing experiments found labeled cell bodies in the nucleus reuniens co-expressing CR[46]. Our results show that CR+ cells are widely expressed across the midline thalamus, and given their anatomical and physiological features suggest that they are likely to be glutamatergic projection cells[1]. Cortical projections from the midline thalamus are not homogeneous across nuclei. Indeed, neurons in dorsal structures preferentially target the medial prefrontal cortex, with little input to the medial temporal lobe[5,24]; neurons in middle regions, project almost exclusively to the medial prefrontal cortex[24,47]; whereas neurons in ventral areas, project mostly to the parahippocampal cortex, with less significant projections to the medial prefrontal cortex[24,27]. Thus, the anatomical organization of synaptic output from the midline thalamus is not homogeneous, with every nucleus displaying distinct efferent connectivity patterns. Interestingly, our results suggest that a major feature in defining the activity pattern of thalamic neurons is not their nuclear location, but the expression profile of calcium-binding proteins, particularly CR.

The different neuronal activity patterns that we describe could be related to the expression of dissimilar intrinsic membrane properties in the midline thalamus. Indeed, we found lower overall spontaneous firing rates and higher proportions of burst discharges in CR+ neurons compared to CR− cells. Both features would be consistent, for example, with more hyperpolarized baseline membrane potential or higher input resistance in CR+ neurons[42]. Further experiments will have to test this possibility with intracellular recordings *in vivo*. Compared to parvalbumin, CR and CB are considered slow Ca^{2+} buffers[10]. Our results suggest that neither of these calcium-binding proteins influences the shape of the action potential, since spike waveforms were similar across thalamic neurons, regardless of their CR or CB expression profile. Nonetheless, both the firing rate and

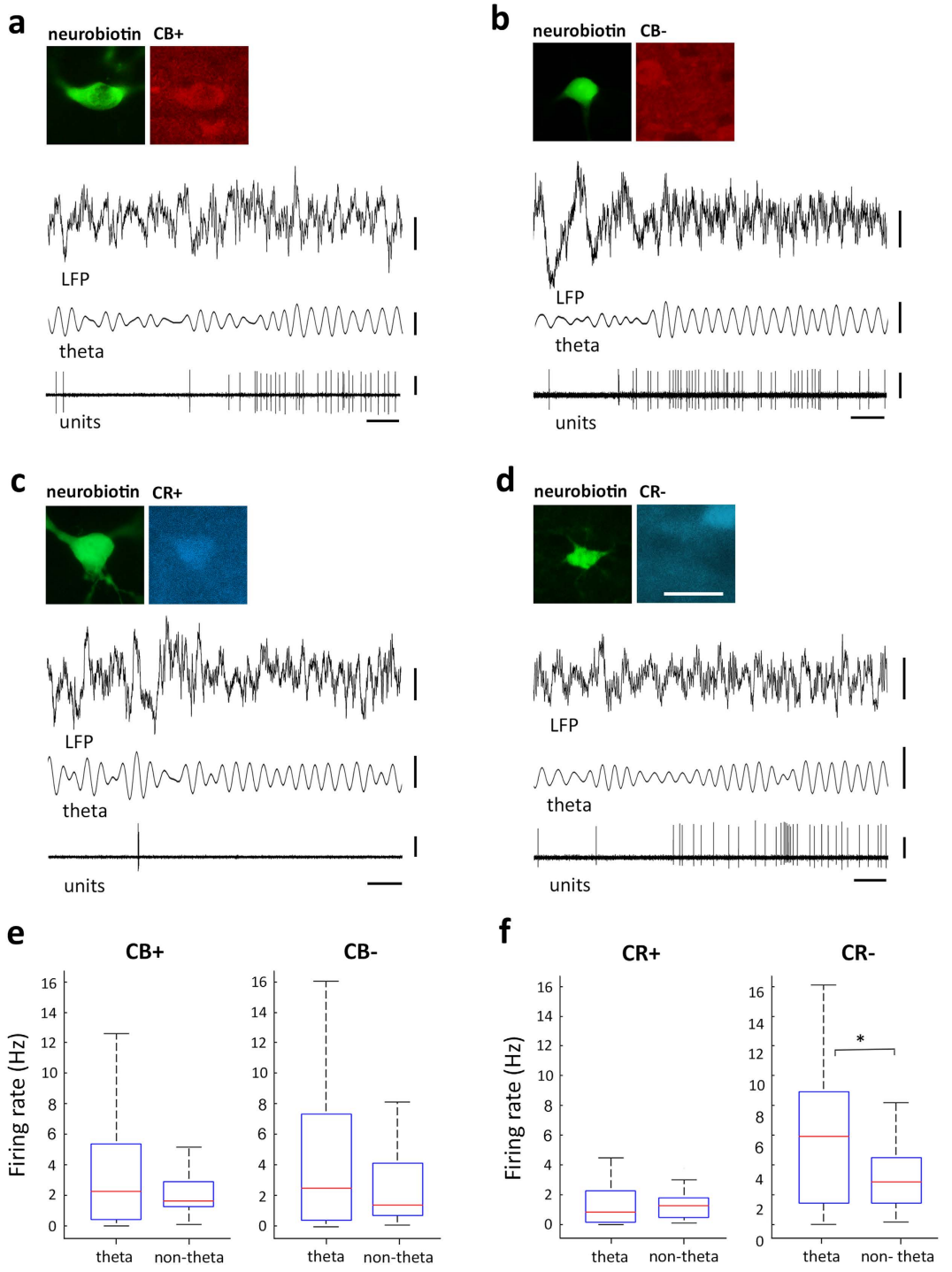

Figure 4. Spike timing of identified neurons in the midline thalamus during transitions to hippocampal theta oscillations. Firing patterns of a midline thalamic CB+ cell (**a**) and a CB− cell (**b**) recorded in VM (AL40c1) and in Sub (AL26c2), respectively. Single cell activity (unit, 0.3–5 kHz) is shown for the transition from non-theta epochs to theta oscillations recorded in the dorsal CA1 area (LFP, 0.3–300 Hz). Theta oscillations are evidenced by LFP filtering (theta, 4–8 Hz) and were automatically detected (see Methods). Note both cells largely increasing their activity during theta oscillations. Immunoreactivity for CR is not shown for clarity; yet AL40c1 and AL26c2 were CR− (Supplementary Figure 6). Firing patterns of a CR+ cell (**c**) and a CR− cell (**d**) recorded in Rh (AL27c3) and Re (AL23c3), respectively. Immunoreactivity for CB is not shown for clarity; yet AL27c3 was CB+ and AL23c3 was CB− (Supplementary Figure 6). Box plot representations of mean firing rates for midline thalamic neurons separated according to the expression of CB (**e**) or CR (**f**). Note that differences in firing rates between non-theta epochs and theta oscillations were significant (asterisk (*)) only for CR−cells. (Wilcoxon signed-rank test, $p = 8.64 \times 10^{-4}$). CB+, n = 28 cells; CB−, n = 32 cells; CR−, n = 29 cells; CR−, n = 31 cells. Scale bars: micrographs 25 μm; recordings, horizontal 500 ms, vertical 0.5 mV.

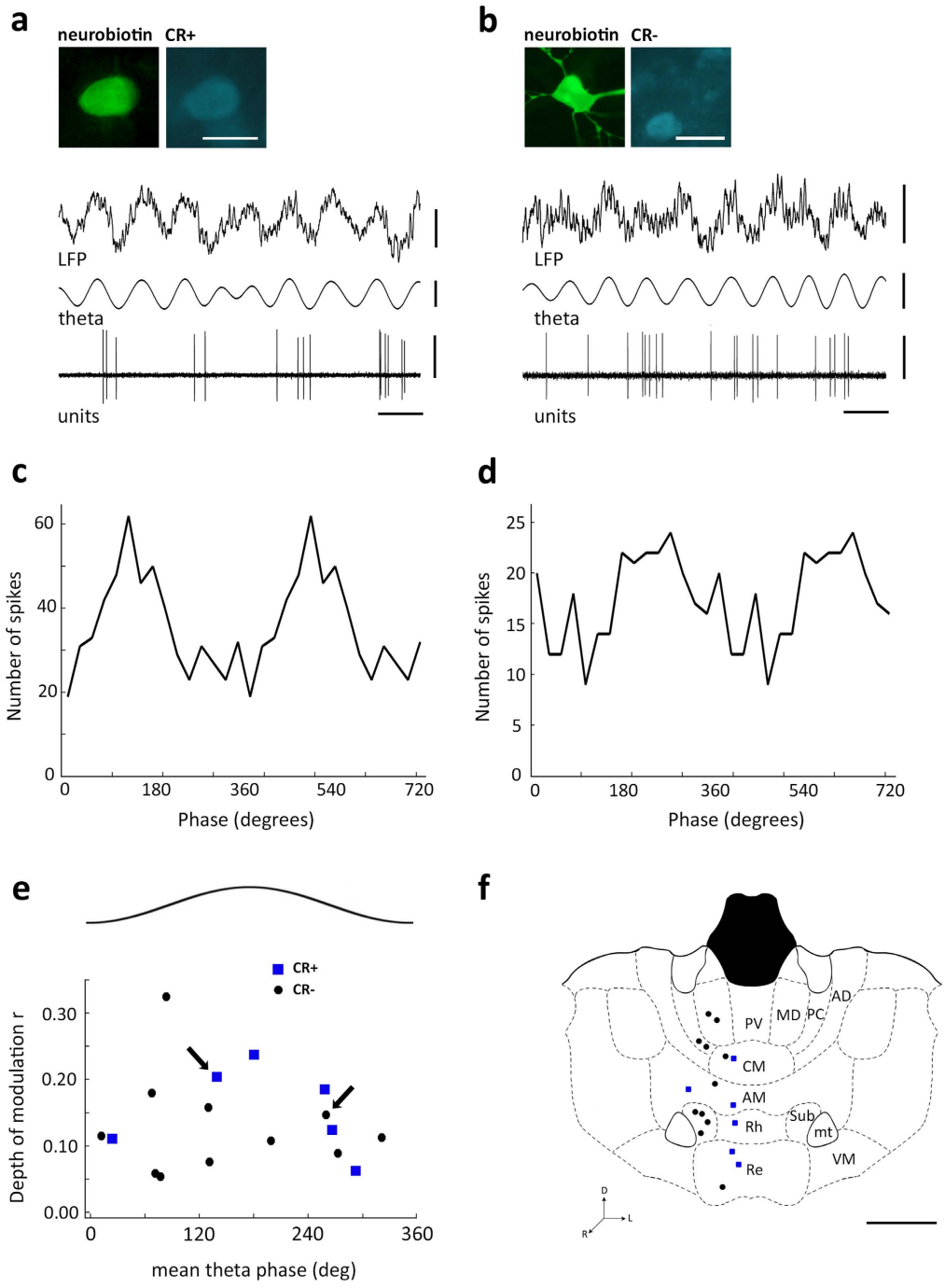

Figure 5. Phase modulation of midline thalamic neurons during hippocampal theta oscillations. (**a**,**b**) Examples of spike timing from a midline thalamic CR+ cell (**a**) and a CR− cell (**b**) in Re (ED15c3) and PC (RC14c2), respectively; recorded during theta oscillations in the dorsal CA1 area (LFP, 0.3–300 Hz). Theta oscillations are evidenced by LFP filtering (theta, 4–8 Hz). Immunoreactivity for CB is not shown for clarity; yet both ED15c3 and RC14c2 were CB+ (Supplementary Figure 6). (**c**,**d**) Examples of theta phase firing probability histograms for the cells depicted in (**a**,**b**) respectively. The same data are repeated in two cycles for theta histograms to indicate oscillations. The trough of the extracellularly recorded oscillations in dorsal CA1 stratum pyramidale are at 0°, 360° and 720°; bin size: 20°. (**e**) Theta-modulated firing of midline thalamic neurons characterized by the depth of modulation (r) and the mean preferred theta phase angle for each identified cell significantly modulated (Rayleigh test, $p < 0.05$). The trough and peak of the field theta cycle are at 0° and 180°, respectively. Blue squares, CR+ (n = 6 cells); black circles, CR− (n = 11 cells). Arrows depict data for example histograms from (**b**,**c**). Histograms of average theta phase discharge probability for neurons (Supplementary Figure 5). (**f**) Coronal view of anatomical location of theta-modulated neurons collapsed in one medial plane based of the mouse brain atlas (plate 39[39]). Color code as in (**e**). Scale bars: (**a**) micrographs 25 μm, LFP 0.5 mV, theta 0.2 mV, units 1 mV, horizontal 250 ms; (**f**) 1 mm.

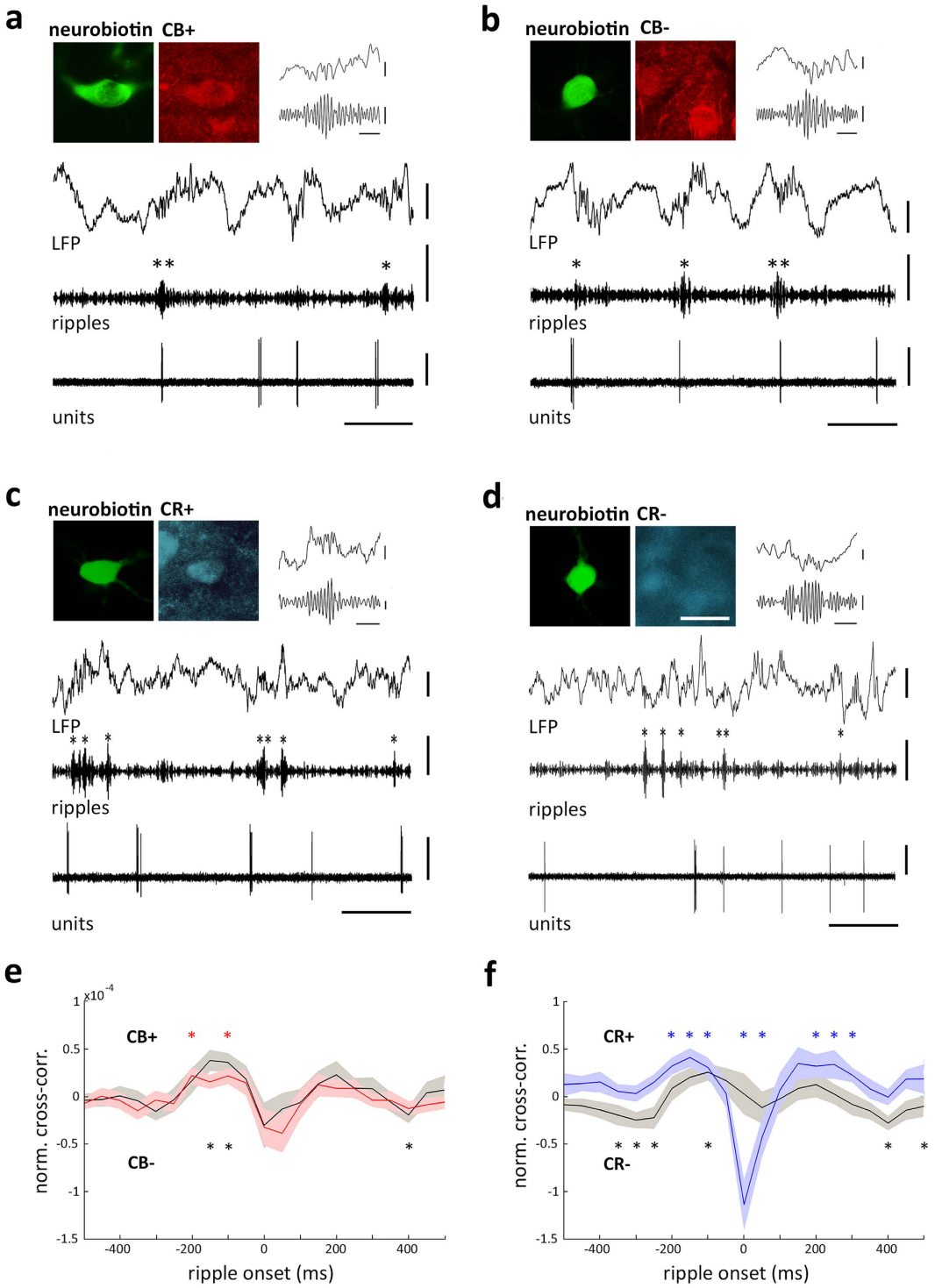

Figure 6. Spike timing of identified neurons in the midline thalamus during hippocampal ripple oscillations. (**a**,**b**) Firing patterns of a midline thalamic CB+ cell (**a**) and a CB− cell (**b**) recorded in VM (AL40c1) and in AM (AL43c1), respectively. Single cell activity (units, 0.3–5 kHz) is shown during non-theta epochs in the dorsal CA1 area (LFP, 0.3–300 Hz). Sharp wave-ripples are evidenced by LFP filtering (ripples, 100–200 Hz). Sharp wave-ripples were detected by filtering and thresholding (see Methods). Single asterisk (*) depict ripple episodes and double asterisks (**) show ripple episodes expanded in insets. Note both cells occasionally discharged in coincidence with hippocampal ripples. Immunoreactivity for CR is not shown for clarity; yet AL40c1 and AL43c1 were CR− (Supplementary Figure 6). (**c**,**d**) Firing patterns of a CR+ cell (**c**) and a CR− cell (**d**) recorded in CM (ED16c5) and Re (RC17c2), respectively. Immunoreactivity for CB is not shown for clarity; yet ED16c5 and RC17c2 were CB+ (Supplementary Figure 6). (**e**,**f**) Normalized cross-correlation (norm. cc) functions between ripples onset and the spike timing of neurons sorted by the expression of CB (**e**) or CR (**f**). Note that neurons when separated into CB+ and CB− populations exhibited similar dynamics during ripple episodes; whereas when using the expression profile of CR, CR+ cells were significantly

modulated during ripple episodes. Asterisks (*) depict individual time-points with statistically significant differences from shuffling (Wilcoxon signed-rank test, $p < 0.05$). Shufflings were controlled for spurious correlations (see Methods). Light areas illustrate standard error for each distribution. In (**e**), Gray and black lines depict average cross-correlograms for CB+ (n = 28 cells) and CB− (n = 37 cells), respectively; whereas in (**f**), Gray and black lines depict average cross-correlograms for CR+ (n = 27 cells) and CR− (n = 38 cells), respectively. Binsize, 50 ms. Scale bars: micrographs 25 μm; LFP 0.5 mV; ripples 0.2 mV; units 0.5 mV; horizontal 500 ms; inset ripples, LFP 0.25 mV, ripples 0.05 mV, horizontal 50 ms.

burst incidence of thalamic neurons were correlated with the expression of CR. This does not mean that CR directly affects the biophysical process of spiking discharge, but it reveals a neurochemical correlate of physiological activity which might be useful in the future to define thalamic cell types. Indeed, the expression of CB and CR has proved to be useful to define cell types in other brains structures such as neocortex[14], hippocampus[13], striatum[48] and cerebellum[49].

The diverse activity patterns detected in midline thalamic neuronal populations could be the result, at least in part, of differential dynamics in synaptic input provided by anatomical innervation arrangements from the hippocampal projection system. Indeed, the subicular formation represents the main output station of the hippocampus and projects extensively to the midline thalamus via the dorsal fornix, reaching bilaterally the reuniens, anteromedial, paraventricular and submedius nuclei[29–31]. Previous studies have found that anterior thalamic nuclei are modulated by hippocampal theta rhythms, likely via subicular projections[25,50,51]. The ultrastructural organization of the subicular input to the midline thalamus has not been documented in detail. Nevertheless, based on our physiological data, it could be reasonable to speculate that a large proportion of subicular axons terminate directly onto CR− neurons, exciting them during hippocampal theta oscillations. Another plausible option for the relay of theta oscillations is the input provided by the entorhinal cortex, which also projects extensively to most of the midline thalamic nuclei[52] and expresses robust theta oscillations that are coherent with hippocampal activity[53]. Additional theta-modulated synaptic drive may arise from the medial prefrontal cortex. Based on connectivity patterns, this could seem as a natural alternative, given the prominent innervation provided by the medial prefrontal cortex to the midline thalamus[54,55]. Nonetheless, the origin of theta oscillations in the medial prefrontal cortex is controversial, as the rhythm is not concurrently expressed in the hippocampus and medial prefrontal cortex[34,56] and there is evidence that theta waves in prefrontal cortex are the result of volume conduction[57]. Conversely, other studies have suggested that theta waves are synaptically generated in the prefrontal cortex and can synchronize with hippocampal rhythms[58–60]. Certainly, the previous possibilities are not exclusive, and a combination of them could operate concurrently in delivering theta oscillatory information to the midline thalamus during active behavior. Indeed, during theta oscillations, the entorhinal performant path strongly drives hippocampal activity[61,62], thus likely contributing to the theta-modulated subicular output to the midline thalamus. Overall, our results show that the theta rhythm can effectively reach the midline thalamus as it is capable of modulating both the discharge rate and phase-coupling of neuronal activity. Both of these elements might contribute to propagate memory signals and synchronize cortical targets during spatial exploration[33,36].

On the other hand, the hippocampal theta rhythm impinging on the midline thalamus is likely to be supplemented by increased cholinergic tone arising from dense pedunculopontine[63] and laterodorsal tegmental[64] projections, which are known to robustly stimulate the thalamus during activated states[65]. An additional mechanism to explain the differential recruitment of thalamic neurons during hippocampal theta oscillations could be related to different expression profiles of muscarinic and nicotinic receptors associated to the expression of CR. Indeed, cholinergic receptors are abundantly expressed in the thalamus[66,67]; yet, it is currently unknown if they are segregated in different neuronal populations. Differential expression of cholinergic receptors would be consistent with *in vitro* and *in vivo* data showing wide ranging effects of acetylcholine in thalamic neurons that were not anatomically identified[68–71]. On other hand, compared to anesthesia preparations the number of theta-modulated neurons is likely to be different in the awake state as the systemic level of neuromodulators is much higher and the network will be actively engaged in faster rhythms. Moreover, different thalamic nuclei show distinct synaptic connectivity, and are accordingly expected to be active during different behavioural contexts[5]. Interestingly, studies in identified neurons in the basal forebrain[72], hippocampus[73], and barrel cortex[74,75] have shown that the spike timing is preserved in relation to network oscillations in anesthesia and wakefulness. This is remarkable given that the frequency of network oscillations is faster and the average neuronal firing rates are much higher in awake animals as compared to anesthetized preparations. This suggests a tight control of network structured activity patterns across a wide dynamic range. Thus, we expect that similar results should hold for the thalamus.

Sharp wave-ripple episodes represent another hallmark hippocampal activity pattern, that is prominent during non-theta states[76,77] and associated to episodic memory consolidation[78–81]. Ripples are locally generated in the hippocampus, but robustly propagate to the cortex[37,82] and produce global effects[37,83], thus defining a brain state. Our data also shows that sharp wave-ripples exert a differential impact on midline thalamic neurons. Recent experiments used NET-fMRI in monkeys to identify the brain areas that consistently modified their activity in relation to sharp wave-ripples. The study showed that ripples were tightly associated with robust cortical activations that occur concurrently with extensive activity suppression in subcortical territories, including: thalamus, basal ganglia, cerebellum, and midbrain–brainstem neuromodulatory structures[83]. Interestingly, our results confirm that the midline thalamus is, at least partially, inhibited during sharp wave-ripples. Moreover, our data suggest that CR+ cells are particularly modulated during sharp wave-ripples as their activity is selectively inhibited. Interestingly, right after the end of ripples, CR+ cells exhibited a small, yet significant, increase in spiking activity, similar to burst rebound responses after active synaptic thalamic inhibition[84]. Since rodents virtually lack GABAergic thalamic interneurons[85], it reasonable to propose that the zona incerta, the main inhibitory drive of

the midline thalamus[86], might be selectively recruited during hippocampal ripples to control synaptic activity of particular domains, in this case, specific neuronal populations, of the midline thalamus.

Memory formation and decision-making largely depend on the coordinated interaction of the medial temporal lobe and medial prefrontal cortex[87,88]. It has been proposed that the medial prefrontal cortex provides context information to the medial temporal lobe during learning and retrieval of position-dependent memories. Similarly, the medial prefrontal cortex could make memory-based inferences by retrieving memories from the medial temporal lobe[89]. We propose that coupling between these multiple oscillatory systems may be a mechanism exploited by the thalamus for linking the medial prefrontal cortex, dedicated to planning and execution, with the medial temporal lobe, dedicated to memory formation and context representation. According to our data the midline thalamus might not be directly associated with the process of memory consolidation, which takes place during sharp wave-ripples, a result consistent with previous data[83]. On the contrary, midline thalamic activity might be detrimental to the process as it seems to be actively inhibited. During theta oscillations, when memory encoding occurs, the activation of a particular thalamic cell population seems to be required to increase cortical excitatory drive. Although at present we do not know the functional consequences of the selective activity patterns displayed by CR+ and CR− cells in the midline thalamus, it is important to remark that they could provide the basis for a differential thalamic contribution to particular stages of memory processing, with CR− neurons being activated by theta oscillations during memory encoding, whereas CR+ neurons are actively inhibited by sharp wave-ripples during memory consolidation. These observations provide support to the presence of specialized neuronal classes in the thalamus, thus sustaining differential synaptic flow between prefrontal medial and temporal lobes[45,90], necessary for memory specificity and generalization[15,17].

Methods

***In vivo* recording and labeling.** Adequate measures were taken to minimize pain or discomfort in experimental animals. Experiments were carried out in accordance with the guidelines published in the NIH *Guide for the Care and Use of Laboratory Animals* (NIH publication no. 86-23, revised 1987), and reviewed and approved by the university (Pontificia Universidad Catolica de Chile) and funding body (Comision Nacional de Investigacion Cientifica y Tecnologica) bioethics committees. Recordings were obtained from adult C57Bl/6 mice (n = 45, from either sex; 20–30 g, 15–20 weeks). Animals were anesthetized with urethane (0.8 g/kg body weight), plus supplemental doses of ketamine and xylazine (20 and 2 mg/kg, respectively) as needed; body temperature was maintained with a heating pad. The head was placed in a stereotaxic frame, the skull was exposed, and a small craniotomy (~1 mm) was made above the hippocampus (anteroposterior, −2.3 mm; mediolateral, +2.3 mm; coordinates from Bregma[39]) to insert a recording electrode at 20° degrees toward the midline. Another hole in the skull was drilled above the midline thalamus (anteroposterior, −0.8 mm; mediolateral, +0.3 mm). Neuronal activity in the midline thalamus was recorded extracellularly with a glass electrode (10–20 MΩ, *in situ* descended 3–5 mm in the dorsoventral axis) filled with 1.5% neurobiotin (Vector Laboratories) in 0.5 M NaCl, and the reference local field potential (LFP) was recorded in the hippocampus with a second glass electrode (10–20 MΩ) located as close as possible to the dorsal CA1 stratum pyramidale, for which the electrode was descended 0.8–1 mm, until ripple oscillations were visually detected online[91]. Single-unit activity and LFP (sampling rate 10 kHz) were analog filtered between 300 Hz–5 kHz and 0.3 Hz–2 kHz, respectively. All of the extracellularly-recorded thalamic cells were individually labeled with neurobiotin using the juxtacellular labeling method, only after data for the firing patterns had been sampled from the unaffected cell. Spike shape and amplitude were monitored during recording and labeling to ensure that the same cell was recorded and labeled. Two to 4 h after labeling, the mice were terminally anesthetized and cardiac perfusion with saline was followed by 20 min fixation with a fixative of 4% paraformaldehyde. Brains were extracted and sectioned coronally (60–70 μm thickness), and sections were further processed for epifluorescence microscopic visualization of labeled neurons. Location of labeled neurons was established in reference to standard brain atlas coordinates[39].

Brain-state and time-frequency analysis. We defined brain-states based on the hippocampal LFP. We recognized theta oscillations, non-theta epochs and ripple episodes, in consistency with previous studies[91]. Unless stated, the LFP from dorsal CA1 stratum pyramidale was considered as the time-frame reference for the spike-timing of recorded cells. Theta oscillations were detected by calculating the continuous ratio between the envelopes of theta (4–8 Hz) and delta (2–3 Hz) frequency bands filtered from the hippocampus LFP, and calculated by the Hilbert transform. A ratio of 1.4 SD or higher, during at least 2 s defined epochs of theta oscillations. Recording episodes outside theta oscillations were defined as non-theta epochs. To determine the phase relationship between single-cell activity and theta cycles, the local field potential during theta episodes was filtered between 4 and 8 Hz, and the troughs of the theta oscillations were detected in the filtered signals. Sharp wave-ripples were recorded in dorsal CA1, as close as possible to stratum pyramidale (Fig. 6) and considered as the time-frame reference for the spike-timing of the recorded neurons and population activity (LFP) in the thalamus. We used a recently described method for ripples detection[83] with some variation. Briefly, the hippocampus LFP was first down-sampled to 1 kHz, then band-pass filtered (100–200 Hz) using a zero phase shift non-causal finite impulse filter with 0.5 Hz roll-off. Next, the signal was rectified and low-pass filtered at 20 Hz with a 4th order Butterworth filter. This procedure yields a smooth envelope of the filtered signal, which was then z-score normalized using the mean and SD of the whole signal in the time domain. Epochs during which the normalized signal exceeded a 3.5 SD threshold were considered as ripple events. The first point before threshold that reached 1 SD was considered the onset and the first one after threshold to reach 1 SD as the end of events. The difference between onset and end of events was used to estimate the ripple duration. We introduced a 50 ms-refractory window to prevent double detections. In order to precisely determine the mean frequency, amplitude, and duration of each event, we performed a spectral analysis using Morlet complex wavelets of seven cycles. The Matlab toolbox used is available online as LANtoolbox (http://lantoolbox.wikispaces.com/).

Cross-correlation analysis. Activity of thalamic neurons and hippocampal ripples was cross-correlated by applying the "sliding-sweeps" algorithm[92]. A time window of ±1 s was defined with the 0 point assigned to the start time of a ripple. The timestamps of the thalamic spikes within the time window were considered as a template and were represented by a vector of spikes relative to t = 0 s, with a time bin of 50 ms and normalized to the total number of spikes. Thus, the central bin of the vector contained the ratio between the number of thalamic spikes elicited between ±25 ms and the total number of spikes within the template. Next, the window was shifted to successive ripples throughout the recording session, and an array of recurrences of templates was obtained.

Both thalamic timestamps and start times of ripples where shuffled by randomized exchange of the original inter-event intervals[93] and the cross-correlation procedure was performed on the pseudo-random sequence. The statistical significance of the observed repetition of spike sequences was assessed by comparing, bin to bin, the original sequence with the shuffled sequence. An original correlation sequence that presented a statistical distribution different from 100 simulated shufflings was considered as statistically significant, with $p < 0.01$ probability, instead of a chance occurrence (see *Statistics*). For every recording with a significant correlation, the average of the simulated shuffling was subtracted from the average of the correlation curve and a representative cross-correlogram was obtained. To reveal repeating event correlations through the population, all representative cross-correlogram curves were pooled together and the statistical significance of a non-zero observed value was computed (see *Statistics*).

Detection of Low-Threshold Spike bursts. Thalamic projection neurons discharge low-threshold Ca2+ spike bursts by of various species during anesthesia, natural sleep, and quiet wakefulness[41,94–96]. Previous analyses have shown that spike bursts are preceded by a silent period (50–100 ms[97]). Spike bursts were extracted according to established criteria used in extracellular unit recordings[84,98]. Accordingly, at least 2 action potentials with an inter spike interval of ≤5 ms, but with a preceding silent period of >100 ms[97]; and a maximum inter spike interval of 10 ms was used to define the end of spike burst[96].

Tissue processing and anatomical analysis. Neurobiotin-labelled cells were revealed by streptavidin conjugated with Alexa Fluor 488. Once located in the corresponding brain section, cells were photographed in other wavelengths to test for bleed through (false positives). After fluorescence testing, horseradish-peroxidase reactions for light microscopy were performed to reveal somatodendritic structure and axonal labelling, with all necessary controls, as described previously[99]. Briefly, for immunocytochemistry, sections were rinsed three times for 10 min each with phosphate buffer (PB), incubated in 1% horse serum supplemented with 0.3% Triton X-100 in PB for 1 h, and then incubated in 1:2000 dilutions of the CR (mouse, code CG1, Swant Inc.) and/or CB (rabbit, code CB-38a, Swant Inc.) antibody for 24 h at 4 °C, followed by a 1:1000 dilution of the secondary antibody for 3–6 hours at room temperature. Secondary antibodies were conjugated to Alexa Fluor 350, 488, 568, or 660 (Invitrogen); and cells were photographed with the appropriate filter cubes (Nikon; UV-2E/C, B-2E-C, G-2E/C, and Cy5-HYQ, respectively) with an epifluorescence microscope (Nikon Eclipse Ci). Antibody dilutions were performed in PB supplemented with 1% horse serum and 0.3% Triton X-100. Sections were mounted on slides with mounting medium and photographed under epiluminescence microscopy. After that, sections were dismounted and rinsed three times for 10 min each in PB, then processed with an ABC kit (Vector Laboratories). Samples were rinsed, and the peroxidase reaction was developed with 0.05% 3,3-diaminobenzidine-4 HCl (DAB) and 0.003% H_2O_2. Sections were mounted on gelatin-coated slides, air-dried, dipped in alcohol/xylene battery for development. Sections were then mounted and photographed under bright-field microscopy.

Statistics. Unless stated, all tabulated data are presented as the mean ± SD and significant differences were accepted at $p < 0.05$. For cross-correlation analysis, a Wilcoxon test was applied to compare two independent samples (rank-sum test) as well as to identify a distribution with a median equal to zero (signed-rank test). Corrected p-values with the false discovery rate method[100] were used to examine statistical significances.

Phase modulation of action potentials was determined by Rayleigh circular statistics[101]. For all circular statistical tests the non-uniformity of the phase distribution, due to skewness of the slow oscillation wave shape, was taken into account using the cumulative density function-based transformation[98,102]. Group comparison tests of circular variables were performed using circular ANOVA.

References

1. Jones, E. G. *The Thalamus* (Cambridge University Press, 2007).
2. Sherman, S. M. Thalamocortical interactions. *Current opinion in neurobiology* **22,** 575–579, doi: 10.1016/j.conb.2012.03.005 (2012).
3. Steriade, M., Jones, E. G. & McCormick, D. A. *Thalamus* (Elsevier Ltd. Oxford, 1997).
4. Vertes, R. P., Linley, S. B. & Hoover, W. B. Limbic circuitry of the midline thalamus. *Neuroscience and biobehavioral reviews*, doi: 10.1016/j.neubiorev.2015.01.014 (2015).
5. Van der Werf, Y. D., Witter, M. P. & Groenewegen, H. J. The intralaminar and midline nuclei of the thalamus. Anatomical and functional evidence for participation in processes of arousal and awareness. *Brain research. Brain research reviews* **39,** 107–140 (2002).
6. Arai, R., Jacobowitz, D. M. & Deura, S. Distribution of calretinin, calbindin-D28k, and parvalbumin in the rat thalamus. *Brain research bulletin* **33,** 595–614 (1994).
7. Bokor, H., Csaki, A., Kocsis, K. & Kiss, J. Cellular architecture of the nucleus reuniens thalami and its putative aspartatergic/glutamatergic projection to the hippocampus and medial septum in the rat. *The European journal of neuroscience* **16,** 1227–1239 (2002).
8. Winsky, L., Montpied, P., Arai, R., Martin, B. M. & Jacobowitz, D. M. Calretinin distribution in the thalamus of the rat: immunohistochemical and *in situ* hybridization histochemical analyses. *Neuroscience* **50,** 181–196 (1992).
9. Schwaller, B. The continuing disappearance of "pure" Ca2+ buffers. *Cellular and molecular life sciences: CMLS* **66,** 275–300, doi: 10.1007/s00018-008-8564-6 (2009).

10. Schwaller, B. Cytosolic Ca2+ buffers. *Cold Spring Harbor perspectives in biology* **2,** a004051, doi: 10.1101/cshperspect.a004051 (2010).
11. Baimbridge, K. G., Celio, M. R. & Rogers, J. H. Calcium-binding proteins in the nervous system. *Trends in neurosciences* **15,** 303–308 (1992).
12. Celio, M. R. Calbindin D-28k and parvalbumin in the rat nervous system. *Neuroscience* **35,** 375–475 (1990).
13. Freund, T. F. & Buzsaki, G. Interneurons of the hippocampus. *Hippocampus* **6,** 347–470 (1996).
14. Kubota, Y. *et al.* Selective coexpression of multiple chemical markers defines discrete populations of neocortical GABAergic neurons. *Cerebral cortex* **21,** 1803–1817, doi: 10.1093/cercor/bhq252 (2011).
15. Penzo, M. A. *et al.* The paraventricular thalamus controls a central amygdala fear circuit. *Nature* **519,** 455–459, doi: 10.1038/nature13978 (2015).
16. Ito, H. T., Zhang, S. J., Witter, M. P., Moser, E. I. & Moser, M. B. A prefrontal-thalamo-hippocampal circuit for goal-directed spatial navigation. *Nature*, doi: 10.1038/nature14396 (2015).
17. Xu, W. & Sudhof, T. C. A neural circuit for memory specificity and generalization. *Science* **339,** 1290–1295, doi: 10.1126/science.1229534 (2013).
18. Cassel, J. C. *et al.* The reuniens and rhomboid nuclei: neuroanatomy, electrophysiological characteristics and behavioral implications. *Prog Neurobiol* **111,** 34–52, doi: 10.1016/j.pneurobio.2013.08.006 (2013).
19. Loureiro, M. *et al.* The ventral midline thalamus (reuniens and rhomboid nuclei) contributes to the persistence of spatial memory in rats. *J Neurosci* **32,** 9947–9959, doi: 10.1523/JNEUROSCI.0410-12.2012 (2012).
20. Cholvin, T. *et al.* The ventral midline thalamus contributes to strategy shifting in a memory task requiring both prefrontal cortical and hippocampal functions. *J Neurosci* **33,** 8772–8783, doi: 10.1523/JNEUROSCI.0771-13.2013 (2013).
21. Jankowski, M. M. *et al.* Nucleus reuniens of the thalamus contains head direction cells. *eLife* **3,** doi: 10.7554/eLife.03075 (2014).
22. Preston, A. R. & Eichenbaum, H. Interplay of hippocampus and prefrontal cortex in memory. *Current biology: CB* **23,** R764–R773, doi: 10.1016/j.cub.2013.05.041 (2013).
23. Euston, D. R., Gruber, A. J. & McNaughton, B. L. The role of medial prefrontal cortex in memory and decision making. *Neuron* **76,** 1057–1070, doi: 10.1016/j.neuron.2012.12.002 (2012).
24. Oh, S. W. *et al.* A mesoscale connectome of the mouse brain. *Nature* **508,** 207–214, doi: 10.1038/nature13186 (2014).
25. Vertes, R. P., Albo, Z. & Viana Di Prisco, G. Theta-rhythmically firing neurons in the anterior thalamus: implications for mnemonic functions of Papez's circuit. *Neuroscience* **104,** 619–625 (2001).
26. Herkenham, M. The connections of the nucleus reuniens thalami: evidence for a direct thalamo-hippocampal pathway in the rat. *J Comp Neurol* **177,** 589–610, doi: 10.1002/cne.901770405 (1978).
27. Vertes, R. P., Hoover, W. B., Do Valle, A. C., Sherman, A. & Rodriguez, J. J. Efferent projections of reuniens and rhomboid nuclei of the thalamus in the rat. *J Comp Neurol* **499,** 768–796, doi: 10.1002/cne.21135 (2006).
28. Dolleman-Van der Weel, M. J., da Silva, F. H. L. & Witter, M. P. Nucleus reuniens thalami modulates activity in hippocampal field CA1 through excitatory and inhibitory mechanisms. *J Neurosci* **17,** 5640–5650 (1997).
29. Canteras, N. S. & Swanson, L. W. Projections of the ventral subiculum to the amygdala, septum, and hypothalamus: a PHAL anterograde tract-tracing study in the rat. *J Comp Neurol* **324,** 180–194 (1992).
30. Meibach, R. C. & Siegel, A. Efferent connections of the hippocampal formation in the rat. *Brain research* **124,** 197–224 (1977).
31. Witter, M. P., Ostendorf, R. H. & Groenewegen, H. J. Heterogeneity in the Dorsal Subiculum of the Rat. Distinct Neuronal Zones Project to Different Cortical and Subcortical Targets. *The European journal of neuroscience* **2,** 718–725 (1990).
32. O'Mara, S. M., Sanchez-Vives, M. V., Brotons-Mas, J. R. & O'Hare, E. Roles for the subiculum in spatial information processing, memory, motivation and the temporal control of behaviour. *Progress in neuro-psychopharmacology & biological psychiatry* **33,** 782–790, doi: 10.1016/j.pnpbp.2009.03.040 (2009).
33. Battaglia, F. P., Benchenane, K., Sirota, A., Pennartz, C. M. & Wiener, S. I. The hippocampus: hub of brain network communication for memory. *Trends in cognitive sciences* **15,** 310–318, doi: 10.1016/j.tics.2011.05.008 (2011).
34. Siapas, A. G., Lubenov, E. V. & Wilson, M. A. Prefrontal phase locking to hippocampal theta oscillations. *Neuron* **46,** 141–151, doi: 10.1016/j.neuron.2005.02.028 (2005).
35. Peyrache, A., Khamassi, M., Benchenane, K., Wiener, S. I. & Battaglia, F. P. Replay of rule-learning related neural patterns in the prefrontal cortex during sleep. *Nat Neurosci* **12,** 919–926, doi: 10.1038/nn.2337 (2009).
36. Buzsaki, G. Theta oscillations in the hippocampus. *Neuron* **33,** 325–340 (2002).
37. Buzsaki, G. & Silva, F. L. High frequency oscillations in the intact brain. *Prog Neurobiol* **98,** 241–249, doi: 10.1016/j.pneurobio.2012.02.004 (2012).
38. Pinault, D. A novel single-cell staining procedure performed *in vivo* under electrophysiological control: morpho-functional features of juxtacellularly labeled thalamic cells and other central neurons with biocytin or neurobiotin. *J Neurosci Meth* **65,** 113–136 (1996).
39. Franklin, K. B. J. & Paxinos, G. *The Mouse Brain in Stereotaxic Coordinates* (Academic Press, 2007).
40. Kölliker, A. *Handbuch der Gerwebelehre des Menschen. Nervensystemen des Menschen und der Thiere.* 6th edn, (Engelmann, 1896).
41. Llinas, R. R. & Steriade, M. Bursting of thalamic neurons and states of vigilance. *J Neurophysiol* **95,** 3297–3308, doi: 10.1152/jn.00166.2006 (2006).
42. Jahnsen, H. & Llinas, R. Electrophysiological properties of guinea-pig thalamic neurones: an *in vitro* study. *The Journal of physiology* **349,** 205–226 (1984).
43. Wolansky, T., Clement, E. A., Peters, S. R., Palczak, M. A. & Dickson, C. T. Hippocampal slow oscillation: a novel EEG state and its coordination with ongoing neocortical activity. *J Neurosci* **26,** 6213–6229, doi: 10.1523/JNEUROSCI.5594-05.2006 (2006).
44. Isomura, Y. *et al.* Integration and segregation of activity in entorhinal-hippocampal subregions by neocortical slow oscillations. *Neuron* **52,** 871–882, doi: 10.1016/j.neuron.2006.10.023 (2006).
45. Vertes, R. P. Analysis of projections from the medial prefrontal cortex to the thalamus in the rat, with emphasis on nucleus reuniens. *J Comp Neurol* **442,** 163–187, doi: 10.1002/cne.10083 (2002).
46. Wouterlood, F. G. *et al.* Origin of calretinin-containing, vesicular glutamate transporter 2-coexpressing fiber terminals in the entorhinal cortex of the rat. *J Comp Neurol* **506,** 359–370, doi: 10.1002/cne.21555 (2008).
47. Uylings, H. B. & van Eden, C. G. Qualitative and quantitative comparison of the prefrontal cortex in rat and in primates, including humans. *Progress in brain research* **85,** 31–62 (1990).
48. Sharott, A., Doig, N. M., Mallet, N. & Magill, P. J. Relationships between the firing of identified striatal interneurons and spontaneous and driven cortical activities *in vivo*. *J Neurosci* **32,** 13221–13236, doi: 10.1523/JNEUROSCI.2440-12.2012 (2012).
49. Bastianelli, E. Distribution of calcium-binding proteins in the cerebellum. *Cerebellum* **2,** 242–262, doi: 10.1080/14734220310022289 (2003).
50. Tsanov, M. *et al.* Theta-modulated head direction cells in the rat anterior thalamus. *J Neurosci* **31,** 9489–9502, doi: 10.1523/JNEUROSCI.0353-11.2011 (2011).
51. Tsanov, M. *et al.* Oscillatory entrainment of thalamic neurons by theta rhythm in freely moving rats. *J Neurophysiol* **105,** 4–17, doi: 10.1152/jn.00771.2010 (2011).
52. Witter, M. P. & Groenewegen, H. J. Connections of the parahippocampal cortex in the cat. III. Cortical and thalamic efferents. *J Comp Neurol* **252,** 1–31, doi: 10.1002/cne.902520102 (1986).

53. Colgin, L. L. *et al.* Frequency of gamma oscillations routes flow of information in the hippocampus. *Nature* **462,** 353–357, doi: 10.1038/nature08573 (2009).
54. Gabbott, P. L., Warner, T. A., Jays, P. R., Salway, P. & Busby, S. J. Prefrontal cortex in the rat: projections to subcortical autonomic, motor, and limbic centers. *J Comp Neurol* **492,** 145–177, doi: 10.1002/cne.20738 (2005).
55. Hoover, W. B. & Vertes, R. P. Anatomical analysis of afferent projections to the medial prefrontal cortex in the rat. *Brain structure & function* **212,** 149–179, doi: 10.1007/s00429-007-0150-4 (2007).
56. Fujisawa, S. & Buzsaki, G. A 4 Hz oscillation adaptively synchronizes prefrontal, VTA, and hippocampal activities. *Neuron* **72,** 153–165, doi: 10.1016/j.neuron.2011.08.018 (2011).
57. Sirota, A. *et al.* Entrainment of neocortical neurons and gamma oscillations by the hippocampal theta rhythm. *Neuron* **60,** 683–697, doi: 10.1016/j.neuron.2008.09.014 (2008).
58. Adhikari, A., Topiwala, M. A. & Gordon, J. A. Synchronized activity between the ventral hippocampus and the medial prefrontal cortex during anxiety. *Neuron* **65,** 257–269, doi: 10.1016/j.neuron.2009.12.002 (2010).
59. Benchenane, K. *et al.* Coherent theta oscillations and reorganization of spike timing in the hippocampal- prefrontal network upon learning. *Neuron* **66,** 921–936, doi: 10.1016/j.neuron.2010.05.013 (2010).
60. O'Neill, P. K., Gordon, J. A. & Sigurdsson, T. Theta oscillations in the medial prefrontal cortex are modulated by spatial working memory and synchronize with the hippocampus through its ventral subregion. *J Neurosci* **33,** 14211–14224, doi: 10.1523/JNEUROSCI.2378-13.2013 (2013).
61. Brun, V. H. *et al.* Place cells and place recognition maintained by direct entorhinal-hippocampal circuitry. *Science* **296,** 2243–2246, doi: 10.1126/science.1071089 (2002).
62. Nakazawa, K. *et al.* Requirement for hippocampal CA3 NMDA receptors in associative memory recall. *Science* **297,** 211–218, doi: 10.1126/science.1071795 (2002).
63. Erro, E., Lanciego, J. L. & Gimenez-Amaya, J. M. Relationships between thalamostriatal neurons and pedunculopontine projections to the thalamus: a neuroanatomical tract-tracing study in the rat. *Experimental brain research* **127,** 162–170 (1999).
64. Kha, H. T., Finkelstein, D. I., Pow, D. V., Lawrence, A. J. & Horne, M. K. Study of projections from the entopeduncular nucleus to the thalamus of the rat. *J Comp Neurol* **426,** 366–377 (2000).
65. Steriade, M. & Biesold, D. *Parallel activation of thalamic and cortical neurons by brainstem and basal forebrain cholinergic systems* Vol. 1 (Oxford University Press, 1990).
66. Oda, S., Kuroda, M., Kakuta, S. & Kishi, K. Differential immunolocalization of m2 and m3 muscarinic receptors in the anteroventral and anterodorsal thalamic nuclei of the rat. *Brain research* **894,** 109–120 (2001).
67. Deutch, A. Y., Holliday, J., Roth, R. H., Chun, L. L. & Hawrot, E. Immunohistochemical localization of a neuronal nicotinic acetylcholine receptor in mammalian brain. *Proceedings of the National Academy of Sciences of the United States of America* **84,** 8697–8701 (1987).
68. McCormick, D. A. & Prince, D. A. Actions of acetylcholine in the guinea-pig and cat medial and lateral geniculate nuclei, *in vitro*. *The Journal of physiology* **392,** 147–165 (1987).
69. Curro Dossi, R., Pare, D. & Steriade, M. Short-lasting nicotinic and long-lasting muscarinic depolarizing responses of thalamocortical neurons to stimulation of mesopontine cholinergic nuclei. *J Neurophysiol* **65,** 393–406 (1991).
70. Ye, M., Hayar, A. & Garcia-Rill, E. Cholinergic responses and intrinsic membrane properties of developing thalamic parafascicular neurons. *J Neurophysiol* **102,** 774–785, doi: 10.1152/jn.91132.2008 (2009).
71. McCormick, D. A. Cellular mechanisms underlying cholinergic and noradrenergic modulation of neuronal firing mode in the cat and guinea pig dorsal lateral geniculate nucleus. *J Neurosci* **12,** 278–289 (1992).
72. Hassani, O. K., Lee, M. G., Henny, P. & Jones, B. E. Discharge profiles of identified GABAergic in comparison to cholinergic and putative glutamatergic basal forebrain neurons across the sleep-wake cycle. *J Neurosci* **29,** 11828–11840, doi: 10.1523/JNEUROSCI.1259-09.2009 (2009).
73. Lapray, D. *et al.* Behavior-dependent specialization of identified hippocampal interneurons. *Nat Neurosci* **15,** 1265–1271, doi: 10.1038/nn.3176 (2012).
74. Crochet, S. & Petersen, C. C. Correlating whisker behavior with membrane potential in barrel cortex of awake mice. *Nat Neurosci* **9,** 608–610, doi: 10.1038/nn1690 (2006).
75. Gentet, L. J. *et al.* Unique functional properties of somatostatin-expressing GABAergic neurons in mouse barrel cortex. *Nat Neurosci* **15,** 607–612, doi: 10.1038/nn.3051 (2012).
76. Buzsaki, G. Hippocampal sharp waves: their origin and significance. *Brain research* **398,** 242–252 (1986).
77. O'Keefe, J. & Nadel, L. *The Hippocampus as a Cognitive Map* (Oxford University Press, 1978).
78. Jadhav, S. P., Kemere, C., German, P. W. & Frank, L. M. Awake hippocampal sharp-wave ripples support spatial memory. *Science* **336,** 1454–1458, doi: 10.1126/science.1217230 (2012).
79. Girardeau, G. & Zugaro, M. Hippocampal ripples and memory consolidation. *Current opinion in neurobiology* **21,** 452–459, doi: 10.1016/j.conb.2011.02.005 (2011).
80. Girardeau, G., Benchenane, K., Wiener, S. I., Buzsaki, G. & Zugaro, M. B. Selective suppression of hippocampal ripples impairs spatial memory. *Nat Neurosci* **12,** 1222–1223, doi: 10.1038/nn.2384 (2009).
81. Ego-Stengel, V. & Wilson, M. A. Disruption of ripple-associated hippocampal activity during rest impairs spatial learning in the rat. *Hippocampus* **20,** 1–10, doi: 10.1002/hipo.20707 (2010).
82. Axmacher, N., Elger, C. E. & Fell, J. Ripples in the medial temporal lobe are relevant for human memory consolidation. *Brain* **131,** 1806–1817, doi: 10.1093/brain/awn103 (2008).
83. Logothetis, N. K. *et al.* Hippocampal-cortical interaction during periods of subcortical silence. *Nature* **491,** 547–553, doi: 10.1038/nature11618 (2012).
84. Domich, L., Oakson, G. & Steriade, M. Thalamic burst patterns in the naturally sleeping cat: a comparison between cortically projecting and reticularis neurones. *The Journal of physiology* **379,** 429–449 (1986).
85. Arcelli, P., Frassoni, C., Regondi, M. C., De Biasi, S. & Spreafico, R. GABAergic neurons in mammalian thalamus: a marker of thalamic complexity? *Brain research bulletin* **42,** 27–37 (1997).
86. Bartho, P., Freund, T. F. & Acsady, L. Selective GABAergic innervation of thalamic nuclei from zona incerta. *The European journal of neuroscience* **16,** 999–1014 (2002).
87. Eichenbaum, H. Declarative memory: insights from cognitive neurobiology. *Annu Rev Psychol* **48,** 547–572, doi: 10.1146/annurev.psych.48.1.547 (1997).
88. Squire, L. R. Memory and the hippocampus: a synthesis from findings with rats, monkeys, and humans. *Psychol Rev* **99,** 195–231 (1992).
89. Eichenbaum, H. & Fortin, N. J. The neurobiology of memory based predictions. *Philos Trans R Soc Lond B Biol Sci* **364,** 1183–1191, doi: 10.1098/rstb.2008.0306 (2009).
90. Eichenbaum, H. A cortical-hippocampal system for declarative memory. *Nat Rev Neurosci* **1,** 41–50, doi: 10.1038/35036213 (2000).
91. Klausberger, T. *et al.* Brain state- and cell type-specific firing of hippocampal interneurons *in vivo*. *Nature* **421,** 844–848 (2003).
92. Abeles, M. & Gerstein, G. L. Detecting spatiotemporal firing patterns among simultaneously recorded single neurons. *J Neurophysiol* **60,** 909–924 (1988).
93. Nadasdy, Z., Hirase, H., Czurko, A., Csicsvari, J. & Buzsaki, G. Replay and time compression of recurring spike sequences in the hippocampus. *J Neurosci* **19,** 9497–9507 (1999).

94. Swadlow, H. A. & Gusev, A. G. The impact of 'bursting' thalamic impulses at a neocortical synapse. *Nat Neurosci* **4,** 402–408, doi: 10.1038/86054 (2001).
95. Ramcharan, E. J., Gnadt, J. W. & Sherman, S. M. Higher-order thalamic relays burst more than first-order relays. *Proceedings of the National Academy of Sciences of the United States of America* **102,** 12236–12241, doi: 10.1073/pnas.0502843102 (2005).
96. Fanselow, E. E., Sameshima, K., Baccala, L. A. & Nicolelis, M. A. Thalamic bursting in rats during different awake behavioral states. *Proceedings of the National Academy of Sciences of the United States of America* **98,** 15330–15335, doi: 10.1073/pnas.261273898 (2001).
97. Lu, S. M., Guido, W. & Sherman, S. M. Effects of membrane voltage on receptive field properties of lateral geniculate neurons in the cat: contributions of the low-threshold Ca2+ conductance. *J Neurophysiol* **68,** 2185–2198 (1992).
98. Nakamura, K. C., Sharott, A. & Magill, P. J. Temporal coupling with cortex distinguishes spontaneous neuronal activities in identified basal ganglia-recipient and cerebellar-recipient zones of the motor thalamus. *Cerebral cortex* **24,** 81–97, doi: 10.1093/cercor/bhs287 (2014).
99. Klausberger, T. *et al.* Complementary roles of cholecystokinin- and parvalbumin- expressing GABAergic neurons in hippocampal network oscillations. *J Neurosci* **25,** 9782–9793 (2005).
100. Hochberg, Y. & Benjamini, Y. More powerful procedures for multiple significance testing. *Stat Med* **9,** 811–818 (1990).
101. Fisher, N. I. *Statistical analysis of circular data* (Cambridge University Press, 1993).
102. Siapas, A. G., Lubenov, E. V. & Wilson, M. A. Prefrontal phase locking to hippocampal theta oscillations. *Neuron* **46,** 141–151, doi: S0896-6273(05)00197-2 10.1016/j.neuron.2005.02.028 (2005).

Acknowledgements

This work was supported by the Comisión Nacional de Investigación Científica y Tecnológica (CONICYT) with grant Fondecyt regular 1141089 and grant CONICYT PIA ACT 1414. AL and ED were supported by a VRI scholarship from the Pontificia Universidad Católica de Chile.

Author Contributions

A.L. and E.D. performed research, M.S. and N.E. analyzed data, P.F. designed research and wrote the manuscript.

Additional Information

Supplementary information accompanies this paper at http://www.nature.com/srep

Competing financial interests: The authors declare no competing financial interests.

How to cite this article: Lara-Vásquez, A. *et al.* Midline thalamic neurons are differentially engaged during hippocampus network oscillations. *Sci. Rep.* **6**, 29807; doi: 10.1038/srep29807 (2016).